TECHNISCHE UNIVERSITÄT MÜNCHEN

Institute for
Experimental Physics E21

Annual Report 2007

Annual Report 2007

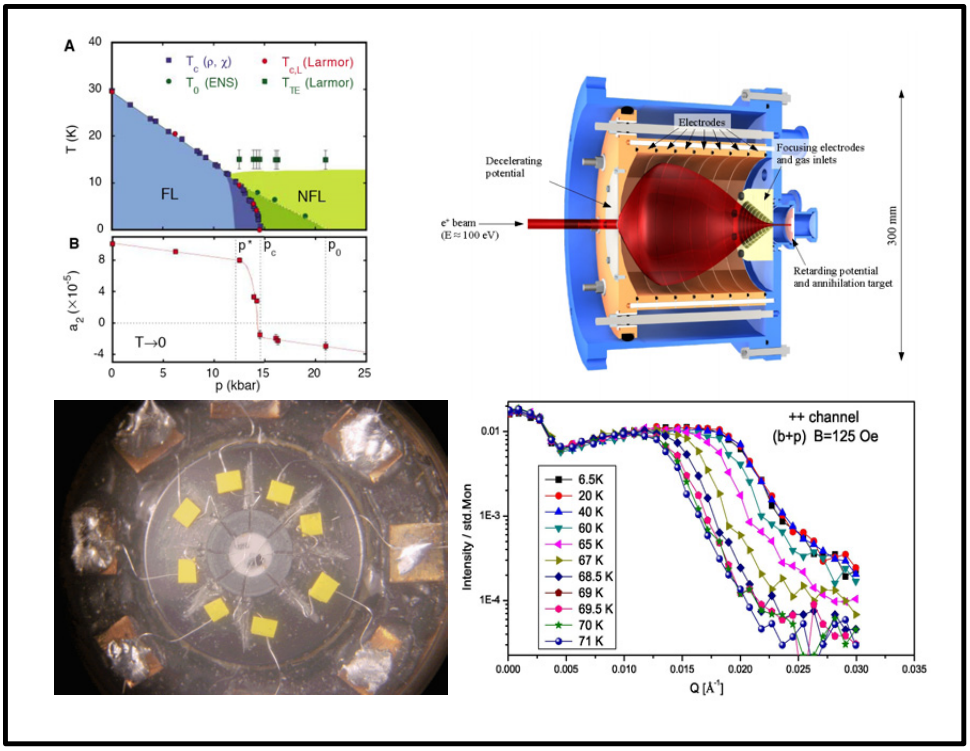

Cover page

Top/left:	Phase diagram of MnSi as a function of pressure (sections 1.2, 1.3, 1.4; C. Pfleiderer et al., Science, 316:1871, 2007; Phys. Rev. Lett., 99:156406, 2007; Y. J. Uemura et al., Nature Physics, 3:34, 2007).
Top/right:	Cross section of the positron gas remoderator (section 3.5).
Bottom/left:	Resistivity set-up in the WC Bridgman cell (section 5.2).
Bottom/right:	Reflectivity profiles of epitaxial EuO on Si (section 1.7, A. Schmehl et al., Nature Materials 6:882, 2007).

Annual Report 2007

of the Institute for Experimental Physics E21
Prof. Dr. P. Böni
Technische Universität München

Annual Report 2007
of the Institute for Experimental Physics E21
published: Feb. 2008
Layout by Nikolas Arend, Florian Grünauer, Stefan Legl
Edited by Stefan Legl
http://e21.frm2.tum.de

Technische Universität München
James-Franck-Straße
D-85748 Garching, Germany

Phone: +49-89-289-14711
Fax: +49-89-289-14713

Copyright:
Inquiries about copyright and reproduction etc.
should be addressed to the authors.

Contents

Preface

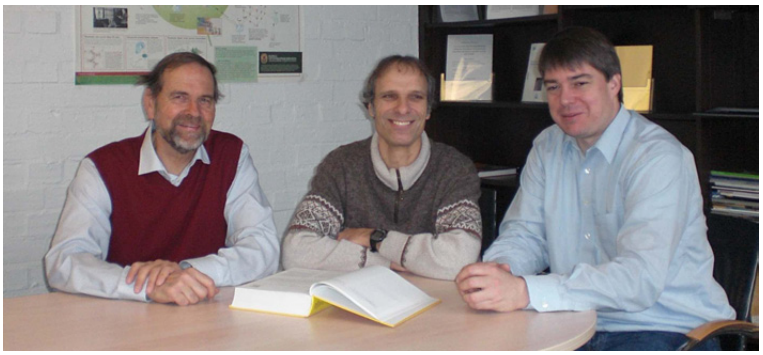

It is with great pleasure to provide with this report an overview of the research and teaching activities of E21 during 2007. Our research areas cover issues ranging from fundamental over applied questions in solid state physics all the way to advanced topics in instrumentation. At FRM II a variety of improvements have been put in place on our beam lines. The polarizing neutron guide of the neutron resonance spin-echo spectrometer RESEDA was successfully replaced by a regular supermirror guide combined with a polarizing cavity. This has solved the problem with the activation of the coatings in the old set-up. In addition, a replacement for the insert of the positron source NEPOMUC has been installed in January 2008. This has further improved the intensity of the positron beam. We also made significant progress in the laboratories at the Physik-Department: Following the refurbishment of the laboratories our top-loading dilution refrigerator now operates very well. The mirror furnace is running excellently and several high quality single-crystals have been manufactured using a new rod-casting-facility.

In early 2007, Philipp Niklowitz has accepted a position as a lecturer at the University of London in Royal Holloway. On the one hand, this is a significant loss for E21, on the other hand this demonstrates yet again the high quality of the staff of E21. His position was filled in September by Dr. Sarah Dunsiger from McMaster University, Hamilton, Canada. As an expert in μSR and neutron scattering she will strengthen the position of E21 in the field of magnetism. For the first year of her stay, funding for her position is supplied by the Physics Department in an effort to increase the number of women in Physics at TUM.

Last year again a large number of experiments have been performed in the laboratories of E21 and our beam lines at FRM II. In addition, beam time at HMI and PSI was acquired. Some of the most important results have been published in leading journals including Science, Nature, and Physical Review Letters. Of course, the output could have been even better, if the dramatic lack of technical support staff at FRM II could be resolved.

E21 has continued acquiring very large support for doing high level research. Unfortunately, most of the funding only appears in the CHE-ranking of the TUM, but not directly as part of the Drittmittel-Fonds of E21. In collaboration with Prof. Markus Braden from the University of Cologne, E21 succeeded to raise funding for a new beam line for polarized neutrons at the FRM II. Again, due to the special relations between TUM and BMBF, the Drittmittel will not appear in the fonds of E21. Last but not least, E21 succeeded to receive funding from DFG for the investigation of quantum phase transitions within the Forschergruppe FOR 960.

In addition to our research efforts, members of E21 have conducted a heavy teaching load. We are very happy to see, that E21 covered essentially the full range of physics, i.e., Experimental Physics for first year Physics students, Solid State Physics, Reactor Physics, and Physics with Neutrons. In addition, E21 contributed in many ways to the activities of the Physik-Department, helping to coordinate the Münchner Physik Kolloquium, the Festkörperkolloquium and tours at FRM II. We are extremely pleased that besides the very hard work we have also found time for social activities including an evening of bowling at the Bürgerhaus in Garching, a very lively visit of the Oktoberfest, and a *Klausabend*. We thank all members of E21 and in particular the young scientists and the technical staff for their dedication and efforts to maintain an excellent atmosphere at our institute.

Garching, January 2008

Peter Böni Christian Pfleiderer Klaus Schreckenbach

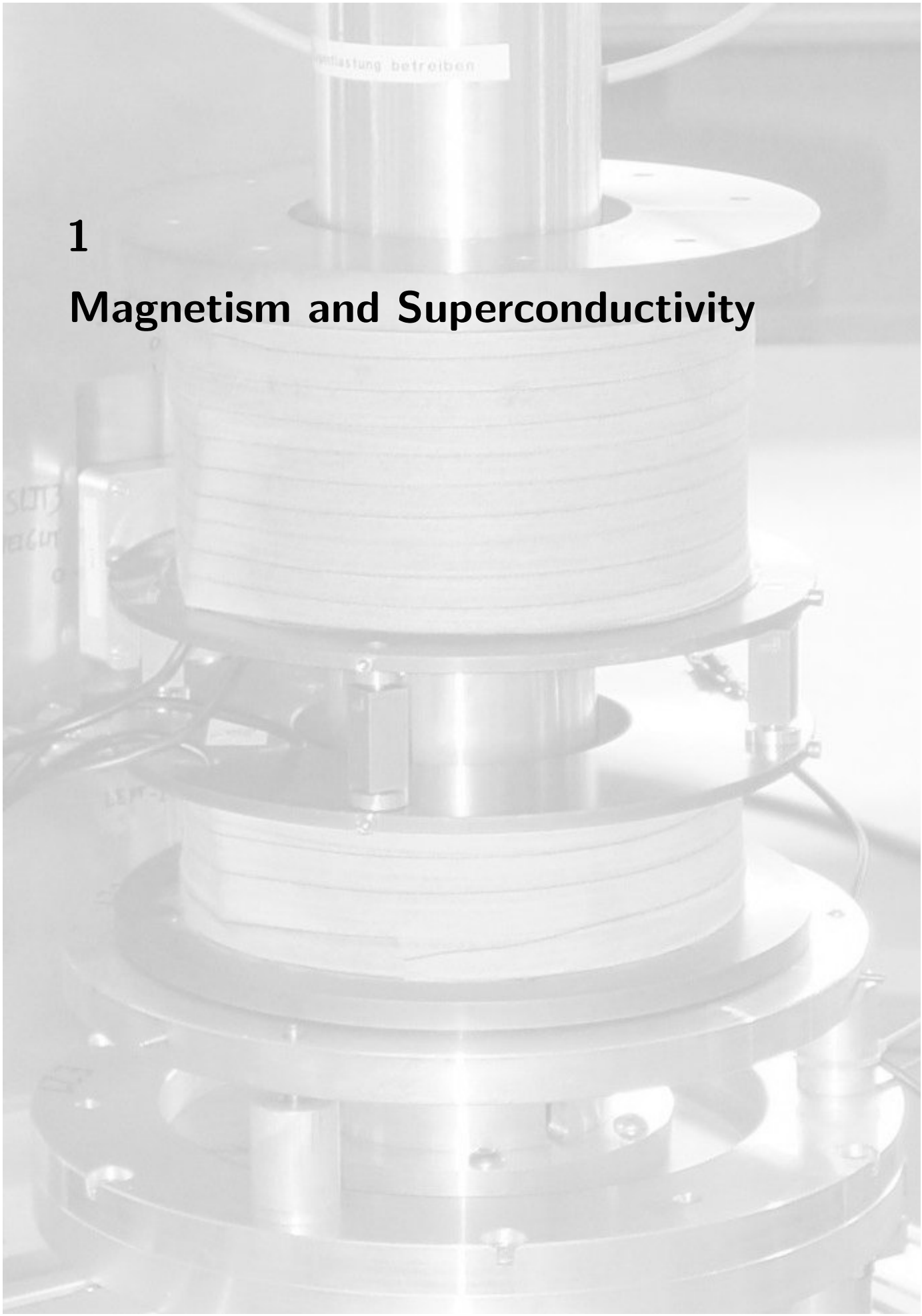

1

Magnetism and Superconductivity

1.1 Neutron diffraction and μSR study on the antiferromagnet $BaCoO_3$

H. Nozaki [3], **M. Janoschek** [1, 2], **B. Roessli** [2], **J. Sugiyama** [3], **L. Keller** [2], **J. H. Brewer** [4], **E. J. Ansaldo** [4], **G. D. Morris** [5], **T. Takami** [6], **H. Ikuta** [6]

[1] *Physik-Department E21, Technische Universität München, D-85748 Garching, Germany*
[2] *Laboratory for Neutron Scattering ETHZ & PSI, CH-5232 Villigen PSI, Switzerland*
[3] *Toyota Central Research and Development Labs. Inc., Nagakute, Aichi 480-1192, Japan*
[4] *TRIUMF, CIAR and Dept. of Physics and Astronomy, Univ. of British Columbia, Vancouver, BC, V6T 1Z1 Canada*
[5] *TRIUMF, 4004 Wesbrook Mall, Vancouver, BC, V6T 2A3 Canada*
[6] *Dept. of Crystalline Materials Science, Nagoya University, Furo-cho, Chikusa-ku, Nagoya, 464-8603 Japan*

Competition between one-dimensional (1D) and two-dimensional (2D) interactions induces complex physics in the class of hexagonal perovskites ABX_3, in which the face sharing BX_6 octahedra form a 1D BX_3 chain. The chains are located on the corners of the 2D triangular lattice and are separated by A ions [1]. If the 2D interaction is antiferromagnetic (AF), geometrical frustration naturally annihilates typical AF long-range order on the 2D triangular lattice, whether the 1D interaction is AF or ferromagnetic (FM). The hexagonal perovskites are however usually classified as a quasi-1D (Q1D) system, because the 1D interaction is superior to the 2D interaction due to the separation between neighboring 1D chains by A ions.

For $BaCoO_3$[2], it was found that a 1D-FM order appears below 53 K, and a sharp bulk 2D-AF transition occurrs at 15 K ($= T_N$) by means of a positive muon spin spectroscopy (μ^+SR) together with heat capacity (C_p) and dc-χ measurements [3, 4, 5], in contrast to the prediction of an electronic structural calculation (LDA+U) — i.e., an FM ground state is the most stable configuration [6]. Very recent μ^+SR experiments under pressure up to 1.1 GPa showed that T_N of $BaCoO_3$ is enhanced by pressure, as expected from the relationship between T_N and the inter-chain distance in the Q1D cobalt oxides [7]. This also strongly supports the role of the 2D-AF interaction on T_N. The zero-field (ZF-) μ^+SR spectrum for $BaCoO_3$ is however found to show clear but complex muon spin oscillations below T_N; that is, it has at least five frequency components (ν_μ = 14.4, 13.5, 6.4, 5.1, and 3.5 MHz) at 1.8 K under ambient pressure, even though the sample is structurally single phase at room T and there is no indication of any structural phase transition down to 4 K[3]. This means that every oxygen is equivalent for the simple hexagonal lattice. As a result, there is naturally only one μ^+ site in the $BaCoO_3$ lattice. On the other hand, the internal magnetic fields of the five signals, i.e., $\nu_{\mu,i}$ with i = 1-5, exhibit a similar T dependence, indicating that the five frequencies are unlikely to be caused by compositional inhomogeneities, but most likely reflect the intrinsic behavior of $BaCoO_3$.

In order to clarify the origin of the multi-frequency components detected by μ^+SR and to determine the AF structure below T_N, we have measured neutron powder diffraction (NPD) spectrum for $BaCoO_3$ down to 1.5 K. In Fig. 1 the difference between the spectrum obtained at 1.5 K and at 20 K is shown. The magnetic Bragg reflections are indexed with a propagation vector $\mathbf{k} = (\frac{1}{3}, \frac{1}{3}, 0)$ — that is, the magnetic unit cell is 3 times larger than the chemical one. Four possible models in agreement with the crystal symmetry and the propagation vector $\mathbf{k}$ were identified by representational analysis. However, only two of them, namely Γ_3 corresponding to an amplitude modulated (am) structure with moments aligned ferromagnetically along the crystallographic c-direction propagating in the (1, 1, 0)-direction with a period of 3**a** and Γ_5 corresponding to a magnetic structure where the spins along the Co chains have an FM arrangment and form a 120° configuration in the hexagonal plane, i.e., 120° structure, gave reasonable fits with almost similar agreement factors $R_M = 6.47$ and $R_M = 6.48$, respectively.

Even though the NPD data alone therefore does not allow to decide between the two magnetic structures the combination of the NPD study with the μSR results yields that the amplitude modulated structure Γ_3 is the correct magnetic model for of $BaCoO_3$. A detailed description of our combined NPD and μSR study can be found in [8].

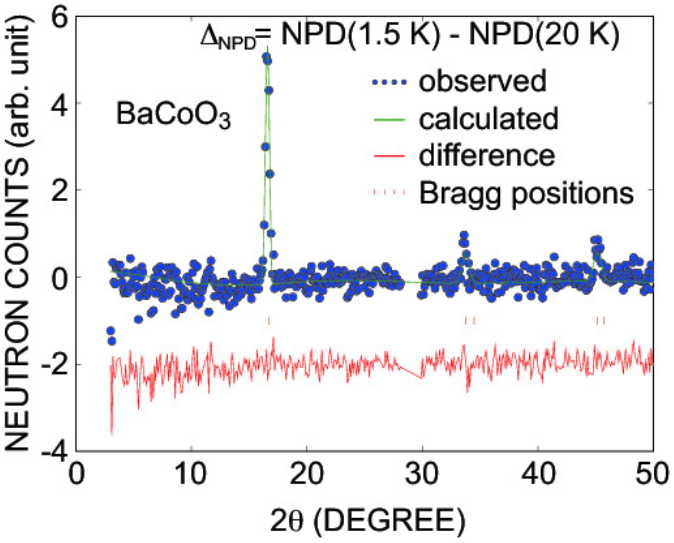

Figure 1: Refinement of the difference diffraction pattern (Δ_{NPD}) for $BaCoO_3$. The Δ_{NPD} pattern was produced by subtracting the $T = 20$ K data set from the data collected at $T = 1.5$ K.

References

[1] T. Li, G. D. Stucky, and G. L. McPherson. *Acta Crystallogr. B*, 29:1330, 1973.
[2] Y. Takeda. *J. Solid State Chem.*, 15:40, 1975.
[3] J. Sugiyama, H. Nozaki, J. H. Brewer, E. J. Ansaldo, T. Takami, H. Ikuta, and U. Mizutani. *Phys. Rev. B*, 72:064418, 2005.
[4] K. Yamaura, H. W. Zandbergen, K. Abe, and R. J. Cava. *J. Solid State Chem.*, 146:96, 1999.
[5] K. Yamaura and R. J. Cava. *Solid State Commu.*, 115:301, 2000.
[6] V. Pardo, P. Blaha, M. Iglesias, K. Schwarz, D. Baldomir, and J.E. Arias. *Phys. Rev. B*, 70:144422, 2004.
[7] J. Sugiyama, H. Nozaki, Y. Ikedo, K. Mukai, D. Andreica, A. Amato, J. H. Brewer, E. J. Ansaldo, G. D. Morris, T. Takami, and H. Ikuta. *Phys. Rev. Lett.*, 96:197206, 2006.
[8] H. Nozaki, M. Janoschek, B. Roessli, J. Sugiyama, L. Keller, J. H. Brewer, E. J. Ansaldo, G. D. Morris, T. Takami, and H. Ikuta. *Phys. Rev. B*, 76:014402, 2007.

1.2 Non-Fermi liquid metal without quantum criticality

C. Pfleiderer [1], **P. Böni** [1], **T. Keller** [2, 3], **U. K. Rößler** [4], **A. Rosch** [5]
[1] *Physik-Department E21, Technische Universität München, D-85748 Garching, Germany*
[2] *Max-Planck Institut für Festkörperforschung, Heisenbergstr. 1, D-70569 Stuttgart, Germany*
[3] *ZWE FRM-II, Technische Universität München, D-85748 Garching, Germany*
[4] *Leibniz-Institut für Festkörper-und Werkstoffforschung(IFW) Dresden, D-01171 Dresden, Germany*
[5] *II. Physikalisches Institut, Universität zu Köln, Zülpicher Str. 77, 50937 Köln, Germany*

Quantum critical points (QCPs) are defined as zero-temperature second-order phase transitions that are tuned by non-thermal control parameters such as hydrostatic pressure or magnetic field. Various novel states of condensed matter originate from QCPs [1]. For instance, superconductivity has been found at the border of antiferromagnetism [2] and at the transition between ferromagnetic states [3], and a nematic electronic phase has been reported at a metamagnetic QCP [4]. In contrast to low-dimensional systems where, for instance, Luttinger liquids provide a well-understood new metallic state in one dimension a breakdown of Fermi liquid theory for three-dimensional metals is expected only at QCPs [5]. However, because strong competing interactions are balanced at QCPs, allowing weak residual interactions to stabilize new behavior, all known examples of non-Fermi liquid (NFL) behavior and novel states at QCPs are extraordinarily sensitive to fine-tuning of the underlying interactions.

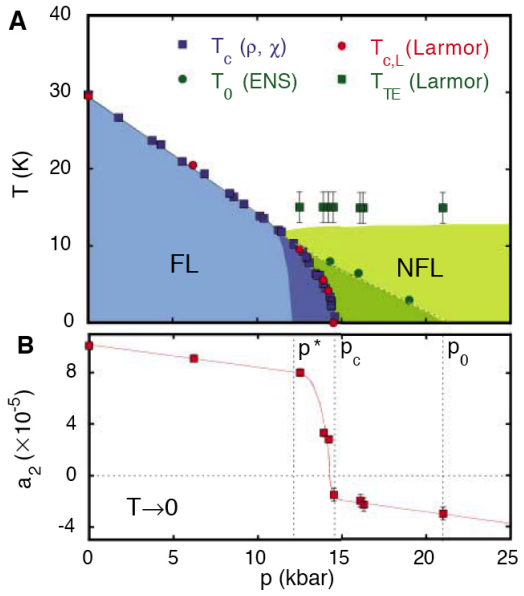

Figure 1: Phase diagram of MnSi as a function of pressure [6]. Data for T_c are based on the resistivity ρ and the ac susceptibility χ reported in [7]. T_0 is based on elastic neutron scattering [8]. The blue shading indicates the regime of Fermi liquid behavior, where dark blue shading shows the regime of phase segregation seen in μ-SR [9]. The green shading represents the regime of NFL resistivity [10], where dark green shading indicates the regime of partial order [8]. The transition temperature $T_{c,L}$ observed in the lattice constant by Larmor diffraction is in excellent agreement with previous work. The crossover temperature T_{TE} represents the appearance of lattice contraction as measured by Larmor diffraction. (B) Extrapolated zero-temperature variation of the electronic contribution to the lattice constant, a_2. The spontaneous magnetostriction varies very weakly under pressure up to $p^* \sim 12.5$ kbar before dropping distinctly and changing sign. It also varies very weakly above p_c. Both the temperature and pressure dependence of the lattice constant establish the absence of a quantum critcal point. Yet a non-Fermi liquid resistivity is observed [10].

A key question in condensed matter physics concerns whether pure three-dimensional metals can always be described as Fermi liquids. Using neutron Larmor diffraction to overcome the traditional resolution limit of diffraction experiments [11], we studied the lattice constants of the cubic itinerant-electron magnet manganese silicide (MnSi) at low temperatures and high pressures [6].

Our results concerning the nature of the phase diagram of MnSi (Fig. 1) show that the transition at p_c is first order [7], and the onset of partial order at T_0 (and thus p_0) seen in neutron scattering [8] is clearly not related to a thermodynamic phase transition. This establishes that the observed NFL behavior [10] is not connected to a QCP. Instead, it is the characteristic of an extended genuine NFL state far from any instability. More generally, this finding suggests that novel forms of order may be expected elsewhere than at quantum phase transitions.

References

[1] G. R. Stewart. *Rev. Mod. Phys.*, 73:797, 2001.
[2] N. D. Mathur et al. *Nature*, 394:39, 1998.
[3] S. S. Saxena et al. *Nature*, 406:587, 2000.
[4] R. A. Borzi et al. *Science*, 315:214, 2007.
[5] A. J. Schofield. *Contemp. Phys.*, 40:95, 1999.
[6] C. Pfleiderer, P. Böni, T. Keller, U. K. Rößler, and A. Rosch. Non-Fermi liquid metal wihtout quantum criticality. *Science*, 316:1871, 2007.
[7] C. Pfleiderer, G. J. McMullan, S. R. Julian, and G. G. Lonzarich. Magnetic quantum phase transition in MnSi under hydrostatic pressure. *Phys. Rev. B*, 55:8330, 1997.
[8] C. Pfleiderer, D. Reznik, L. Pintschovius, H. v. Löhneysen, M. Garst, and A. Rosch. Partial magnetic order in the non-Fermi liquid phase of MnSi. *Nature*, 427:227–230, 2004.
[9] Y. J. Uemura, T. Goko, I. M. Gat-Malureanu, J. P. Carlo, P. L. Russo, A. T. Savici, A. Aczel, G. J. MacDougall, J. Rodoriguez, G. M. Luke, S. R. Dunsiger, A. McCollam, J. Arai, Ch. Pfleiderer, P. Böni, K. Yoshimura, E. Baggio-Saitovitch, M. B. Fontes, J. Larrea, Y. V. Sushko, and J. Sereni. Phase separation and suppression of critical dynamics at quantum transitions of itinerant magnets: MnSi and $(Sr_{1-x}Ca_x)RuO_3$. *Nature Physics*, 3:34, 2007.
[10] C. Pfleiderer, S. R. Julian, and G. G. Lonzarich. Non-Fermi liquid nature of the normal state of itinerant-electron ferromagnets. *Nature*, 414:427–430, 2001.
[11] M. T. Rekveldt, T. Keller, and R. Golub. Larmor precession, a technique for high-sensitivity neutron diffraction. *Eur. Phys. Lett.*, 54:342–346, 2001.

1.3 Magnetic field and pressure dependence of small angle neutron scattering in MnSi

C. Pfleiderer [1, 2, 3], **D. Reznik** [3], **L. Pintschovius** [3], **J. Haug** [4]
[1] *Physik-Department E21, Technische Universität München, D-85748 Garching, Germany*
[2] *Physikalisches Institut, Universität Karlsruhe, D-76128 Karlsruhe, Germany*
[3] *Forschungszentrum Karlsruhe, Institut für Festkörperphysik, D-76021 Karlsruhe, Germany*
[4] *Hahn-Meitner-Institut, Glienicker Straße 100, D-14109 Berlin, Germany*

At ambient pressure and low temperatures the cubic B20 compound MnSi is well described as a weakly spin-polarized Fermi liquid. When the magnetic transition temperature decreases and vanishes under pressure at $p_c \approx 14.6$ kbar the resistivity snaps from a Fermi liquid (FL) temperature dependence T^α with $\alpha \approx 2$ to a non-Fermi liquid (NFL) dependence with $\alpha \approx 3/2$ that ranges over 3 orders of magnitude from a few mK to a few K [1, 2]. Because the suppression of magnetic order at p_c is first order [3, 4], an important question is whether some mechanism exists that stabilizes the NFL behavior. In the most likely scenario the NFL behavior may be related to the magnetic properties of MnSi, which exhibit a hierarchy of three energy scales: (i) a tendency to ferromagnetic spin alignment as the strongest scale, (ii) long-wavelength spin rotations with a periodicity ahe 180 Å due to isotropic Dzyaloshinsky-Moriya (DM) spin-orbit interactions on an intermediate scale, and (iii) very weak crystal-field interactions that pin the direction of the helical order to the cubic space diagonal $\langle 111 \rangle$. At $p = 0$ magnetic field unpins the helical order for $B_{c1} \approx 0.1$ T and destroys it above $B_{c2} \approx 0.6$ T [5, 6].

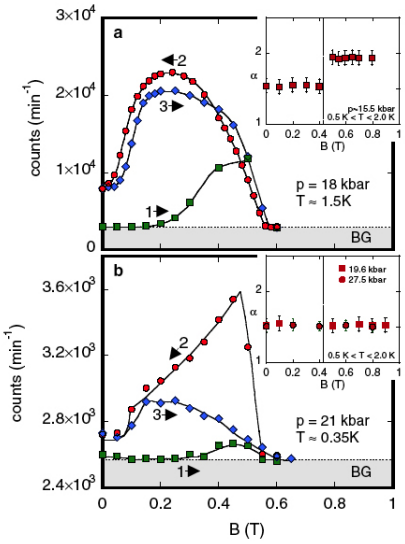

Figure 1: Typical magnetic field dependence of the SANS intensity in MnSi above p_c, where $B \parallel \langle 110 \rangle$ [7]. Data were recorded at 1.5 K and 0.35 K in panel (a) and panel (b), respectively. Gray shading shows the background (BG) signal. The magnetic field history following ZFC is: (1) ramp to 0.7 T, (2) ramp down, and (3) ramping field up again. Inset: Exponent α of the T dependence of the resistivity as reported in Ref. [1].

We have used small angle neutron scattering of spontaneous and magnetic field aligned components of the helical spin polarization in MnSi for temperatures T down to 0.35 K, at pressures p up to 21 kbar, and magnetic field B up to 0.7 T [8]. The parameter range of our study spans the first order transition between helical order [3, 9] and partial magnetic order [7] at $p_c = 14.6$ kbar, which coincides with the onset of an extended regime of non-Fermi liquid resistivity [2, 1]. Experiments were carried out at the polarized SANS instrument V4 at the Hahn Meitner Institute in Berlin. Our study suggests that MnSi above p_c is not dominated by the remains of the first order transition at p_c, e.g., in the form of metastable droplets, but that a mechanism actively drives the system away from helical order. In fact, the hysteresis we observe supports a recent study showing that the NFL resistivity is not related to quantum criticality [4]. If the NFL resistivity is related to DM-interactions, the effects of these interactions must be much more stable against applied magnetic field than the helical order. A candidate are multidimensional magnetic textures, which were theoretically found to be more stable under certain conditions than helical order [10, 11, 12]. Alternatively the NFL resistivity may even be completely unrelated to DM-interactions.

References

[1] N. Doiron-Leyraud, I. R. Walker, L. Taillefer, M. J. Steiner, S. R. Julian, and G. G. Lonzarich. Fermi-liquid breakdown in the paramagnetic phase of a pure metal. *Nature*, 425:595–599, 2003.

[2] C. Pfleiderer, S. R. Julian, and G. G. Lonzarich. Non-Fermi liquid nature of the normal state of itinerant-electron ferromagnets. *Nature*, 414:427–430, 2001.

[3] C. Pfleiderer, G. J. McMullan, S. R. Julian, and G. G. Lonzarich. Magnetic quantum phase transition in MnSi under hydrostatic pressure. *Phys. Rev. B*, 55:8330, 1997.

[4] C. Pfleiderer, P. Böni, T. Keller, U. K. Rößler, and A. Rosch. Non-Fermi liquid metal wihtout quantum criticality. *Science*, 316:1871, 2007.

[5] Y. Ishikawa and M. Arai. Magnetic field and pressure dependence of small angle neutron scattering in MnSi. *J. Phys. Soc. Jpn.*, 53:2726, 1984.

[6] C. Thessieu, C. Pfleiderer, A. N. Stepanov, and J. Flouquet. Magnetic field and pressure dependence of small angle neutron scattering in MnSi. *Phys. Condens. Matter*, 9:6677, 1997.

[7] C. Pfleiderer, D. Reznik, L. Pintschovius, H. v. Löhneysen, M. Garst, and A. Rosch. Partial magnetic order in the non-Fermi liquid phase of MnSi. *Nature*, 427:227–230, 2004.

[8] C. Pfleiderer, D. Reznik, L. Pintschovius, and J. Haug. Magnetic field and pressure dependence of small angle neutron scattering in MnSi. *Phys. Rev. Lett.*, 99:156406, 2007.

[9] Y. J. Uemura, T. Goko, I. M. Gat-Malureanu, J. P. Carlo, P. L. Russo, A. T. Savici, A. Aczel, G. J. MacDougall, J. Rodoriguez, G. M. Luke, S. R. Dunsiger, A. McCollam, J. Arai, Ch. Pfleiderer, P. Böni, K. Yoshimura, E. Baggio-Saitovitch, M. B. Fontes, J. Larrea, Y. V. Sushko, and J. Sereni. Phase separation and suppression of critical dynamics at quantum transitions of itinerant magnets: MnSi and $(Sr_{1-x}Ca_x)RuO_3$. *Nature Physics*, 3:34, 2007.

[10] Sumanta Tewari, D. Belitz, and T. R. Kirkpatrick. Blue quantum fog: Chiral condensation in quantum helimagnets. *Phys. Rev. Lett.*, 96(4):047207, Feb 2006.

[11] B. Binz, A. Vishwanath, and V. Aji. Theory of the helical spin crystal: A candidate for the partially ordered state of MnSi. *Phys. Rev. Lett.*, 96(20):207202, May 2006.

[12] U. K. Rößler, A. N. Bogdanov, and C. Pfleiderer. Spontaneous skyrmion ground states in magnetic metals. *Nature*, 442:797, 2006.

1.4 Phase separation and suppression of critical dynamics at quantum phase transitions of MnSi and $(Sr_{1-x}Ca_x)RuO_3$

Y. J. Uemura [1], T. Goko [1, 2], I. M. Gat-Malureanu [1, 3], J. P. Carlo [1], P. L. Russo [1], A. T. Savici [1], A. Aczel [4], G. J. MacDougall [4], J. A. Rodriguez [4], G. M. Luke [4], S. R. Dunsiger [4], A. McCollam [5], J. Arai [2], C. Pfleiderer [6], P. Böni [6], K. Yoshimura [7], E. Baggio-Saitovich [8], M. B. Fontes [8], J. Larrea [8], Y. V. Sushko [9], J. Sereni [10]

[1] *Department of Physics, Columbia University, New York, New York 10027, USA*
[2] *Department of Physics, Tokyo University of Science, Noda, Chiba 278-8510, Japan*
[3] *Department of Science, SUNY Maritime College, Throggs Neck, New York 10465, USA*
[4] *Department of Physics and Astronomy, McMaster University, Hamilton, Ontario L8S 4M1, Canada*
[5] *Department of Physics, University of Toronto, Toronto, Ontario M5S 1A7, Canada*
[6] *Physik-Department E21, Technische Universität München, D-85748 Garching, Germany*
[7] *Department of Chemistry, Kyoto University, Kyoto 606-8502, Japan*
[8] *Centro Brasilieiro de Pesquisas Fisicas, Rua Xavier Sigaud 150 Urca, CEP 22290-180 Rio de Janeiro, Brazil*
[9] *Department of Physics and Astronomy, University of Kentucky, Lexington, Kentucky 40506-0055, USA*
[10] *Laboratorio de Bajas Temperaturas, Centro Atomico Bariloche, 8400 San Carlos de Bariloche, Argentina*

Quantum phase transitions (QPTs) at zero temperature are generally studied by means of pressure or composition tuning. Volume integrated probes such as neutron and magnetization measurements, as well as pressure uncertainties in NMR studies using powder specimens, however, have limited the characterization of magnetism and detection of discontinuous changes at QPTs. Overcoming these limitations, we carried out muon spin relaxation measurements that have a unique sensitivity to volume fractions of magnetically ordered and paramagnetic regions, and studied QPTs from itinerant helimagnet or ferromagnet to paramagnet transitions in MnSi (single crystal; varying pressure) and $(Sr_{1-x}Ca_x)RuO_3$ (ceramic specimens; varying x) [1]. Our results provide evidence that both cases are associated with phase separation and suppression of dynamic critical behaviour, reveal slow dynamics of the partial order diffuse spin correlations in MnSi above the critical pressure and suggest the possibility that a majority of QPTs in correlated electron systems involve first-order transitions and/or phase separation.

References

[1] Y. J. Uemura, T. Goko, I. M. Gat-Malureanu, J. P. Carlo, P. L. Russo, A. T. Savici, A. Aczel, G. J. MacDougall, J. Rodoriguez, G. M. Luke, S. R. Dunsiger, A. McCollam, J. Arai, Ch. Pfleiderer, P. Böni, K. Yoshimura, E. Baggio-Saitovitch, M. B. Fontes, J. Larrea, Y. V. Sushko, and J. Sereni. Phase separation and suppression of critical dynamics at quantum transitions of itinerant magnets: MnSi and $(Sr_{1-x}Ca_x)RuO_3$. *Nature Physics*, 3:34, 2007.

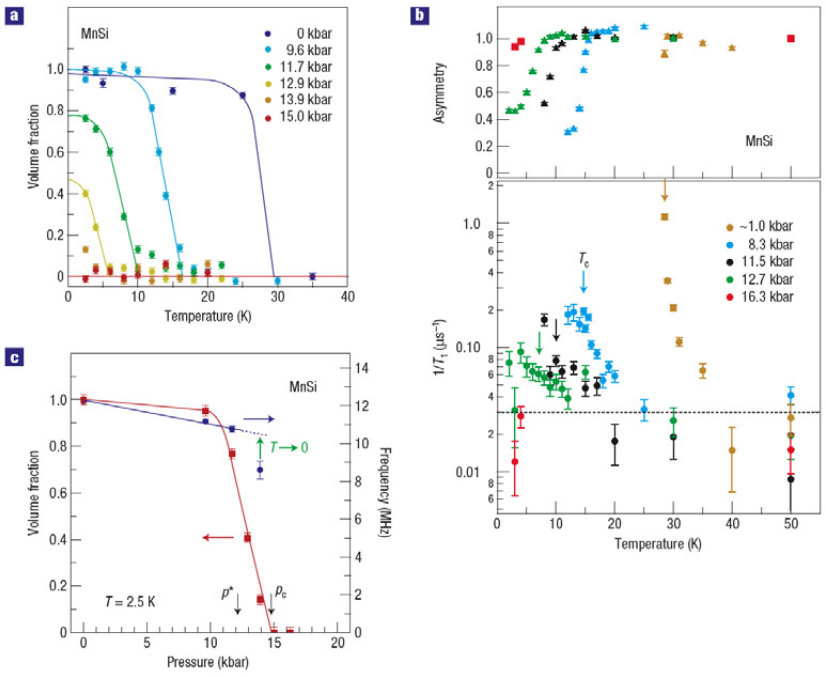

Figure 1: μSR results on the volume fraction, relaxation rate and spin precession frequency in MnSi. (a) Temperature and pressure dependences of the volume fraction, V_f, with static magnetic order determined in transverse field of 100 G. V_f remains finite at $T \to 0$ for pressure p between 11.7 and 13.9 kbar, indicating phase separation between magnetically ordered and paramagnetic volumes. (b) The muon spin relaxation rate $1/T_1$ and the relative magnitude of the corresponding muon asymmetry in MnSi in an longitudinal field of 200 G. Divergent critical behaviour of $1/T_1$, seen at $p \sim 1$ kbar, is gradually suppressed with increasing pressure. No anomaly of $1/T_1$ is seen at T_c (indicated by arrows) at $p = 12.7$ kbar ($p^* < p < p_c$). At $p = 16.3$ kbar, $1/T_1$ becomes smaller than the technical limit of detection, indicated by the dashed line. (c) Pressure dependence of V_f and the zero-field muon spin precession frequency at $T = 2.5$ K. The finite frequency near p_c indicates a first-order phase transition. The frequency at $p = 13.9$ kbar at $T = 2.5\,\mathrm{K} \sim 0.5T_c$ is expected to increase for $T \to 0$ as illustrated by the green arrow.

1.5 Study of magnetically induced variations in phonon frequencies in Ni

Severian N. Gvasaliya [1], **Klaudia Hradil** [3, 2], **Peter Böni** [4], **Bertrand Roessli** [1]
[1] *Laboratory for Neutron Scattering ETH & PSI, CH-5232 Villigen PSI, Switzerland*
[2] *ZWE FRM-II, Technical University Munich, D-85747 Garching, Germany*
[3] *IPC Universität Göttingen, Institut für Physikalische Chemie, D-37077 Göttingen, Germany*
[4] *Physics Department E21, Technical University Munich, D-85747 Garching, Germany*

The fundamental physics of the magnetism in metals has not been satisfactorily understood and continues to be an active field of research both theoretically and experimentally. Despite this activity the mutual influence of the magnetism and lattice dynamics is rarely taken into account [1]. Rather recently Raman scattering studies of the thin films of the metallic oxide $SrRuO_3$ revealed an anomalous softening of the optic phonons and it turned out that the damping of these phonons was strongly affected by the ferromagnetic transition [2]. The origin of these anomalies was ascribed to the reorganization of the electronic band structure, but no quantitative analysis was made, partially due to the complexity of the problem.

J.-H. Lee *et al.* performed a systematic first-principle study of the phonon dispersion of FCC Ni as a function of its magnetic moment [1]. The main qualitative result of Ref. [1] is that due to the interplay between the electronic screening and the magnetostriction the phonon frequencies of Ni show a noticeable change as the magnetic moment of Ni varies. The following features of the dispersion are expected according to Ref. [1]. First, the changes exhibit a strong q-dependence. Second, the calculated values of the relative change of the phonon frequencies may be as large as ~ 30 cm^{-1} (~ 4 meV). Finally, the phonon frequency changes its sign at some q-s. We note that according to other first-principle studies of the phonons in Ni [3], one should not expect a noticable change in the phonon frequency due to the magnetism.

In order to check the predictions of the theory we have measured the temperature dependence of the phonon frequencies on a large (100 g) isotopically enriched single crystal of ^{58}Ni along the main high symmetry directions with emphasis on [$\xi\xi$0] and [00ξ] directions using the PUMA spectrometer at FRM II. The sample was aligned in the $< 110 > / < 001 >$ scattering plane. The spectrometer equipped with a PG monochromator and analyser was operated in the constant-final-energy mode. Most of the data were collected in the following two configurations:
PG(002) monochromator and PG(002) analyzer, k_f = 2.662 Å and open-24′-sample-45′-60′ collimations
PG(004) monochromator and PG(002) analyzer, k_f = 4.1 Å and open-24′-sample-45′-60′ collimations
These two configurations gave us desirable focusing for the phonons under interest.

We have collected the data along main high symmetry directions of the FCC lattice of Ni. Fig. 1 shows an example of the phonon dispersions with $\mathbf{q} \parallel$ [$\xi\xi$0] obtained at room temperature. Our results in this and other $\mathbf{q}$-directions are in agreement with earlier reports [4, 5]. Fig. 2 shows a phonon lineshape taken at $\mathbf{Q} = (0.4\ 0.4\ 2)$ at $T = 298$ K, $T = 580$ K, and $T = 645$ K $> T_C \sim 630$ K. One can see that the higher the temperature the lower the phonon peak position. Also, the phonon is broader at higher temperatures. These facts are in agreement with published results [5] and do not support the first-principles study [1]. A very surprsing feature is a constant integrated intensity of the phonon in the temperature range 298 K – 645 K, as according to the Bose factor the intensity should be higher by $\sim 60\%$.

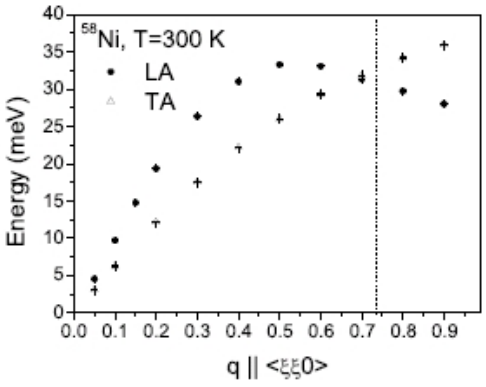

Figure 1: Dispersion of the phonons in ^{58}Ni at $T = 300$ K along the [$\xi\xi$0]- direction. The results are in agreement with earlier measurements Refs. [4, 5] using natural Ni composition. The dotted vertical line shows the Brillouin zone boundary in the $\xi\xi$0-direction.

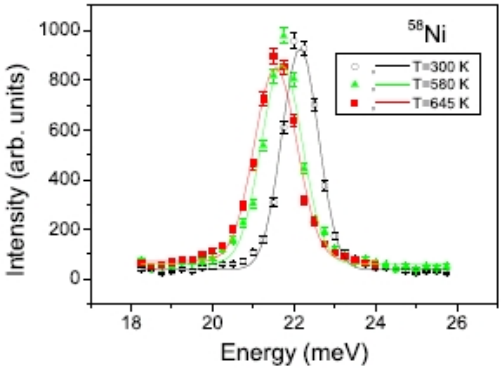

Figure 2: T-evolution of the TA phonon lineshape measured at $\mathbf{Q} = (0.40.42)$. Symbols denote the data. The lines indicate fits to Gaussian functions.

The conclusions are a need to investigate (i) the phonons of Ni in the $< 100 > / < 010 >$ scattering plane in order to further check the predictions of [1] and (ii) the issue of the phonon intensity.

References

[1] J. H. Lee, Y.-C. Hsue, and A. J. Freeman. *Phys. Rev. B*, 73:172405, 2006.
[2] D. Kirillov, Y. Suzuki, L. Antognazza, K. Char, I. Bozovic, and T.H. Geballe. *Phys. Rev. B*, 51:12825, 1995.
[3] A. dal Corso and S. de Gironcoli. *Phys. Rev. B*, 62:273, 2000.
[4] R. J. Birgeneau, J. Cordes, G. Dolling, and A. D. B. Woods. *Phys. Rev.*, 136:A1359, 1964.
[5] G. A. de Witt and B. N. Brockhouse. *J. Appl. Phys.*, 39:451, 1968.

1.6 Symmetry breaking vortex lattice structures in pure Niobium

Sebastian Mühlbauer [1], **Peter Böni** [1], **Christian Pfleiderer** [1], **Robert Georgii** [2], **E. M. Forgan** [3], **M. Laver** [3], **A. Wiedenmann** [4]

[1] *Physik-Department E21, Technische Universität München, D-85748 Garching, Germany*
[2] *ZWE FRM-II, Technische Universität München, D-85748 Garching, Germany*
[3] *School of Physics and Astronomy, Condensed Matter Group, Birmingham UK*
[4] *Hahn-Meitner-Insitut, D-14109 Berlin, Germany*

Small angle neutron scattering (SANS) directly maps the vortex lattice (VL) of a type II superconductor, revealing both individual sample properties as e.g., pinning potentials and purity - but also reflecting the symmetry of the underlying Fermi-surface as well as the symmetry of the superconducting wavefunction ψ. Especially in high-T_c and heavy-fermion superconductors, the symmetry of ψ and the pairing mechanism are of great interest, being so called unconventional nature. As the symmetry of the VL is influenced by anisotropies of the underlying Fermi-surface, non-local corrections to the free energy and ψ itself, conventional superconductors have attracted great interest as model systems, where certain parameters can be tuned with high precision.

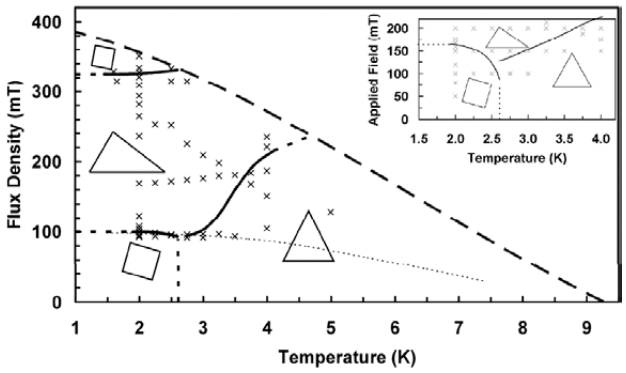

Figure 1: VL structure phase diagram of Niobium with the magnetic field applied along the four fold (100) crystal axis. Plot taken from ref. [1].

Niobium (Nb) is understood to be a classical type II superconductor. The morphology of the VL in Nb with the magnetic field applied parallel to the four-fold (100) crystal axis is characterized by a rich VL phase diagram, consisting of a high field square phase, separated by an intermediate scalene VL phase from a low field square phase in the low T regime as shown in [1]. All VL phases break crystal symmetry, being not aligned with the crystal axes [1]. The fundamental origin of this symmetry breaking transition is not understood. While in general the appearance of a low field square phase may be described by Fermi velocity anisotropy and the high field square phase by non-local corrections to the superconducting gap function [2] little is known about the triangular VL phases.

We have carried out SANS experiments on V4 (HMI) on ultra-pure Nb single crystals, characterized by a residual resistivity ratio around 10000. The samples had specially treated surfaces and showed neither bulk nor surface pinning.

In our studies we observed for the first time a complete field exclusion in the Meissner-phase independent of the path chosen in the phase diagram even close to T_c at 8.8 K. This therefore gives the unique possibility to study the morphology of an undisturbed bulk VL in a well defined way without essentially surface or pinning effects. The experiments showed that the symmetry breaking transition vanishes in the high field square, intermediate scalene phase and isosceles phase if the magnetic field is rotated approximately 17° away from the (100) axis in a (110) plane, as shown in Fig. 1. As magnetoresistance measurements of similar samples show characteristic features at similar angles [3], the origin of the symmetry breaking transition is supposed to be related to the topology of the Fermi surface. Further experiments on Nb are in progress to complete the understanding of the interplay of Fermi topology and VL symmetry.

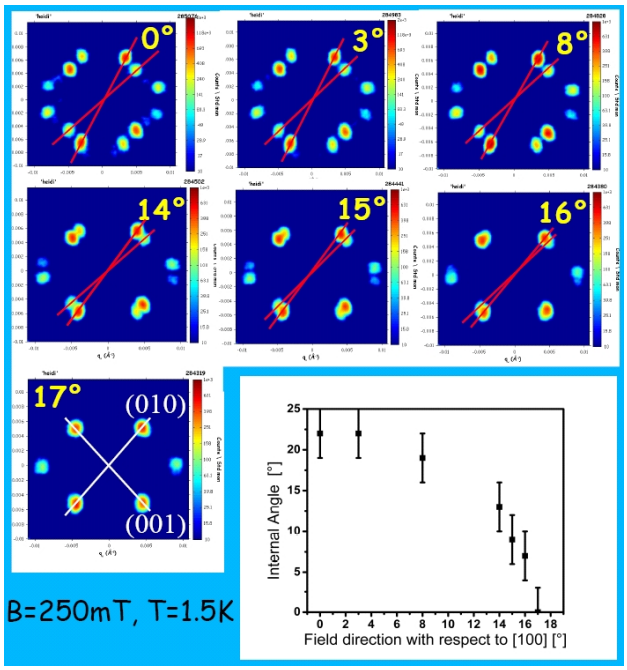

Figure 2: VL scattering pattern showing the evolution of two degenerate scalene VL domains, each rotated 11° off the (010) direction. The yellow number gives the orientation of the magnetic field B with respect to the (100) crystal direction in a (110) plane. B=250 mT, T= 2K. The symmetry breaking of the VL vanishes, as the magnetic field is rotated by 17°. The (010) and (001) axes The inset shows the evolution of the internal angle, separating the two scalene VL domains as a function of magnetic field direction.

References

[1] M. Laver et al. Spontaneous symmetry breaking vortex lattice transitions in pure niobium. *Phys. Rev. Lett*, 96:167002, 2006.
[2] N. Nakai et al. *Phys. Rev. Lett.*, 89:237004, 2002.
[3] Fawcett et al. *Phys. Rev.*, 159:553, 1967.

1.7 Magnetic Moment in Epitaxially Grown EuO Films

Sebastian Mühlbauer [1, 2], **Peter Böni** [1], **Robert Georgii** [2], **D. G. Schlom** [3], **A. Schmehl** [3], **J. Mannhart** [4]

[1] *Physik-Department E21, Technische Universität München, D-85748 Garching, Germany*
[2] *ZWE FRM-II, Technische Universität München, D-85748 Garching, Germany*
[3] *Department of Materials Science and Engineering, Pennsylvania State University, Pennsylvania, USA*
[4] *Experimentalphysik VI, Elektronische Korrelationen und Magnetismus, Institut für Physik, Universität Augsburg*

Ferromagnetic EuO exhibits a metal-insulator transition showing a very large colossal magneto-resistance. Recently, it became possible to grow epitaxial films of semiconducting EuO_{1-x} on Si with spin polarization above 90 percent [1]. The direct integration of EuO with Si will allow the fabrication of model systems for studying devices in the field of spintronics. In order to determine non-destructively the magnetic properties of thin films of EuO on Si, we have measured the critical angle of reflection by using polarized neutrons. The results confirm that the magnetic moment in the films, $\mu_{sat} = 6.6\mu_B$, is consistent with the bulk value of EuO. he reflectivity measurements were performed on the beam line for very cold neutrons MIRA at the FRM II [2]. A magnetic field was applied parallel to the incident neutron beam with a wavelength $\lambda = 9.7 \pm 0.05$ Å and parallel to the surface of the EuO film (Fig. 1). As the magnetic field is also guiding the neutron polarization, $\mathbf{P}$ is parallel or antiparallel to the sample and perpendicular to $\mathbf{Q}$.

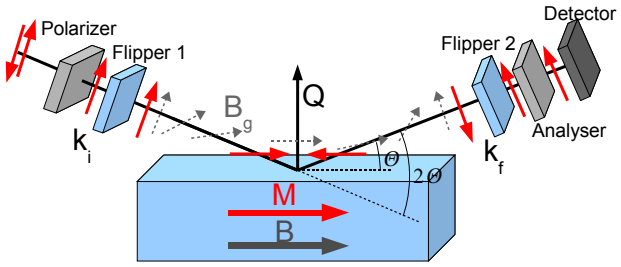

Figure 1: Schematics of the polarized neutron reflectometer MIRA. The incoming neutrons $\mathbf{k}_i$ are elastically reflected by the sample. $\mathbf{Q}$ designates the momentum transfer. The polarization of the neutron beam is selected by means of spin flippers before and after the sample. The polarization of the neutrons follows adiabatically along the direction of the guide field $\mathbf{B}_g$. This setup allows the measurement of the four cross-sections I_{++}, I_{--}, I_{-+} and I_{+-}.

The amplitude of the magnetic moments can be determined by two means: i) either by conducting measurements up to reasonably large q and fitting the data with a model that includes the EuO film and the Si substrate or by ii) determining the angle of total reflection that is given by

$$\Theta_c = \lambda\sqrt{(\rho/\pi)(b_{nuc} \pm b_{mag})},$$

which can be converted to a momentum transfer q_c characterizing the drop of the intensity on a q-scale. Here, ρ designates the density of the nuclei, b_{nuc} the nuclear scattering length, and b_{mag} the magnetic scattering length given by $b_{mag} = (\gamma r_0/2)gS$. For convenience we have chosen method ii).

Figs. 2 and 3 show typical reflectivity profiles of the EuO sample recorded at various temperatures in a field $B_g = 125$ Oe. The direct beam is visible around 0^0. Due to footprint effects, the plateau of total reflection for I_{++} and I_{--} is reached at the lowest temperatures at roughly 0.011 $Å^{-1}$.

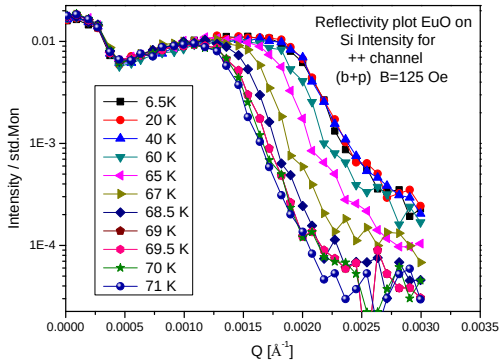

Figure 2: Reflectivity profile of EuO on Si (001) for temperatures 6 K $< T <$ 71 K, $H = 125$ Oe, I_{++}.

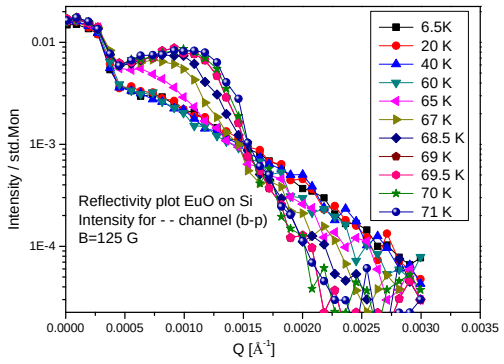

Figure 3: Reflectivity profile of EuO on Si (001) for 6 K $< T <$ 71 K, $H = 125$ Oe, I_{--}.

The merging of the critical angles for $T = T_C = 69$ K indicates the vanishing of the ferromagnetism, i.e. the Curie temperature T_C agrees with the value from bulk samples. With $\gamma r_0/2 = 0.2695 \cdot 10^{-12}$ cm a magnetic moment $\mu_{sat} = 6.6 \pm 0.7\mu_B$ is obtained also in excellent agreement with the bulk value. In addition, the results show that the change of magnetization is caused by a repopulation of domains and not by domain rotation. These results demonstrate the high potential of EuO as spin emitters for spintronic devices [1].

References

[1] A. Schmehl, V. Vaithyanathan, A. Herrnberger, S. Thiel, C. Richter, M. Liberati, T. Heeg, M. Röckerath, L. F. Kourkoutis, S. Mühlbauer, P. Böni, D. A. Muller, Y. Barash, J. Schubert, Y. Idzerda, J. Mannhart, and D. Schlom. *Nature Materials*, 6:882, 2007.

[2] S. Mühlbauer, P. Böni, R. Georgii, D. G. Schlom A. Schmehl, and J. Mannhart. *J. Phys.: Condens. Matter*, 2008. in print.

2

Large Scale Structures

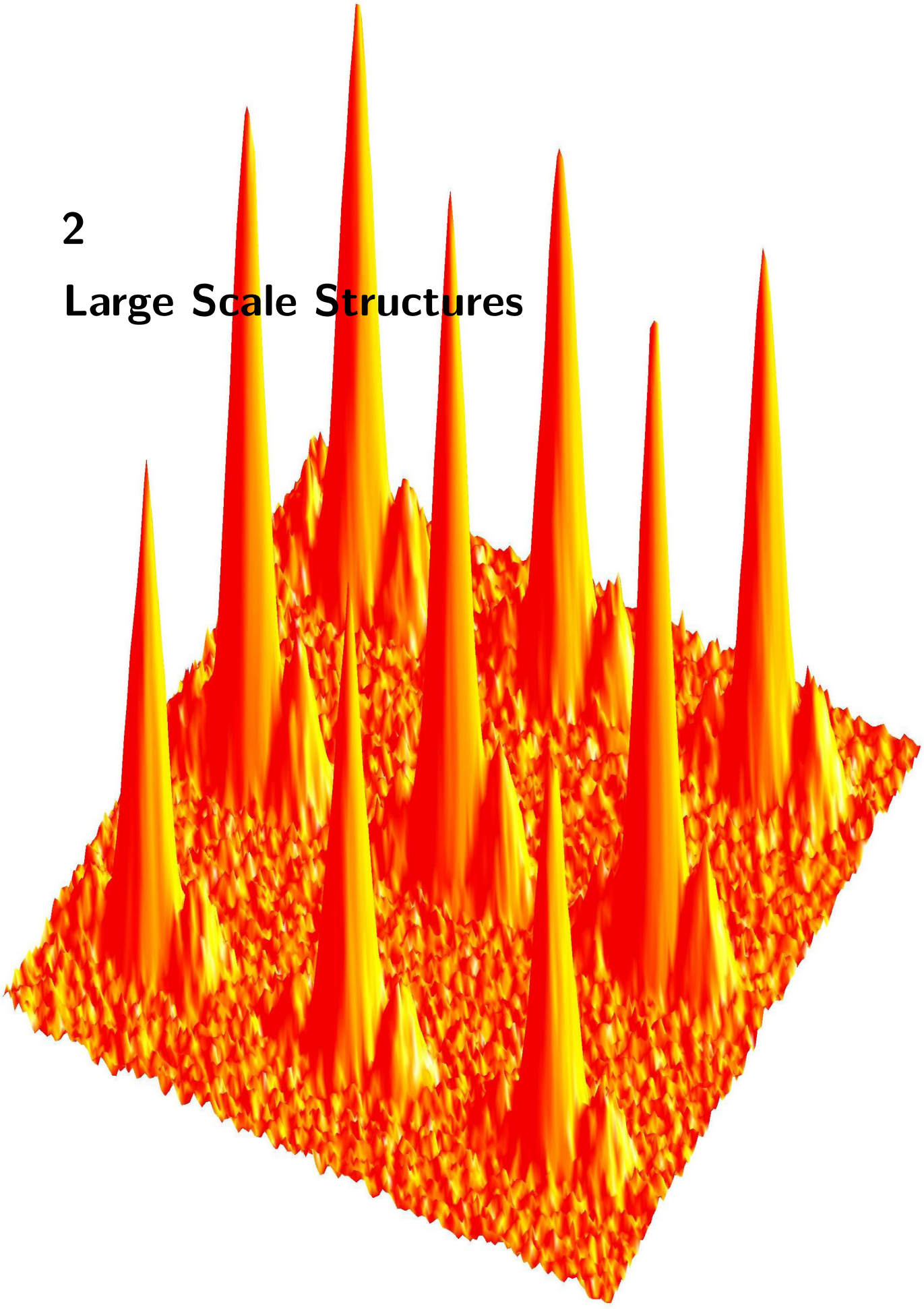

2.1 SANS measurements with polarization analysis on protein solutions

Ana Gaspar [1, 2], **Marie-Sousai Appavou** [1], **Sebastian Busch** [1], **Wolfgang Doster** [1], **Robert Georgii** [2, 3], **Wolfgang Häussler** [2, 3], **Sergey Masalovich** [2]

[1] *Physik-Department E13, Technische Universität München, D-85748 Garching, Germany*
[2] *ZWE FRM-II, Technische Universität München, D-85748 Garching, Germany*
[3] *Physik-Department E21, Technische Universität München, D-85748 Garching, Germany*

The intention of these investigations was to obtain quantitative information on the fraction of coherent to spin-incoherent nuclear scattering from a representative set of protein samples. Such a method had so far limited application in the study of amorphous materials, despite of its potential. Its use in spectroscopic measurements would allow experimentally separating the self and the collective terms of the dynamic structure factor, while in a diffractometer it would also allow obtaining structure factors uncontaminated by incoherent scattering from the non-exchangeable hydrogens of the proteins. In this experiment the method was first tested at MIRA in measurements of the static structure factors of different protein samples investigated before by us at the time-of-flight instrument TOFTOF.

A π-spin flipper (of efficiency determined to be $\approx$1) was introduced before the sample to reverse the polarization of the incident neutron beam for spin-flip and non-spin-flip measurements. After the sample a super mirror analyzer, diverting the neutrons with the right polarization into a finger detector (^{3}He gas filled) of 2.54 cm circular section was used. The total neutron transmission through the analyzer was determined to be $\approx$ 40%, with a flipping ratio of $R \approx 11.5$ (effective polarization 84%).

The experiment performed relied on the principle that if we can polarize the incident beam and we can count separately neutrons scattered with and without spin-flip with regards to the incident beam polarization, we can then separate coherent from spin-incoherent nuclear scattering processes. This is because only $1/3$ of the spin-incoherent events are without spin-flip (the other $2/3$ being with spin flip), while all the coherent nuclear scattering events correspond to scattering without spin flip. Hence from $I_{NSF} = I_{coh} + 1/3I_{inc}$ and $I_{SF} = 2/3I_{inc}$ one directly obtains $I_{coh} = I_{NSF} - 1/2I_{SF}$ and $I_{inc} = 3/2I_{SF}$. In practice, the scattered intensities have to be corrected for the finite flipping ratio R. Figure 1 illustrates how this separation was successfully achieved at MIRA for several D2O protein solutions and Figure 2 displays the fraction of coherent and spin-incoherent scattering events determined from the data.

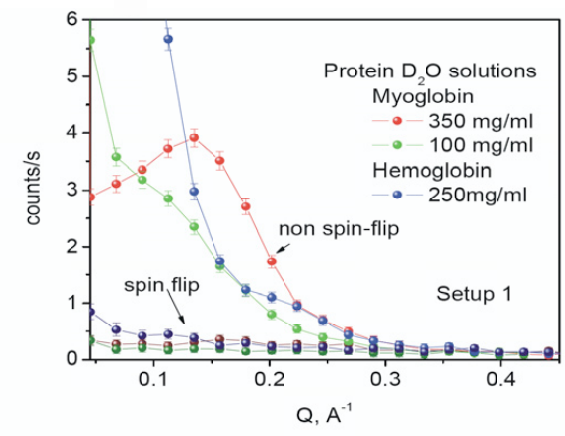

Figure 1: Corrected spin and non spin-flip scattering

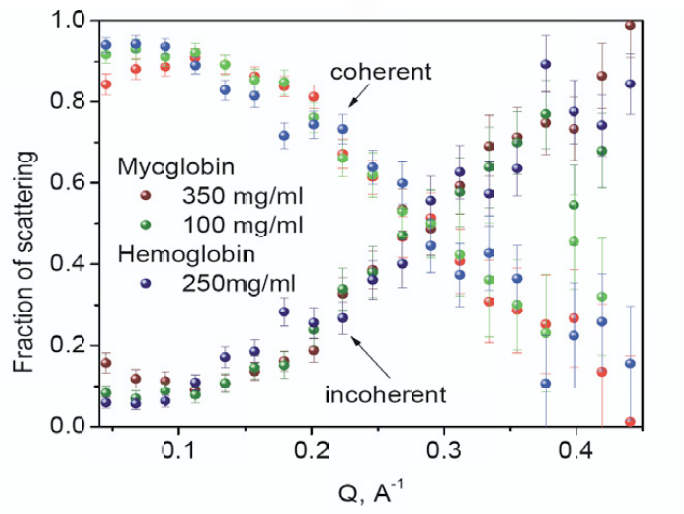

Figure 2: Coherent and inhoherent scattering from different protein solutions.

2.2 Neutron reflectivity study of water-uptake in biocompatible hydrogel films

Ali Ezzeldin Metwalli [1], **Robert Georgii** [2, 3], **Peter Müller-Buschbaum** [1]
[1] *Physik-Department E13, Technische Universität München, D-85748 Garching, Germany*
[2] *ZWE FRM-II, Technische Universität München, D-85748 Garching, Germany*
[3] *Physik-Department E21, Technische Universität München, D-85748 Garching, Germany*

Hydrogel films are used for immobilization of proteins for microarray applications. The protein microarray is a crucial biomaterial for the rapid and high-throughput assay of many biological events where proteins are involved. The hydrated, porous nature of the hydrogel coatings can mimic the conditions found in vivo and can ideally ensure that the adsorbed proteins remains hydrated, functional and properly folded. Aldehyde or amino functional polyethylene glycol is currently used for this application. Since the hydration layer is very important, the film is typically immersed in buffer solution prior to protein immobilization to ensure high water content.

Here the water-uptake of the hydrogel film was investigated as function of time. Silicon wafers were ultrasonically cleaned in dicholormethane, rinsed in DI water, and immersed in the cleaning bath containing a mixture of NH_3, H_2O_2 and H_2O for 2 h at 75^{o}C. The cleaned substrates are further rinsed in DI water and finally spin dried. Deuterated polyethylene glycol (dPEG) with a molecular weight $M_n = 40$ k was dissolved in D_2O and applied to the cleaned silicon wafer via spin coating method. As-prepared films were mounted in a home-made vapour chamber and were investigated with NR at the MIRA instrument at wavelength of 9.83 $\AA$. The q_z range from 0.004 $\AA^{-1}$ to 0.12 $\AA^{-1}$ was probed with high resolution (motor steps of $D_q = 0.01^o$). Neutron reflectivity of the dry film was first measured and the swelling experiments were performed by inserting D_2O vapor in the chamber. The temperature of the chamber was kept constant at 30^{o}C using a water thermostat. A full NR curve was collected every 12 hrs in presence of D_2O vapor. A cycling swelling/deswelling experiment was also performed on hydrogel film by exposure to D_2O vapor at room temperature for 12 h followed by opening the chamber to air for 12 h. Additional samples were pre-heated at different temperatures viz. 20^{o}C, 30^{o}C and 70^{o}C in vacuum oven and the NRs were collected for these dry films. Figure 1 shows the neutron reflectivity data for the studied samples. The scattering length density of our dPEG film is 7.05 x $10^{-6}\AA^{-2}$, and the critical edge (q_c) is expected to shifts towards lower q_z values as D_2O 6.36 x $10^{-6}\AA^{-2}$ is incorporated into the swollen film. In Figure 1a, the critical edge shifts to lower q values from dry to hydrated film after 12 hour of exposure to D_2O vapor. The hydrated gel film shows an equilibrium state as observed from unchanged reflectivity with increasing swelling time to 24 and 36 h. From Figure 1b, the film shows a kinetic behavior as the critical edge responds to the film environment (D_2O vapor and air). The swelling/deswelling behavior indicates that the hydrogel films are very sensitive to humidity and the observed high inconsistencies in the microarray results can be avoid if the humidity is well controlled during the microarray experiment. In the last set of experiments, the as-prepared films are dried using vacuum oven prior to the NR measurements in air. Preliminary data analyses were performed using Parratt32 as well as Motofit and indicate that the shrinkage of the film thickness from 112 nm (as-prepared film) to 71 nm may reveal a possible collapse of the porous hydrated film upon heating.

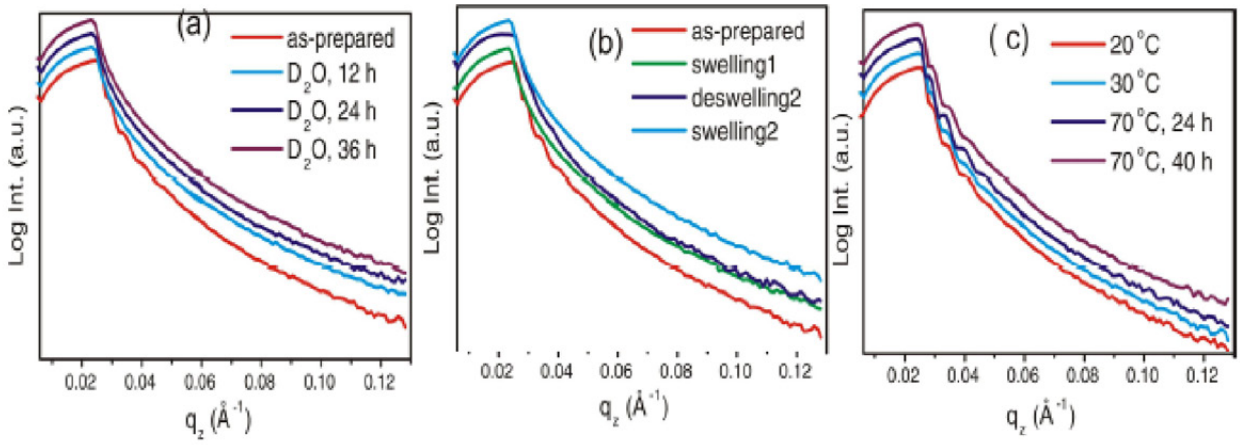

Figure 1: Neutron reflectivity data of deuterated polyethylene glycol (dPEG) films on precleaned silicon surfaces. (a) Dry versus hydrated films for different time periods; in situ experiment, (b) swelling and deswelling effect on the hydrogel film, (c) temperature effect on the hydrogel film structure. The critical edge (q_c) shifts towards lower q values as the dPEG film swells in D_2O vapor. Hydrated films have weak fringes compared with the asprepared and dry ones.

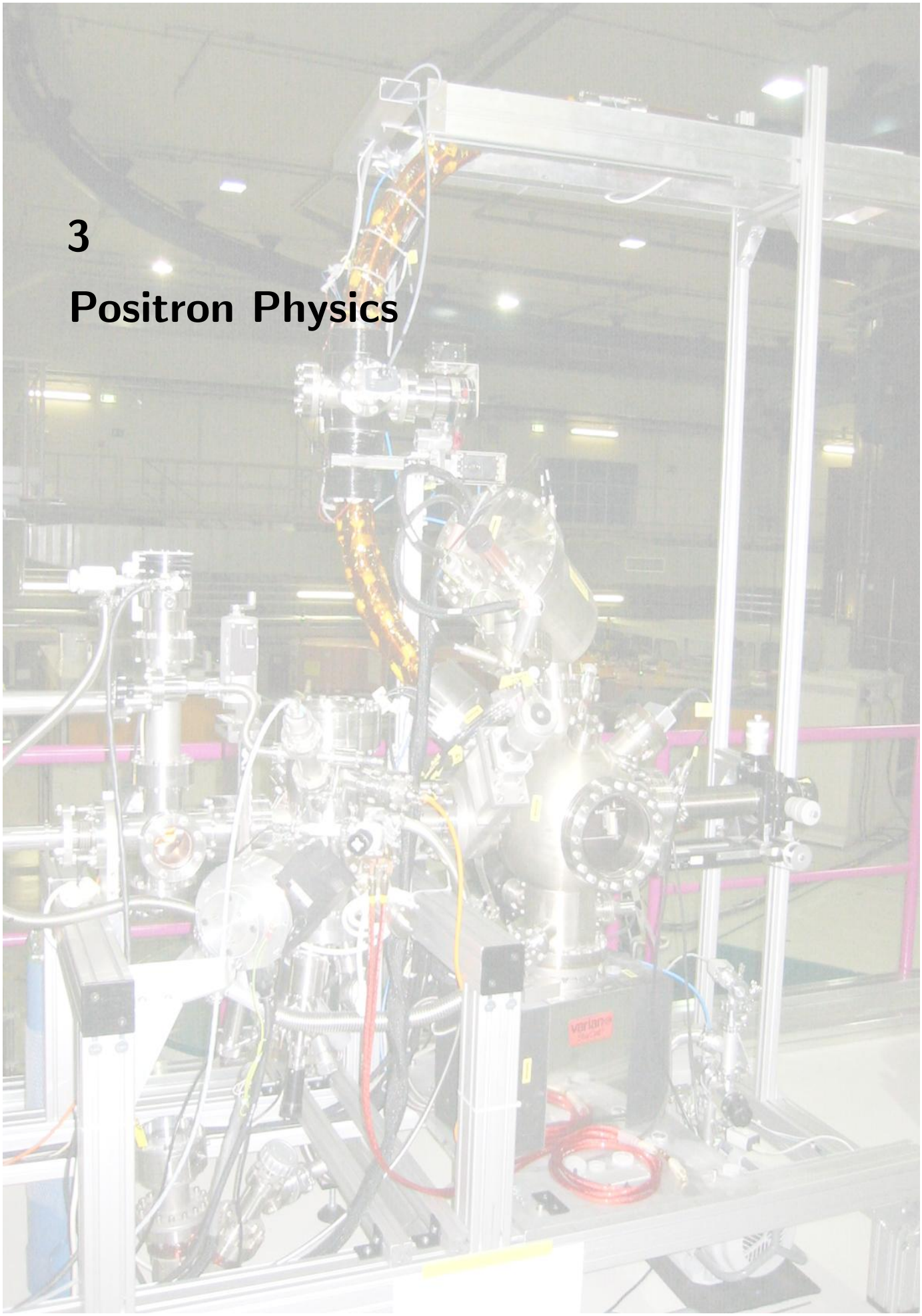

3

Positron Physics

3.1 Investigation of embedded submono-layers in Al using positron annihilation

Christoph Hugenschmidt [1, 2], **Philip Pikart** [1, 2], **Martin Stadlbauer** [1, 2], **Klaus Schreckenbach** [1, 2]

[1] *Physik-Department E21, Technische Universität München, D-85748 Garching, Germany*
[2] *ZWE FRM-II, Technische Universität München, D-85748 Garching, Germany*

In the presented work we demonstrate that metal layers in the sub-monolayer range embedded in a matrix are revealed with unprecedented sensitivity by coincident Doppler-broadening spectroscopy (CDBS) of the positron annihilation using a mono-energetic positron beam. Besides the application of a non-destructive technique, one aim has been to reveal the elemental signature of Sn of various thickness in the CDB-spectra in order to investigate the positron trapping properties of the embedded Sn layer.

A set of four layered samples was prepared in an UHV-chamber: Pure Al was evaporated onto water-cooled glass substrates ($\geq$ 99.99%, thickness of 5.5 $\pm$ 0.3 μm). Afterwards, the Sn layer ($\geq$ 99.999%) of various thickness d_{Sn} (d_{Sn} = 0.10 $\pm$ 0.03 nm, 1.60 $\pm$ 0.1 nm, 25 $\pm$ 1 nm, and 200$\pm$8 nm) was evaporated on top of the Al, which was finally by 200$\pm$8 nm Al. Annealed Al and annealed Sn serve as reference materials. We performed calculations of the Makhovian implantation profile (before diffusion) of the layered samples in order to maximize the overlap of the positron distribution with the Sn layer by variation of the kinetic energy of the positrons. As a result of these calculations the kinetic energy was set to 6 keV for the three samples with a Sn-thickness of 0.10 nm, 1.6 nm, and 25 nm, respectively, and to 15 keV for the others.

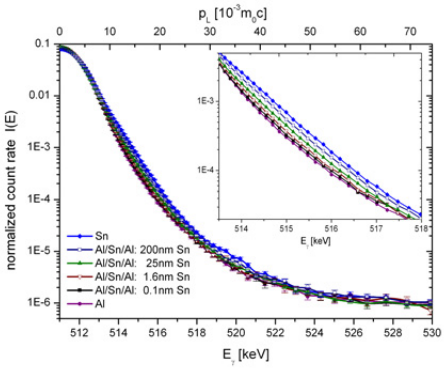

Figure 1: CDBS of the 511 keV annihilation line for pure Al, Sn, and the Al/Sn/Al layered samples.(normalized to same intensity).

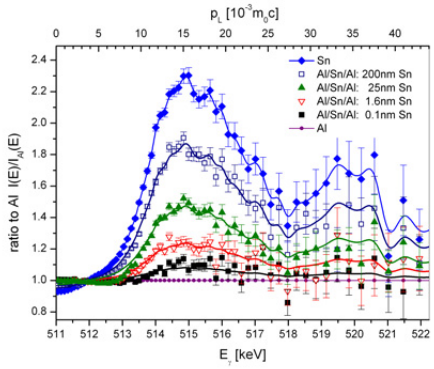

Figure 2: Ratio curves of the photon intensities: All spectra (see fig. 1) are divided by the Al reference spectrum. The uppermost curve shows the elemental signature of Sn. (Details see text.)

The measurements were carried out with the CDB-spectrometer [1] located at the high intensity positron source NEPOMUC – NEutron induced POsitron source MUniCh [2]. The raw data of the CDB-spectra are normalized to the same integrated intensity of the 511 keV photo-peak (figure 1). Note the low background leading to a peak-to-background ratio of better than 10^5. For a more detailed view, all spectra have been divided by the spectrum obtained for pure annealed Al in order to reveal the element specific contribution of Sn (figure 2). The solid lines represent least-square fits of a linear combination of the photon intensities recorded for pure Sn and pure Al with only one free fit parameter, which corresponds to the amount of positrons annihilating in the Sn layer.

The higher photon intensity for larger electron momenta with increasing amounts of Sn is attributed to the higher binding energy of the annihilating core electrons in Sn. Even at an amount of 0.1 nm Sn below the 200 nm Al coating, the photon intensity increases significantly for $10 \cdot 10^{-3} m_0 c < p_L < 25 \cdot 10^{-3} m_0 c$. The strongly disproportional increase of the positron annihilation rate with core electrons from Sn is interpreted as follows: After implantation, thermalized positrons diffuse to the Al/Sn-interface, where they are efficiently trapped in open-volume defects and hence could annihilate with localized core electrons of Sn atoms. The number of those defects are expected to be particularly large due to the lattice mismatch at the Al/Sn-interface. On the other hand, the smaller core annihilation probability for positrons trapped in open volume defects would lead to a lower photon intensity in the high electron momentum range than annihilation in the unperturbed Sn lattice. It is hence unlikely that defect trapping is solely responsible for the large enhancement of the Sn signature. The main reason for the observed high annihilation rate in the Sn layer can be understood in terms of the element specific positron affinity: Due to the much stronger positron affinity of Sn compared to that for Al, the Sn layer can be regarded as a well with a potential depth of $\sim$ 3.2 eV. Therefore, positrons thermalized inside the Sn layer are repelled at the Sn/Al interface during their diffusion, and a certain amount of those thermalized in Al diffuse to the Sn layer where they are efficiently trapped inside the Sn layer or Sn clusters.

With this experiment we demonstrated that CDBS with mono-energetic positrons is clearly a very powerful technique for the investigation of thin layered structures that are hidden below coatings of hundreds of atomic layers. We envisage to investigate layers of various elements embedded in a matrix by CDBS as a function of positron implantation energy not only to reveal the elemental information of the embedded layer but also to determine its depth below the coating.

References

[1] M. Stadlbauer, C. Hugenschmidt, B. Strasser, and K. Schreckenbach. *Appl. Surf. Sci.*, 252:3269–3273, 2006.

[2] C. Hugenschmidt, K. Schreckenbach, M. Stadlbauer, and B. Strasser. *Nucl. Instr. Meth. A*, 554:384–391, 2005.

3.2 Investigation of AZ31 and ion irradiated Mg with the coincident Doppler broadening spectrometer CDBS

Martin Stadlbauer [1, 2], **Christoph Hugenschmidt** [1, 2], **Klaus Schreckenbach** [1, 2]
[1] *Physik-Department E21, Technische Universität München, D-85748 Garching, Germany*
[2] *ZWE FRM-II, Technische Universität München, D-85748 Garching, Germany*

We have investigated defects and their chemical surrounding in Mg and the Mg-alloy AZ31 with Doppler broadening spectroscopy of the positron annihilation radiation. In these Doppler spectra the chemical information and the defect contribution have to be thoroughly separated. For this reason samples of annealed Mg were irradiated with Mg-ions in order to create exclusively defects. In addition Al- and Zn-ion irradiation on Mg-samples was performed in order to create samples with defects and impurity atoms. The ion irradiated area on the samples was investigated with laterally and depth resolved positron Doppler broadening spectroscopy (DBS) and compared with preceding SRIM-simulations of the vacancy distribution. The investigation of the chemical vicinity of crystal defects in AZ31 was performed with coincident Doppler broadening spectroscopy (CDBS) by comparing Mg-ion irradiated AZ31 with Mg-ion irradiated Mg.

Samples of pure Mg and AZ31 have been used for the investigations. Pieces with $20 \times 20 \times 3\,\mathrm{mm}^3$ were produced which fit into the CDB-spectrometer at NEPOMUC. Every sample has been polished and subsequently annealed in a CO_2-atmosphere for 1 h before the ion irradiation. The temperature was set to 693 K for the Mg-samples, whereas the AZ31-samples were annealed at 653 K. For temperatures higher than 400 K even defect clusters are completely removed in Mg [1]. The ion irradiation was performed at the 3 MeV-Tandetron in Rossendorf, where a maximum mean implantation depth for Zn-ions into Mg of 2.3 μm was achievable. In order to obtain the same ion distribution for the Mg- and Al-ions, the respective energy of the ion beam was set to 1.4 and 1.6 MeV respectively. The diameter of the ion beam was reduced to 5 mm in order to facilitate spatially resolved scans with the positron beam with a resolution of 2 mm [2].

Measurements of the S-parameter, which quantifies the width of the annihilation line, as a function of the positron energy in the irradiated area as well as in the untreated region were performed. As an example for all samples, figure 1 compares the untreated with the Zn-ion irradiated region of the Mg-sample irradiated with Zn-ions at $3 \cdot 10^{14}\,\mathrm{cm}^{-2}$ ion dose [3]. The S-parameter differs at the sample surface (between 1 and roughly 4 keV) and for larger positron penetration depths (between 9 and 29 keV). This is ascribed to defects which have been created during the irradiation procedure. Since the defect profile stretches to the surface, the positrons are trapped and hence detained from diffusing back to the surface which reduces the rising of the S-parameter for low energies and therefore very small positron penetration depths. The difference between the two curves reaches its maximum between 13 and 21 keV, whereas for higher positron energies it starts to decrease, which is due to the shape of the vacancy distribution with a maximum defect concentration at 2.3 μm according to 17 keV positron energy.

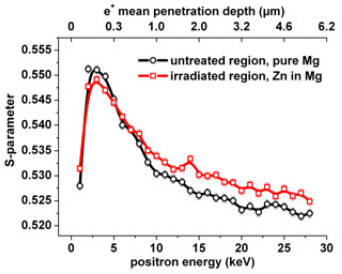

Figure 1: Energy dependent measurement of the S-parameter at a Zn-ion irradiated Mg-sample.

Figure 2 presents the three CDBS-curves of the Mg-, Al- and Zn-ion irradiated Mg-samples relative to untreated Mg ($3 \cdot 10^{14}\,\mathrm{cm}^{-2}$ dose each). All three signatures reveal a reduced contribution of high momentum electrons, as expected due to the irradiation induced defects. The signatures of the Mg/Mg- and the Al/Mg-sample are similar and the Zn/Mg-sample reveals the most distinct deviation [3].

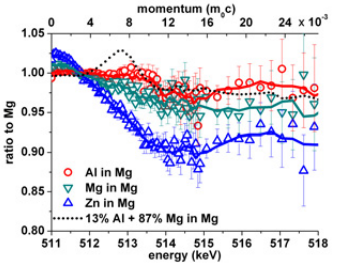

Figure 2: CDBS ratio curves of Mg-, Al- and Zn-ion irradiated Mg. The heavy Zn-ions create the most distinct deviation from annealed Mg.

Mg-ion irradiated AZ31 has been investigated with CDBS and compared to annealed Mg and also to Mg-ion irradiated Mg with the same ion dose. This normalization cancels out the contribution of defects in pure Mg in the high momentum region. No change of the high momentum part of the annihilation line could be detected due to this irradiation procedure. This behavior shows, that neither Zn- nor Al-atoms agglomerate in the vicinity of ion irradiation induced defects in AZ31. Consequently, the chemical vicinity of crystal defects produced by Mg-ion irradiation remains unchanged compared to the annealed bulk material [3].

It is planned to determine the absolute defect concentration in more detail with positron lifetime spectrometry at PLEPS [4].

References

[1] P. Erhart. In H. Ullmaier, editor, *Landolt-Börnstein - Atomic defects in metals*, volume III/25, page 274. Springer Verlag Berlin, Heidelberg, 1991.

[2] M. Stadlbauer, C. Hugenschmidt, and K. Schreckenbach. *Phys. Stat. Sol.*, 4:3489, 2007.

[3] M. Stadlbauer, C. Hugenschmidt, K. Schreckenbach, and P. Böni. *Phys. Rev. B*, 76:174104, 2007.

[4] W. Bauer-Kugelmann, P. Sperr, G. Kögel, and W. Triftshäuser. *Mat. Sci. For.*, 363-365:529, 2001.

3.3 PAES-measurements of pure Cu and Au coated Cu

Jakob Mayer [1], **Christoph Hugenschmidt** [1, 2], **Klaus Schreckenbach** [1, 2]
[1] *Physik-Department E21, Technische Universität München, D-85748 Garching, Germany*
[2] *ZWE FRM-II, Technische Universität München, D-85748 Garching, Germany*

PAES-facility at the FRM II

Positron **A**nnihilation induced **A**uger **E**lectron **S**pectroscopy is a very sensitive and non destructive method in surface physics. The main difference to conventional Auger electron spectroscopy (AES) is the ionization process. Whereas at AES the incoming particles (e.g. electrons, ions, photons) require high energies (several keV) to ionize the atoms by impact, at PAES the energy of the positrons can be chosen very low, typically 20 eV since the initial hole is produced via the annihilation of a positron with an electron. Due to the low incident energy there is no secondary electron background in the region of the Auger peaks. Furthermore most of the impinging positrons diffuse back to the surface where they are trapped in a surface state and can initiate the Auger process. This behaviour of the positrons makes PAES to a powerful technique for surface investigations, since only the topmost atomic layer is examined. The main challenge of PAES are the comparatively low positron currents of lab beams which lead to long measurement times. The high intensity positron source NEPOMUC at the FRM II enables PAES-measurements on a reasonable time scale for the first time.

Measurements and results

As a consequence of the low background the signal to noise ratio (SNR) with PAES is much higher than with conventional EAES. The SNR of a PAES-spectrum of polycrystalline copper measured at NEPOMUC was even at the first measurements better (SNR $\approx$ 1.5, open squares in fig. 1) than with EAES (SNR on the order of typically 1/2). Since one part of the unexpectedly high electron background stemmed from (n,γ)-reactions in the aluminum construction of a neutron scattering experiment nearby a lead shielding wall has been constructed (open circles in fig. 1). After the installation of the new remoderation stage the SNR has been increased to currently 4.5 (solid triangles in fig. 1).

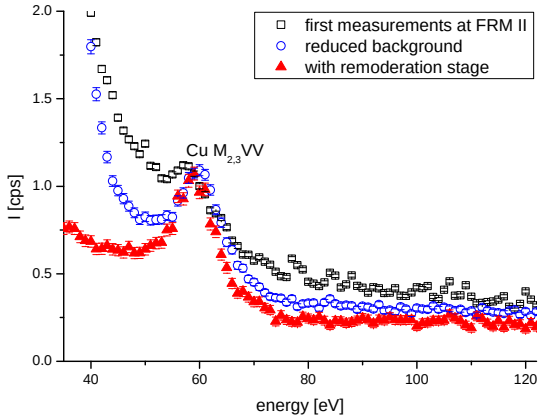

Figure 1: Enhancement of the SNR at the PAES-facility of the NEPOMUC beamline. The spectra are normalized to the Cu $M_{2,3}VV$ peak height obtained with the remoderated beam (solid triangles). For details see text.

The extreme surface sensitivity can be seen in figure 2 where the PAES-spectra of clean polycrystalline copper and copper coated with 0.5 ML (monolayer) and 5.5 ML Au are shown respectively. It is evident that the intensity of the Cu $M_{2,3}VV$ Auger-transition decreases significantly with only 0.5 ML on top of the copper. The slight increase in the region of 40 eV is consequently attributed to the Au $O_2, 3VV$ transition. The reason why the gold peak can not be clearly seen even with 5.5 ML Au is due to two points, which both show again the surface selectivity of PAES. Firstly the gold layer on the top of the copper is not stable at room temperature where the experiment has been performed and hence intermixing of gold and copper may occur. This explains also why the Cu $M_{2,3}VV$ peak is still slightly visible. Secondly the surface of the coated sample may have been contaminated with carbon. EAES-measurements confirm this assumption [1].

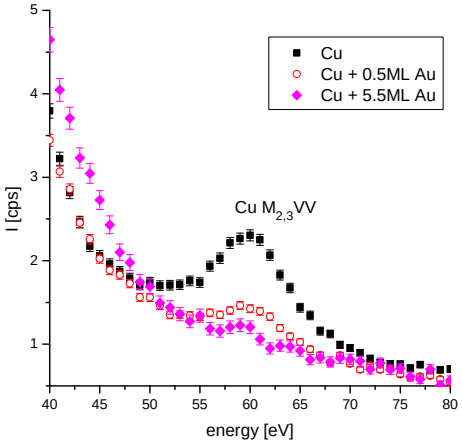

Figure 2: PAES-spectra for a clean polycrystalline Cu surface and for copper covered with 0.5 ML and 5.5 ML Au, respectively.

Outlook

The results of the measurements with the current PAES-facility show the high potential of this technique. However the long measurement times of typically 12 hours constrict the possibility for surface investigations in routine operation. The long measurement times originate first of all in the low efficiency of the actual electron energy analyzer. Thus a new state of the art electron energy analyzer has been purchased and installed at the end of this year. In the next reactor cycle it will be adjusted and first results are expected to reveal the gain in measurement time and spectrum quality.

References

[1] C. Hugenschmidt, J. Mayer, and K. Schreckenbach. Surface investigation of Si(1 0 0), Cu, Cu on Si(1 0 0), and Au on Cu with positron annihilation induced Auger-electron spectroscopy. *Surf. Sci.*, 601:2459–2466, 2007.

3.4 A new device for a pulsed positron beam at the NEPOMUC positron facility

Christian Piochacz [1, 2, 3], **Gottfried Kögel** [3], **Werner Egger** [3], **Peter Sperr** [3], **Günther Dollinger** [3]

[1] *Physik-Department E21, Technische Universität München, D-85748 Garching, Germany*
[2] *ZWE FRM-II, Technische Universität München, D-85748 Garching, Germany*
[3] *UniBw München, Institut LRT2, Werner-Heisenberg-Weg 39, D-85577 Neubiberg*

Positron annihilation is a highly sensitive method to study defects of atomic size. Both, the types and the concentrations of defects can be determined by positron lifetime measurements. To perform such measurements with micrometer spatial resolution, a pulsed positron beam is focused down to micrometer spot size in the Munich Scanning Positron Microscope (SPM). For a much higher event rate it is intended to operate this SPM at the high intense positron source NEPOMUC at the FRM II. Since the beam of NEPOMUC has a higher longitudinal energy spread than the beam used in the lab, an interface is under construction, which prepares the beam according to the demands of the last optical column of the SPM. In this interface the dc beam of NEPOMUC is pulsed with a repetition rate of 50 MHz and the energy is raised by new developed high frequency devices. More over this interface will enhance the beam brilliance [1].

To achieve both, sharp pulses and a high efficiency, the pulsing is done by two different devices. Both perform a linear energy modulation in order to accelerate positrons, which are behind the reference particle and slow down those, which pass too early. After a certain distance the faster positrons will close on the slower positrons and therefore the positrons drift together to short bunches. The devices differ in the manner the energy modulation is done. The first device is a prebunching unit, whose primary aim is not to form very sharp pulses, but to compress as many positrons as possible into a time window of some nanoseconds while the beam is disturbed as less as possible. This buncher utilize a sawtooth function with a long linear part and therefore it can compress a large amount of the incoming positrons. The following buncher uses a sine function and therefore high amplitudes could be reached due to resonant amplification. A further advantage of the sine wave is that the leading and the trailing edge can be used to achieve a small time focus. The disadvantage, that only these positrons could be compressed, which pass the buncher during the small linear parts of the sine wave, is overcome by means of the pre-buncher.

In order to measure the pulse width and the efficiency of the setup both bunching units were connected to the NEPOMUC beam facility. The sawtooth and the sine wave amplifier where triggered by the same 50 MHz Master oscillator, which was also used to derive the stop signal for the timing measurement. The start signal was obtained by the annihilation radiation from the positrons hitting a target at the end of a drift tube. The γ-Quanta were detected by a BaF-Scintillator connected to a photo multiplier tube (PMT). Two signals from two different dynods were taken. One was used in a fast circuit to get the timing information and the other one was used in a slow circuit to select only the photo peak.

The timing spectra taken with this system are shown in Figure 1 and 2. In the first the influence of the pre-buncher on the dc beam is shown. The device is able to compress nearly 50 % of the dc beam into a time window of 5 ns. The large peak in the second figure shows the bunching capability of the buncher together with the pre-buncher. The FWHM of this peak is 860 ps and on the left side already a contribution from a long positron lifetime in the target could be seen. In a 2 ns region around this peak are about 62% of the dc beam intensity collected and in a 1 ns frame there are still about 45%. The second peak in this figure shows only the sine buncher in operation, what leads to a broadened peak (1010 ps) and less intensity of about 34% respective 23%.

The successful measurements show that the pre-buncher can compress a wide range of the NEPOMUC beam to a sufficiently small pulse, which could be entirely accepted by the following sine wave buncher and focused down to a very small spot in time. Therefore another step toward the final implementation of the SPM at the NEPOMUC beam facility was done and the further assembly of the interface will be continued.

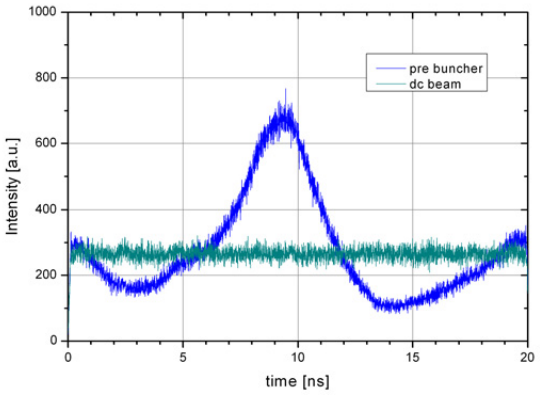

Figure 1: This time spectrum shows the influence of the prebuncher on the dc beam provided by the NEPOMUC positron beam facility. It forms a pulse, which is short enough, to be accepted by the following sine wave buncher.

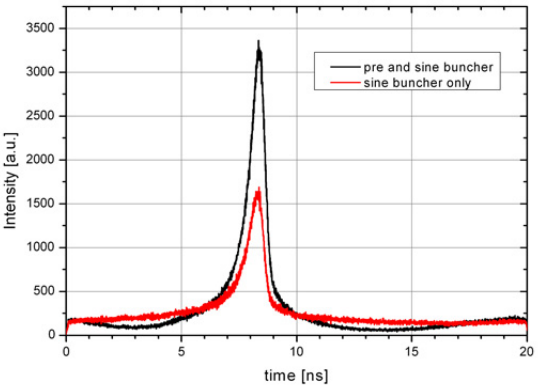

Figure 2: The higher peak shows the performance of both bunchers together. The lower curve shows the influence of the sine wave buncher alone. The pre-buncher leads to a reduced pulse width and a nearly doubled intensity.

References

[1] C. Piochacz, W. Egger, C. Hugenschmidt, G. Kögel, K. Schreckenbach, P. Sperr, and G. Dollinger. *phys. stat. sol. (c) 4*, 10:4028, 2007.

3.5 Development of a gas moderator for positrons

Benjamin Löwe [1, 2], **Klaus Schreckenbach** [1, 2], **Christoph Hugenschmidt** [1, 2]
[1] *Physik-Department E21, Technische Universität München, D-85748 Garching, Germany*
[2] *ZWE FRM-II, Technische Universität München, D-85748 Garching, Germany*

Introduction

A variety of low energy positron experiments will take advantage of a beam with a high brilliance. A highly brilliant beam implies a low divergence and a sharp energy distribution for the positrons. To prevent losses of intensity, the use of collimators has to be avoided in favor of moderation. The state-of-the-art method of remoderation is the tungsten solid state moderator in reflexion or transmission geometry. Tungsten has a negative work function for positrons so thermalized positrons that diffuse to the surface can leave the solid. These positrons then have a sharp kinetic energy of 3 eV and a low divergence. The maximum efficiency for this kind of remoderator is usually on the order of 5-20 %. In order to also achieve a good remoderation efficiency for a beam with large phase space, we have developed a new type of remoderator which is based on inelastic scattering and the drift of positrons in a gas. Experiments by Surko et al. have shown that it is possible to decelerate positrons in nitrogen gas and store them in a penning trap [1]. The positrons are decelerated by interactions with the gas molecules in the following ways: elastic scattering, vibrational/rotational excitations, electronic excitation and direct ionization. Positron annihilation in the gas mainly happens after positronium formation, which starts at energies above 8.8 eV and reaches the same order of magnitude as the moderating interactions above 11 eV. Due to inelastic scattering, the mean free path for positrons in nitrogen is on the order of millimeters at 0.1 mbar.

Experimental Setup

The present setup of the gas moderator consists of the gas cell and the annihilation target (see fig. 1). The cell is connected via a pumping unit (not shown) to the NEPOMUC beamline on the left side and has a flange for a turbo pump on the bottom. The positrons are magnetically guided before they are decelerated at the entrance of the gas cell by an electric field. They enter the gas cell through a 3 mm pinhole. In the cell, positrons scatter with gas molecules causing the beam to expand. For this reason, a longitudinal magnetic field is applied to force the positrons into a gyration motion. The positrons lose their kinetic energy through collisions with the nitrogen molecules and then drift along a focusing electric field towards the exit of the cell. The thermalized positrons then leave the cell and annihilate at a beam catcher whose retarding potential can be adjusted. With the help of two BGO scintillators, the annihilation radiation at the beam catcher is detected in coincidence. By varying that retarding potential, it is possible to determine the energy distribution of the outgoing beam. One challenge of the gas moderator is a suitable differential pumping. The positrons have to be injected into the gas cell through a small hole to ensure that the vacuum pumps are capable of lowering the pressure in front of the gas cell over a very short distance. This is important to avoid losses due to positrons scattering in front of the gas cell.

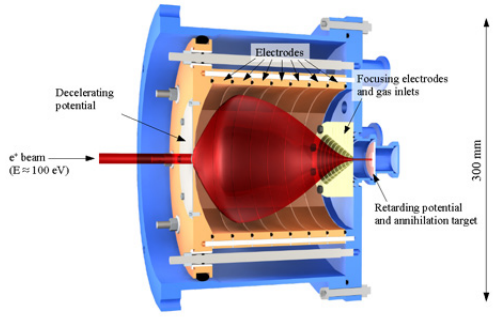

Figure 1: Cross sectional view of the positron gas moderator stage with the potential rings and double walled cell. In the first experiments the beam was caught at a target.

Measurements and results

For our first measurement at the NEPOMUC beamline, a 94 eV positron beam was decelerated to about 46 eV at the entrance of the gas cell. In figure 2 the spectral distribution of the positrons at the beam catcher, which was determined by the derivative of the measured intensity as a function of the retarding potential is shown. The data are shown for three different gas pressures of nitrogen in the gas moderator. At this pressures of nitrogen, a clear peak emerges at approx. 48 V, which corresponds to positrons with an energy of about 2.5 eV.

We succeeded in moderating positrons with a novel remoderator which uses inelastic scattering and the drift of positrons in a gas. The intensity of the observed peak at 48 eV is of the order of up to 6 % of the intensity of the incoming beam. Technical improvements are envisaged in order to increase the moderation efficiency.

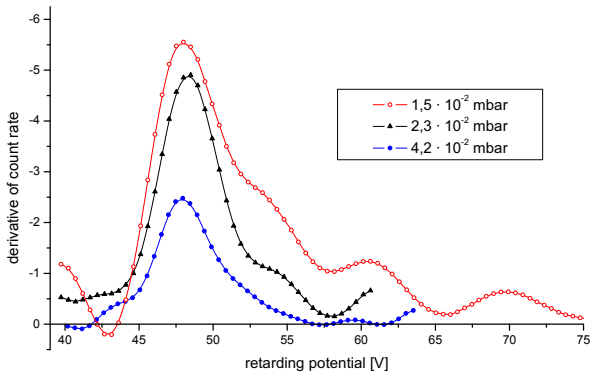

Figure 2: Spectral distribution of positrons at the beam catcher for three different nitrogen gas pressures in the gas moderator.

References

[1] C. M. Surko, M. Leventhal, and A. Passner. Positron plasma in the laboratory. *Phys. Rev. Lett.*, 62(8):901–904, Feb 1989.

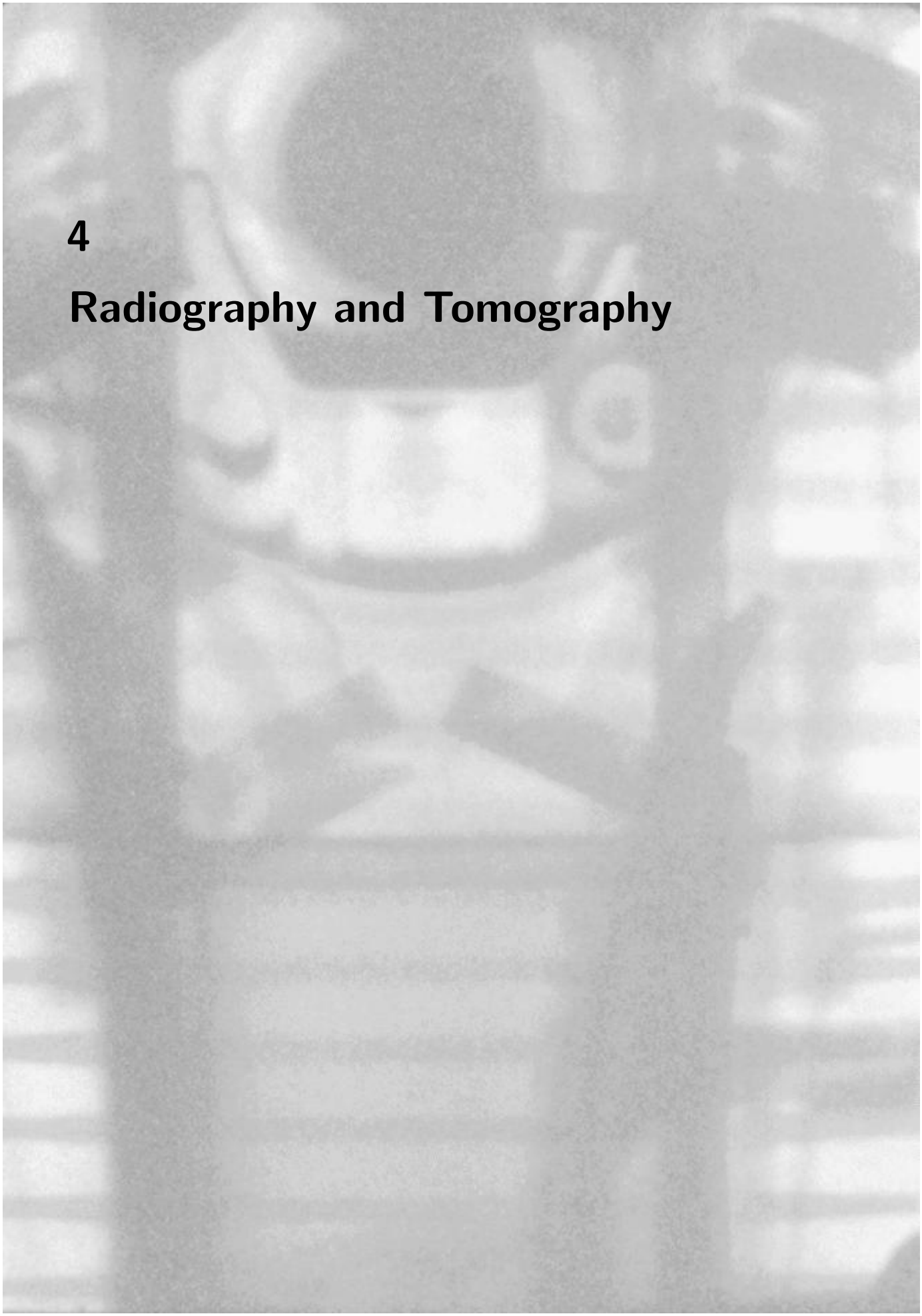

4

Radiography and Tomography

4.1 High-resolution differential phase contrast imaging using microfocus x-ray sources

Martin Engelhardt [1, 2], **Joachim Baumann** [2], **Manfred Schuster** [2], **Christian Kottler** [3], **Christian David** [3], **Oliver Bunk** [3], **Franz Pfeiffer** [3, 4]

[1] *Physik-Department E21, Technische Universität München, D-85748 Garching, Germany*
[2] *Siemens AG, Corporate Technology, D-81739 Munich, Germany*
[3] *Paul Scherrer Institut, 5232 Villigen PSI, Switzerland*
[4] *Ecole Polytechnique Fédérale de Lausanne, 1015 Lausanne, Switzerland*

Abstract

The applicability of absorption imaging is limited for weakly absorbing structures. Phase sensitive x-ray imaging can overcome these shortcomings since it has the potential for a significantly increased contrast. A new setup for phase contrast imaging was developed. This setup is a combination of a grating-based interferometer [1] with projection magnification using a high-brilliance microfocus x-ray source. In contrast to propagation based methods [2] and previous grating based methods [1], it can be combined with scintillators and detector systems with moderate spatial resolution. This offers increased detection efficiency even at higher photon energies.

Setup

The setup (Fig. 1) comprises a phase grating with phase shifting lines and an analyzer grating with absorbing lines. With the aid of the phase grating, an interference pattern is generated. Objects in the beam path slightly refract the beam, which causes a shift of the interference pattern. This shift is determined by scanning the interference pattern with the analyzer grating. It is proportional to the differential phase shift induced by sample. Images, which show the differential and total phase shift induced by the sample magnified by the projection geometry of the setup, can be derived from the data.

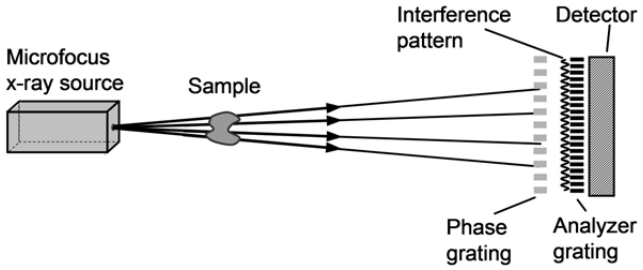

Figure 1: Setup for high-resolution differential phase contrast imaging.

Applications

Phase tomography of biological samples: For demonstration, a wasp was investigated (Fig. 2) [3]. A magnification factor of 3.5 was chosen, which gives a spatial resolution of approx. 30 μm.

Inspection of refractive x-ray lenses: The method described gives a direct measure of the beam refraction angle induced by the sample. This was used to investigate the refractive properties of a (single) Be x-ray lens [4]. In Fig. 3, the deviation $\Delta\gamma$ of the measured beam deflection angle from its target value is displayed. For x-rays transmitted through the lens within the innermost contour line the error $\Delta\gamma$ of the beam deflection angle is smaller than 0.012 arcsec. This gives a focus size of approx. 9 μm. However, at a distance of 300 μm from the center of the lens, a deviation $\Delta\gamma$ of 0.13 arcsec was determined, which results in a focus size of 83 μm. This is not acceptable for imaging and focusing application. The defective lens was chosen for demonstration purposes.

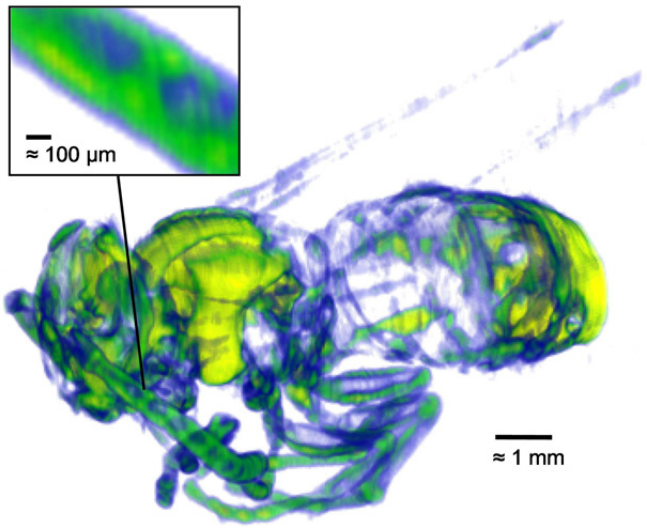

Figure 2: Phase tomography of a wasp in a quantitative rendered 3D representation of the refractive index decrement δ.

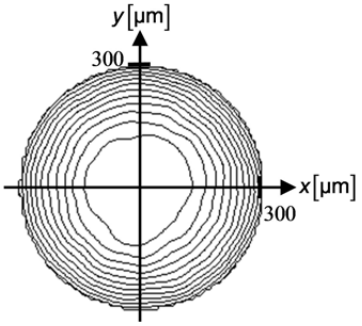

Figure 3: Quality validation of a refractive x-ray lens made of beryllium based on the beam deflection angle. The figure exhibits the deviation $\Delta\gamma$ of the measured beam deflection angle in radial direction from its target value. The contour lines correspond to a deviation of 0.012 arcsec, 0.024 arcsec, 0.036 arcsec, etc.

References

[1] F. Pfeiffer, T. Weitkamp, O. Bunk, and C. David. Phase retrieval and differential phase-contrast imaging with low-brilliance x-ray sources. *Nature Phys.*, 2:258, 2006.

[2] S. W. Wilkins, T. E. Gureyev, D. Gao, A. Pogany, and A. W. Stevenson. Phase-contrast imaging using polychromatic hard x-rays. *Nature*, 384:335, 1996.

[3] M. Engelhardt, J. Baumann, M. Schuster, C. Kottler, F. Pfeiffer, O. Bunk, and C. David. High-resolution differential phase contrast imaging using a magnifying projection geometry with a microfocus x-ray source. *Appl. Phys. Lett.*, 90(22):224101, 2007.

[4] M. Engelhardt, J. Baumann, M. Schuster, C. Kottler, F. Pfeiffer, O. Bunk, and C. David. Inspection of refractive x-ray lenses using high-resolution differential phase contrast imaging with a microfocus x-ray source. *Rev. Sci. Instrum.*, 78(9):093707, 2007.

4.2 Polarised neutron radiography: Ferromagnetism in Fe and Ni

Michael Schulz [1], **Robert Georgii** [1, 2], **Sebastian Mühlbauer** [1, 2]
[1] *Physik-Department E21, Technische Universität München, D-85748 Garching, Germany*
[2] *ZWE FRM-II, Technische Universität München, D-85748 Garching, Germany*

In this experiment the instrument MIRA was used to measure the beam polarization transmitted through a ferromagnetic sample of Fe and Ni. All experiments were carried out at a wavelength of 10 Å where no Bragg scattering in the materials is possible. The aperture installed in the monochromator shielding of the instrument was set to a size of 5x5mm which gives - with a flight path length to the sample of approx. 280cm - an L/D ratio of 560. This yields a reasonable geometrical resolution of 1.4mm at the detector position, which is good enough for the 2mm spatial resolution of the position sensitive detector available on MIRA. Between the aperture and the PSD detector, guide fields were installed to conserve the beam polarization. Furthermore a spin flipper was used to change the sign of the beam polarization. As polarization analyzer a ^{3}He cell was used which does not affect the geometrical resolution as much as i.e. a bender due to its influence on beam divergence. To magnetize the sample a pair of water cooled Helmholtz coils was used. These could produce fields up to approx. 3kG at the sample position being parallel to the neutron polarization. The maximum field used in the experiment was however only 1.4kG since higher fields produced severe stray fields that depolarized the beam.

The polarization of a neutron beam is defined as $P = (I_+ - I_-)/(I_+ + I_-)$, where I_+ and I_- are the intensities of neutrons polarized in the +z and -z direction respectively. The polarization measured on the detector is given by $P_{det} = P \cdot F \cdot P_S \cdot P_A$ Here P is the incident beam polarization, P_A is the analyzing efficiency of the ^{3}He cell, F is the flipping efficiency of the spin flipper and P_S describes the influence of the sample. The incoming beam polarization was determined to be P = 0.94. The flipping efficiency F was determined to be very close to unity and thus will be neglected in the further discussion. Using a position sensitive detector to image the depolarization of the beam over the area of the sample yields 2D information about the macroscopic magentization of the sample. As a sample a Ni slab of 3.5mm thickness which had a smaller slab of iron of 3mm thickness mounted on its side was used. The sample could be magnetized with the Helmholtz magnet. Since the permeability μ of Iron is much bigger than that of Ni a major part of the magnetic flux is bypassed through the Iron slab in the middle of the sample. This leads to a lower magnetization M in this region. Iron however does not come close to saturation in the applied fields. The sample was magnetized in four different external fields from 400G to 1400G. The beam polarization P_S transmitted through the sample was calculated from I_+ and I_- for each of these fields. The images shown (see Figure 1) are in agreement with the expectation that the Fe slab on the left side bypasses a major part of the magnetic flux and therefore decreases the flux density in the Ni slab. This leads to a higher depolarization of the beam. What can also be seen is that the lower the external magnetic field, the lower the magnetization of the bulk material. This leads to a higher depolarization of the beam. As said above Iron is far from saturation even at an external field of 1400G. This is why it completely depolarizes the beam in all images.

This experiment has proven that it is possible to image the depolarization of a neutron beam by a ferromagnetic sample. In future experiments this technique could be used to visualize magnetic flux density distributions in samples of a more complicated shape.

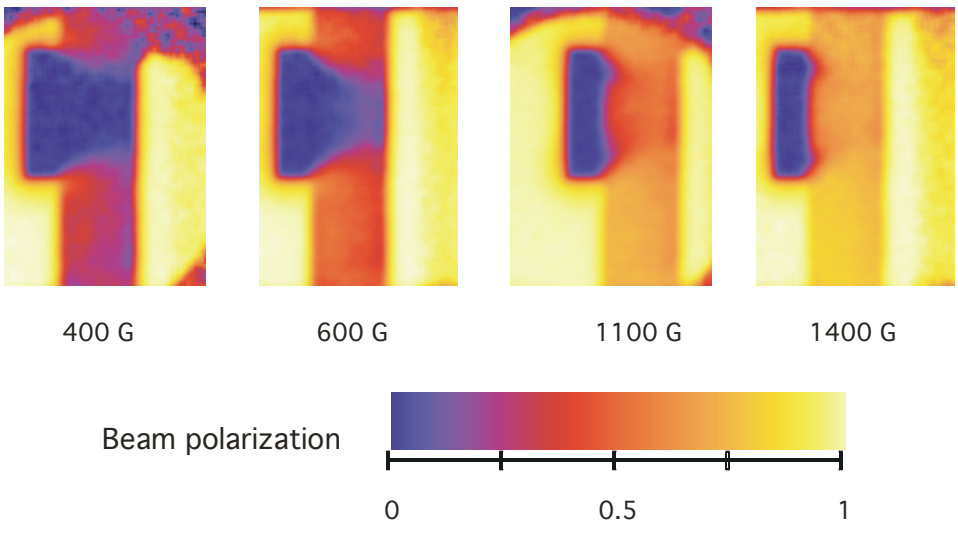

Figure 1: Beam polarization in dependence of the magnetic field

4.3 A Double Crystal Monochromator Option for ANTARES

Michael Schulz [1, 2], **Elbio Calzada** [1, 2], **Martin Mühlbauer** [1, 2], **Burkhard Schillinger** [1, 2], **Peter Böni** [1]

[1] *Physik-Department E21, Technische Universität München, D-85748 Garching, Germany*
[2] *ZWE FRM-II, Technische Universität München, D-85748 Garching, Germany*

A monochromator has been installed at the ANTARES beamline close to the collimator where the beam size is still only a few centimeters. Using this new setup it is now possible to do monochromatic neutron imaging in a wavelength range from 2.7Å to 6.5Å with a wavelength resolution $\Delta\lambda/\lambda$ of $1\%-3\%$. Most of the Bragg edges of materials of interest for neutron radiography lie in this wavelength region. Exposure times of the order of 300 s per radiograph are feasible with this new setup.

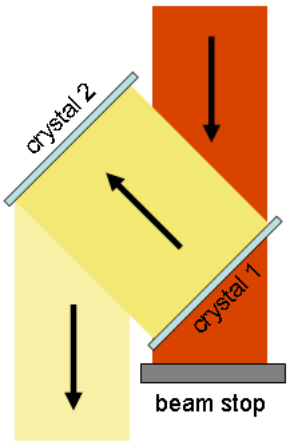

Figure 1: Schematic of the double crystal monochromator

The monochromator is a double crystal type, which consists of two pyrolytic graphite [002] monochromator crystals with a mosaic spread of approx. 0.7°. Each of the crystals is mounted on a rotary stage, respectively. The wavelength is selected with the first crystal and reflected out of the original beam. The remaining polychromatic beam transmitted through the first crystal is stopped by a beam dump. The second crystal is additionally mounted on a linear stage. Setting it to the correct linear position and the same Bragg angle as the first crystal, a zig-zag reflection of the monochromatic beam results (see Fig. 1). The monochromatic neutron beam thus has the same direction but is shifted by 105 mm with respect to the primary beam, the size of which is approx. $80 \times 80\,\mathrm{mm}^2$ at this position. The diameter of the evacuated neutron flight tube is big enough to carry the shifted monochromatic beam to the block house where the sample position is located. The beam size at this position is approx. $20 \times 20\,\mathrm{cm}^2$ which is sufficient for typical samples. The collimation of the beam remains basically unaffected by the monochromator thus yielding high resolution radiographs comparable to those with a polychromatic beam. The first monochromator crystal and the beam stop can be moved into and out of the beam by remote control allowing to switch from monochromatic to polychromatic imaging without any manual interaction.

Using monochromatic neutrons for imaging, one can avoid the effect of beam hardening which results from the wavelength dependence of the mass attenuation coefficient μ (see Fig. 2). For the small wavelength band of the monochromatic neutron beam this effect is negligible, which leads to a plain exponential decrease of intensity transmitted through the sample with increasing thickness d. $I = I_0 \exp^{-\mu d}$. This is especially important for reducing the error in quantitative measurements of material thicknesses.

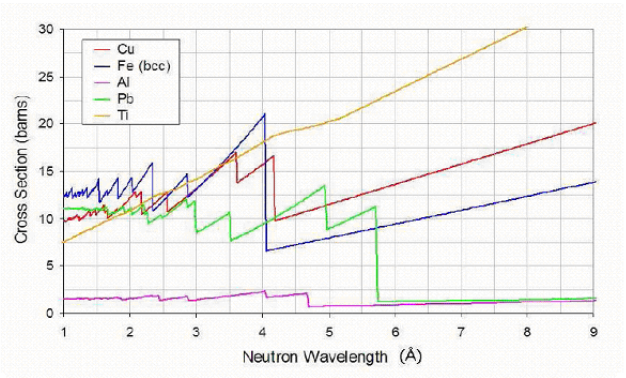

Figure 2: Wavelength-dependence of the total cross section for different materials.

Another application is the possibility to trace changes of the position of the Bragg edge of a certain material. Every polycrystalline material has a so called Bragg edge. When the wavelength reaches twice the maximum lattice distance of a material, coherent Bragg scattering is no longer possible. This leads to a significant decrease in the attenuation coefficient above this wavelength. If for some reason the lattice constant changes, the Bragg edge is slightly shifted towards higher or lower wavelengths. Taking radiographs with the wavelength set to that of the Bragg edge, even small changes in the position of the edge lead to a detectable variation of transmitted intensity. This can happen i.e. due to the heat influence in a welding process. Imaging such a weld one can then obtain information about the deformations introduced in the material. By this method the impact of different welding techniques on the material can be studied.

4.4 Examination of rat lungs by neutron computed micro tomography

Burkhard Schillinger [1, 2], **Elbio Calzada** [1, 2], **Andrew Comerford** [3], **Robert Metzke** [3], **Martin Mühlbauer** [1, 2], **Josef Guttmann** [4], **Hanna Runck** [4], **Matthias Schneider** [4], **Claudius Stahl** [4], **Lena Wiechert** [3], **Wolfgang Wall** [3]

[1] *Physik-Department E21, Technische Universität München, D-85748 Garching, Germany*
[2] *ZWE FRM-II, Technische Universität München, D-85748 Garching, Germany*
[3] *Chair for Computational Mechanics, D-85748 Garching, Germany*
[4] *Department of Anesthesiology and Critical Care Medicine, University of Freiburg, Germany*

Abstract

The ANTARES facility for neutron imaging has recently used a thinned scintillation screen and a high resolution optical system to reach effective resolution of the order of 30 micrometers. This setup was used to gather structural information of freshly extracted rat lungs. The aim of the measurement is the development of a numerical lung model for improvement of artificial respiration in human medicine in hospitals.

Introduction

Patients who need artificial respiration in a hospital over several days often suffer lung damages because the respiration pressure cannot be set with sufficient precision due to insufficient knowledge about the exact composition of the lung. The chair for computational mechanics of TU München aims to develop a numerical model of a lung in order to simulate pressure and air flow in the branching of the air vessels. As it turned out, the structure of the lung is known in principle, but not in detail, and very little is known about the actual branching and diameters of the pulmonary air passages. As the volume of the lung consists mostly of air, with very thin air and blood vessels, normal X-ray examinations deliver insufficient contrast of the tissue to image the structure of the lung. Neutron imaging delivers a high contrast of the hydrogen content in the tissue and was successfully employed to deliver 3D images of the lung structure.

Experimental setup

Since neutron imaging employs a parallel beam, there is no inherent magnification of the sample, and the image resolution is limited to the actual detector resolution. ANTARES used a thinned scintillation screen (50 μm thickness) and a ZEISS planar high resolution lens on a 2048 x 2048 pixel cooled CCD camera. With an effective pixel size of 20 μm, the achieved resolution (due to blurring of the scintillation screen) was estimated in the order of 40 μm. Live laboratory rats were delivered to the engineering faculty, were anaesthetised and killed. The lungs were extracted and sewn with their main air pipe onto on a plastic tube, then put inside an aluminium tube that both simulated the confinement of the rib cage and also fixated the lung against movement during the measurement. The lung was then inflated with 20-30 mbar air pressure and mounted on a rotation table in front of the detector.

Measurement

At this high resolution, the incident neutron flux per pixel is very low. One projection required between 13 and 80 seconds exposure time, totalling in 2.5 to 9 hours for 400 projections for the computed tomography. Additional experiments were conducted with a gadolinium containing contrast agent that was directly injected into the main airway. Due to the capillary forces, this contrast agent penetrated into the finest air vessels.

Fig. 1 shows one projection of a lung confined in the aluminium tube, fig. 2 shows a lung with added gadolinium contrast agent. Fig. 3 shows a lung that was taken out of the aluminium container and had consecutively inflated to double its original volume. Fig. 4 shows a three-dimensional reconstruction of a lung with the threshold set so high as to see only larger air vessels. Fig. 5 shows another lung with a lower threshold level, showing many fine vessels as well as apparently a major blood vessel that branches towards different sections of the lung.

Fig. 6 shows a lung filled with gadolinium contrast agent that had dissipated into the findest branches. Since the liquid had followed gravity during injection, the upper parts of the lung were not filled.

Conclusion

For the first time, neutron computed tomography has been used for the detemination of the structure of lung tissue. The results will be employed in the development of a numerical model of a lung in order to improve clinical treatment of human patients. Further examinations are under way.

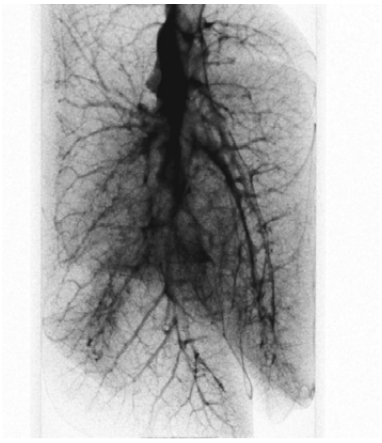

Figure 1: One projection of a lung confined in the aluminium tube

Figure 2: A lung with added gadolinium contrast agent

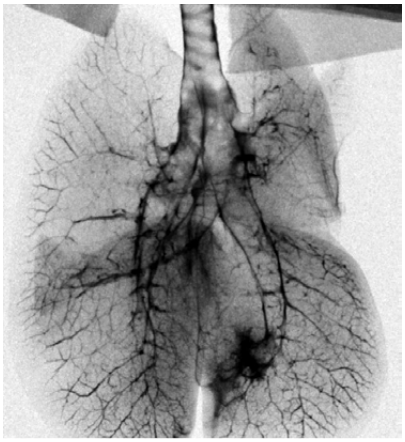

Figure 3: A lung that was taken out of the aluminium container and had consecutively inflated to double its original volume

Figure 4: A three-dimensional reconstruction of a lung with the threshold set so high as to see only larger air vessels

Figure 5: Another lung with a lower threshold level, showing many fine vessels as well as apparently a major blood vessel that branches towards different sections of the lung

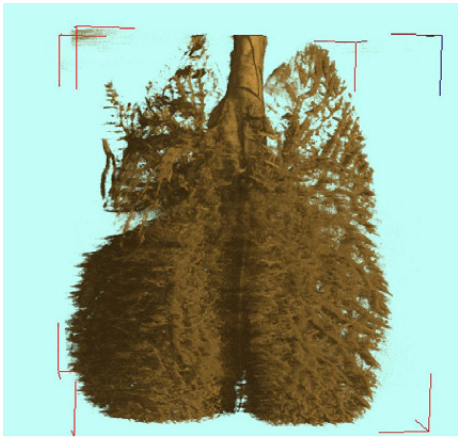

Figure 6: A lung filled with gadolinium contrast agent that had dissipated into the findest branches. Since the liquid had followed gravity during injection, the upper parts of the lung were not filled

4.5 Neutron phase contrast imaging at ANTARES

Klaus Lorenz [1, 2], **Burkhard Schillinger** [1, 2]
[1] *Physik-Department E21, Technische Universität München, D-85748 Garching, Germany*
[2] *ZWE FRM-II, Technische Universität München, D-85748 Garching, Germany*

Theory

The refractive index $n = 1 - \delta + i\beta$ of a material consists in general of a real and an imaginary part. The imaginary part causes the attenuation of the neutron beam, what is used in conventional radiography and tomography to visualize the structure of an object. The real part causes a phase shift

$$\phi(x, y) = -\frac{2\pi}{\lambda} \int \delta(x, y, z) dz \qquad (1)$$

with regard to propagation in free space. At edges and interfaces this leads to strong deviations of the wavefronts of an incoming wave. If the detector plane has a certain distance from the object, an increase in the contrast occurs at those edges and interfaces. This interference effect is called phase contrast [1].

Experimental setup

The simplest way to get phase contrast is the propagation based method. Unlike interferometric measurement methods, no complicated experimental setup is necessary. Basically the same setup as for conventional neutron radiography can be used with two additional requirements:

1. The neutron beam must have a high transversal spatial coherence at the sample position.
2. The detector plane must be in the near field region.

The high coherence is achieved by the introduction of pinhole apertures with a diameter of 2mm and less in the beam at a distance of 14m to the sample position [2].

Applications

In figure 1 the result of a conventional radiography of a step wedge out of $AlMg_{4.5}Mn$ with another aluminum alloy $AlSi_9Cu_4$ cast around it are compared with a phase contrast image of this sample. The effect is only used in a qualitative way for contrast enhancement at edges and interfaces. The phase contrast image is slightly bigger than the conventional one because of the magnification due to the greater sample-detector distance.

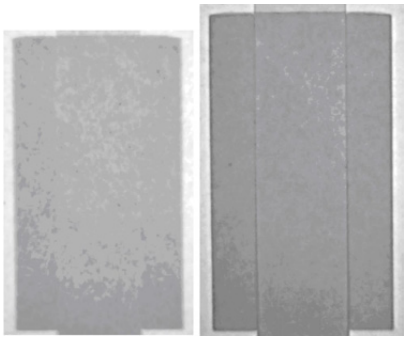

Figure 1: Conventional (left) and a phase contrast radiography (right) of a $AlMg_{4.5}Mn$ step wedge with $AlSi_9Cu_4$ cast around it.

Both materials have very similar attenuation coefficients and produce close to no absorption contrast in conventional neutron imaging. Under phase contrast conditions, due to the fact that manganese causes a negative and copper a strong positive phase shift, phase contrast occurs at the inner interfaces which are parallel to the direction of the neutron beam. The representation of the mass attenuation coefficient and the δ-values of the elements in figure 2 helps to find material compositions where phase contrast can bring advantages in non-destructive testing.

References

[1] John M. Cowley. In *Diffraction Physics*. Elsevier, Amsterdam, Netherlands, 1995.
[2] Eberhard Lehmann, Klaus Lorenz, Erich Steichele, and Peter Vontobel. Non-destructive testing with neutron phase contrast imaging. *Nucl. Instr. and Meth. in Phys. Res. A*, 542:95–99, 2005.

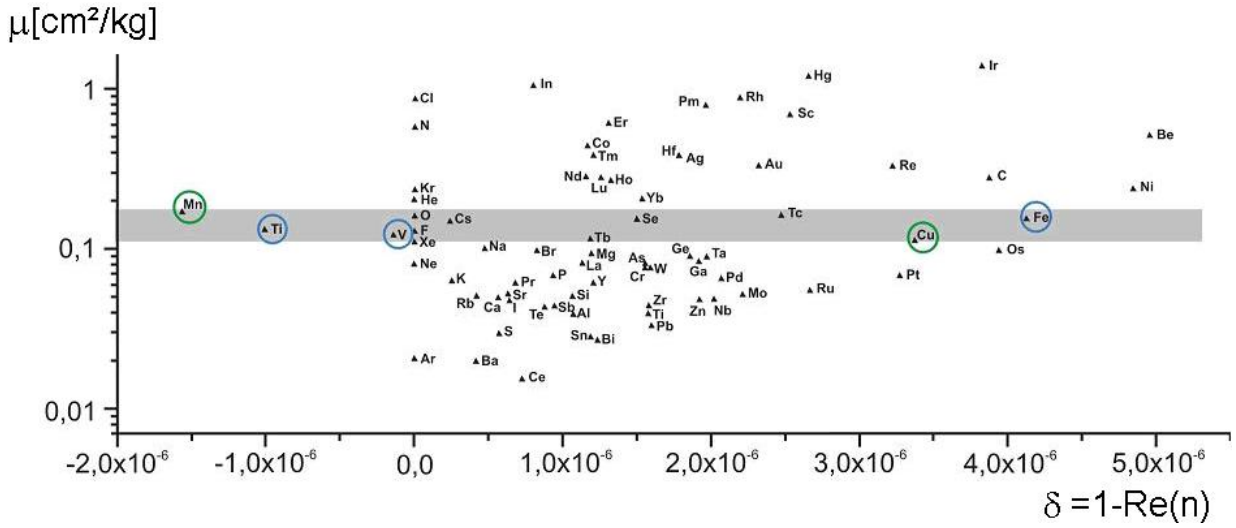

Figure 2: Comparison of the mass attenuation coefficient μ and the δ-values of the elements.

5

Instrument Development

5.1 Inelastic Neutron Scattering From Very Small Single Crystals

Richard A. Mole [1], **Klaudia Hradil** [1, 2], **Sebastian Mühlbauer** [1, 3], **Andreas Ostermann** [1], **Peter Böni** [3]

[1] *ZWE FRM-II, Technische Universität München, D-85748 Garching, Germany*
[2] *IPC Universität Göttingen, Institut für Physikalische Chemie, D-37077 Göttingen, Germany*
[3] *Physik-Department E21, Technische Universität München, D-85748 Garching, Germany*

Triple axis spectrometers (TAS) allow the measurement of excitations with good energy resolution. However, due to the low flux of neutrons usually large samples with dimensions of the order of cubic centimeters have to be used. There are many areas of scientific interest, where measurements are prohibited because of the difficulty of growing large, high quality single crystals. The topics of interest range from lattice and spin dynamics in condensed matter physics to excitations in biomolecules and molecular materials, where TAS methods are very infrequently used due to the problems with crystal growth.

The problem with intensity occurs also in experiments using extreme environments, such as high pressure, where the sample size is restricted too. One method to get around this problem is to use inelastic X-ray scattering, however the energy resolution of this technique is often too coarse. Therefore, we have investigated the use of focusing devices using supermirrors [1].

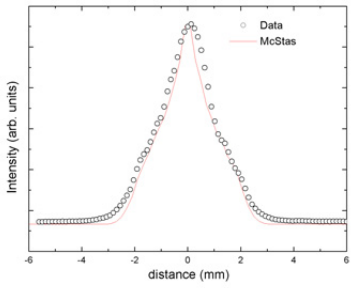

Figure 1: Black: Horizontal beam profile measured with a delCAM neutron CCD camera. Red line: Simulation of the horizontal beam profile.

The used focusing guide has a length of 500 mm and has been described previously [2]. It was installed on PUMA between the monochromator and the sample. In the first instance we used a neutron CCD camera to both correctly align the guide and to analyze the shape and intensity of the beam at the sample position. These measurements, along with Monte-Carlo simulations of the profile are shown in Fig. 1. Both, measurement and simulation show that the beam has a FWHM of approximately 2 mm in the horizontal direction and 8 mm in the vertical direction. Such a profile is ideal for studying small samples, unlike the conventional PUMA profile, where the primary beam has dimensions of roughly 25 mm in the horizontal and vertical direction and must be restricted by means of adjustable apertures. In addition, the images also revealed that the guide reduces the background rather dramatically.

In a first experiment, a small single crystal of Cr with dimensions $2 \times 2 \times 2$ mm^3 was investigated. Samples of this size can typically be used in Paris Edinburgh high pressure cells. Using the focusing guide, we were able to observe amongst other things the change in intensity of the magnetic excitations in the transversely polarized spin density wave phase with temperature (Fig. 2).

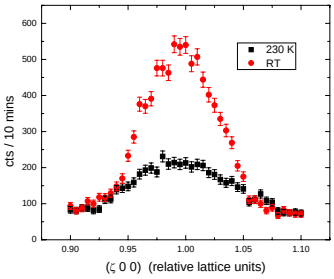

Figure 2: Temperature dependence of the spin excitations at 4 meV in the longitudinal spin density wave phase in Cr. The data was collected at 295 K and 230 K around the (1 0 0) Bragg reflection.

The second experiment was performed using samples of quartz (SiO2), including one with a volume of approximately 8 mm^3 (Fig. 3). This experiment allowed a direct comparison between the conventional PUMA configuration and the focusing set-up, showing that the sample with a volume that is 250 times smaller than the original crystal can be measured. Note the low background and the improved energy resolution.

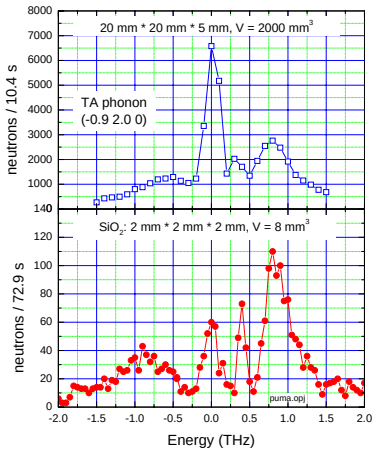

Figure 3: Measurement of a transverse acoustic phonon in quartz. Top: Normal PUMA configuration and large crystal, bottom: Same measurement using the focusing guide with a sample that is 250 times smaller.

In conclusion we have shown that using a focusing guide allows the measurement of excitations in tiny crystals by means of a thermal TAS, while still having excellent energy resolution thus allowing to explore small samples in areas of science, where traditionally experiments have been restricted due to the small sample size.

References

[1] C. Schanzer, Peter Böni, and Uwe Filges. Advanced geometries for ballistic neutron guides. *Nucl. Inst. and Meth. A*, 529:63–68, 2004.

[2] Sebastian Mühlbauer, Martin Stadlbauer, Peter Böni, Christian Schanzer, Jochen Stahn, and Uwe Filges. Performance of an elliptically tapered neutron guide. *Physica B*, 385-386:1247–1249, 2006.

5.2 Bridgman-cells for high-pressure resistivity measurements

P. G. Niklowitz [1], **R. Ritz** [1]
[1] *Physik-Department E21, Technische Universität München, D-85748 Garching, Germany*

The pressure cell is based on a design by D. Braithwaite at the CEA-Grenoble and is a scaled-down version of a design by Wittig [1]. The cell parts are shown in Figure 1. l the parts, except the anvils and a brass centering ring around the anvils, are made of non-magnetic Cu-2%Be. Like the diamond anvil cells (DACs), the Bridgman cell offers a minimalist design with respect to the tasks of pressure application and anvil alignment. The brass centering ring holds the anvil in place by fitting tightly around the anvils and in indentations in the bottom screw and in the piston. As a result of the simple design, the maximal cell diameter is only 30 mm, and the length less than 70 mm and its weight 275 g [2].

The anvil has cylindrical symmetry. WC (tungsten-carbide) anvils (outer culet diameter 3.5 mm) support pressures up to 100 kbar and sintered-diamond anvils (outer culet diameter 2 mm) allow experiments up to several hundred kbar. For the geometry of the anvils used the tensile strength of the support material has to be about 4-5 kbar. Consequently, Cu-2%Be is suitable as anvil support material.

A photo of the resistivity set-up on the lower anvil developed by Wittig [1] is shown in Figure 2. The use of the solid pressure transmitting medium steatite makes the sample space much less compressible than when filled with a rare gas. Therefore the requirements on the plastic flow properties of the gasket are not very high and the gasket can be made from an insulating material. The gasket is made of pyrophyllite and has an outer diameter to fit the culet, and a sample space with a diameter of 1-2 mm. The shear strength of pyrophyllite is large enough that a gasket with a thickness of 250 μm can support a pressure of 100 kbar in the sample space. The gasket is glued on the culet of the lower anvil with a 2:3 mixture of silicate and water or with varnish.

The bevel of both conducting anvils is insulated with standard Araldite. The insulation also gives massive support to the pyrophyllite gasket on the lower anvil. Slits in the gasket for the electrical leads, somewhat more than half the gasket thickness, are cut into the gasket with a razor blade. We found it helpful to cut the slits at a slight angle with respect to the vertical direction, such that the leads are better protected against short-circuiting to the upper WC anvil.

A steatite disk and a sample with thickness of the order of 100 μm and with a length up to 1 mm is placed in the sample space. A Pb sample is used as a pressure gauge. 25 μm Pt wires are strong enough to survive the pressurisation of the cell. When softened by annealing them in a flame, the Pt wires are easily bent into the right position on the sample. To ensure electrical contact the wires are flattened at the ends which touch the sample.

A second steatite disc is placed carefully on top of the resistivity set-up to fully surround the setup with the pressure medium. After insulating the electrical leads from the upper anvil by filling the slits with pyrophyllite powder, the pressure cell is assembled and pressurised.

Figure 1: Parts of the Bridgman cell: the bottom screw with the lower anvil (a) is fixed tightly to the cell body (b). The electrical leads leave the pressure cell through the windows in the cell body. The piston with the upper anvil (c) is pushed up-side down the cylinder towards the lower anvil by an external force generating mechanism via the hole in the top screw. The plate (d) is placed between the piston and the top screw to reduce stress during tightening the top screw (e).

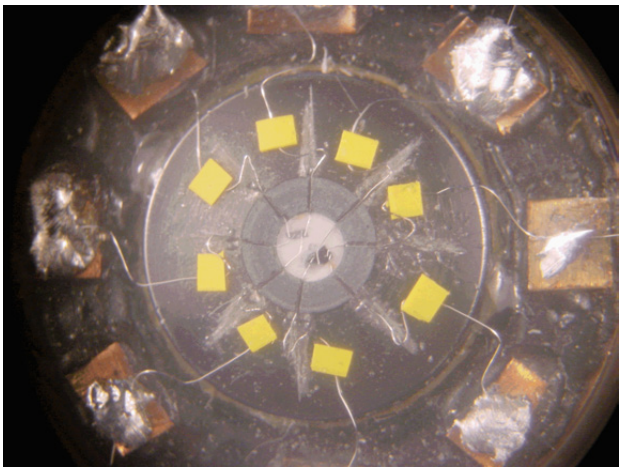

Figure 2: Resistivity set-up in the WC Bridgman cell. The pyrophyllite gasket is glued on the culet of the WC anvil. Inside the gasket is a steatite disc (the pressure transmitting medium) on which samples and Pt wires are placed. The Pt wires go through slits in the gasket from the samples to solder joints from where Cu wires (not shown) build a link to the outside of the pressure cell.

The pressure in the WC Bridgman cell is determined by the pressure dependent superconducting transition temperature T_c of the pressure gauge (see for example [3]). Since T_c can be suppressed by a magnetic field, the presence of a residual field during the pressure determination leads to a measured pressure, which is higher than the actual pressure. Some anvils are Co bonded and are possibly a source of residual magnetic fields. Therefore whenever an external field has been applied onto a WC Bridgman cell with Co bonded anvils, the anvils have to be demagnetised before the next pressure determination. Pressure inhomogeneities are estimated by the width of the superconducting transition and should be smaller than one tenth of the applied pressure.

References

[1] J. Wittig. *Z.Phys.*, 195:215, 1966.
[2] R. Ritz, 2007. Diploma Thesis.
[3] A. Eichler and J. Wittig. *Z.Angew.Phys.*, 25:319, 1968.

5.3 Spherical neutron polarimetry in reflection geometry: Proof of principle

Marc Janoschek [1, 2], **Florian Bernlochner** [1], **Sebastian Mühlbauer** [1], **Peter Boeni** [1]
[1] *Physik-Department E21, Technische Universität München, D-85748 Garching, Germany*
[2] *Paul-Scherrer-Institut, CH-5232 Villigen, Switzerland*

Polarized neutron reflectometry (PNR) is a standard tool to measure inter- and intralayer magnetic correlations in magnetic thin films and multilayers [1]. However, in the standard PNR setup only the component of the final polarisation vector parallel to the direction of the magnetic guide field can be measured. Hence, not the full information contained in the polarisation vector is measured. A method capable of measuring the the full change of the polarisation vector during the scattering process is spherical neutron polarimetry (SNP). At the FRM-II research reactor this method is available through the new SNP option MuPAD [2] that is maintained and operated by our group.
Within the scope of a spherical neutron polarimetry experiment conducted in October 2007 on the very cold neutron beamline MIRA we tested the suitability of MuPAD for doing reflectometry measurements. A non-magnetic TiC multilayer with 20 alternating titanium and carbonium layers of 90 Å thickness was used as a test sample. The wavelength employed in this experiment was $\lambda \approx 11$ Å and therefore the Bragg peak originating from the superstructure was observed in a θ-2θ scan at $\theta = 1.7°$. The scan performed is shown in Fig. 1.

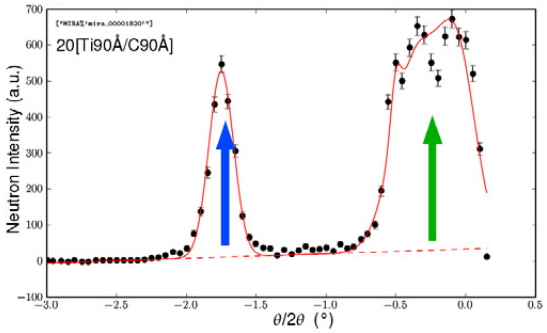

Figure 1: θ-2θ on the TiC multilayer. The green and the blue arrows mark the positions of the polarisation tensors shown in Tab. 1

We measured full polarisation tensors over the range $-3.0° < \theta < 0.2°$ in the scan. The green and the blue arrows mark the positions where the two example polarisation tensors shown in Tab. 1 were measured. Since the used TiC multilayer is non-magnetic, the polarisation vector is not expected to be turned during the scattering process. According to the Blume-Maleyev equations (s. references 1-5 in [2]), the matrix is predicted to have the following form:

$$\vec{P}_{ij} = \begin{pmatrix} 1 & 0 & 0 \\ 0 & 1 & 0 \\ 0 & 0 & 1 \end{pmatrix} \quad (1)$$

This form of the polarisation tensor is observed in the measurement (s. Tab. 1). The diagonal elements deviate from one as the used benders for polarizing and analyzing the beam are not perfect. The off-diagonal elements are non-zero because of the long wavelength of 11 Å available on MIRA (intensity maximum). Therefore low speed neutrons with such a long wavelength are most sensitive to magnetic stray fields. At the beginning of the year 2008 MIRA will be equipped with a new monochromator that will allow to use MuPAD with 5 Å neutrons. Thus, the accuracy of MuPAD installed on MIRA will increase significantly.
In summary we showed that MuPAD can be used in combination with a neutron reflectometer in order to measure the maximum of information available from polarized neutron reflectometry measurements on multilayers.

1	P_{out}		
P_{in}	x	y	z
x	0.78(1)	0.16(2)	-0.18(2)
y	-0.12(2)	0.80(1)	0.07(2)
z	0.01(2)	-0.05(2)	0.82(1)
2	P_{out}		
P_{in}	x	y	z
x	0.787(5)	0.18(1)	-0.19(1)
y	-0.15(1)	0.845(4)	0.03(1)
z	0.03(1)	-0.12(1)	0.850(4)

Table 1: Polarization matrices as measured on the positions of the direct beam marked by the green arrow (1) and the diffracted beam (blue arrow, 2) in the θ-2θ scan shown in Fig. 1. The diagonal elements are reduced from 1 due to a non-perfect polarizer and analyzer.

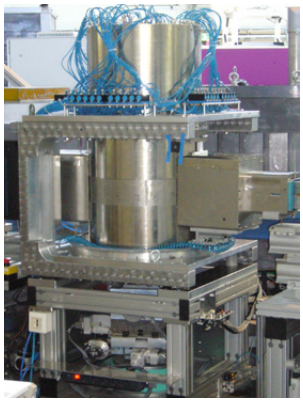

Figure 2: The MuPAD option mounted on MIRA.

References

[1] M.R. Fitzsimmons and C.F. Majkrzak. *Modern Techniques for Characterizing Magnetic Materials*, chapter Application of Polarized Neutron Reflectometry to Studies of Artificially Structured Magnetic Materials. Springer, 2005.
[2] M. Janoschek, S. Klimko, B. Roessli, R. Gähler, and P. Böni. *Physica B*, 397:125–130, 2007.

5.4 TASRESFIT - easy fitting of three-axis-spectrometer data

F. Bernlochner [1], **M. Janoschek** [1, 2]
[1] *Physik-Department E21, Technische Universität München, D-85748 Garching, Germany*
[2] *Paul-Scherrer-Institut, CH-5232 Villigen, Switzerland*

It is one of the most important aspects of analysing inelastic neutron scattering data obtained on a three axis spectrometer to understand and properly take into account the experimental resolution. It is determined by various spectrometer components (neutron guide divergence, quality and mosaic of monochromator and analyser crystal, distances, focussing, collimation) and the properties of the sample (size, form, mosaic spread) and is therefore strongly dependent on the experimental conditions. This is especially true if modern focussing optics are used. Luckily, the formalism to calculate the resolution taking into account the known experimental conditions and the sample properties is well understood today (s. [1]). Hence the deconvolution of the real shape of neutron scattering cross-section from the measured data is theoretically a relatively simple task, especially as today's computing power allows for quick numerical integrations. Such a data treatment is performed in the following steps:

1. calculate the resolution function at EACH data point with the given spectrometer configurations and sample parameters
2. numerical convolution of this resolution function and theoretical cross section
3. fitting convoluted cross section to this data

However, this kind of analysis is still hard, most of all as the software packages used for this task, are either not really user-friendly or often rely on commercial numerical packages like MATLAB.

Here we report on the availability of the new software TASRESFIT, that was written in the language PYTHON [2]. Using PYTHON had several distinct advantages for us:

- PYTHON is free of charge
- PYTHON is platform independent (with some limitations)
- PYTHON is already in use to control the triple axis spectrometers PANDA and PUMA at FRM-II. This will allow for easy integration of parts of TASRESFIT in the control program (a project to do so was already started for PANDA)

TASRESFIT is a command line based program that is based onto the python package 'neutrons' developed by M. Janoschek. All important tasks, e.g. the calculation of the resolution, are part of the neutrons package and therefore can be also used by other programs. TASRESFIT was developed to perform standard tasks without efforts. Therefore it allows for direct import of instrumental data files (currently: TASP, IN14, PANDA) through a powerful and easily extendable import filter system. Further, the loaded data can be treated further within the program (e.g. correct monitor, flipping ratio, sum and merge scans) and hence it is straight forward to start fitting the data immediately. Some of its further features are:

- the neutron cross-section to be fitted to the data can be easily loaded into the program
- TASRESFIT allows for simulation of scans taking into account the loaded cross-section
- most of the resolution parameters (e.g. collimators) can be changed from within the program
- the change of the resolution function can be simulated and plotted over a scan

A screenshot of the program is shown in Fig. 1. TASRESFIT and the neutrons package are freely distributed to scientists interested.

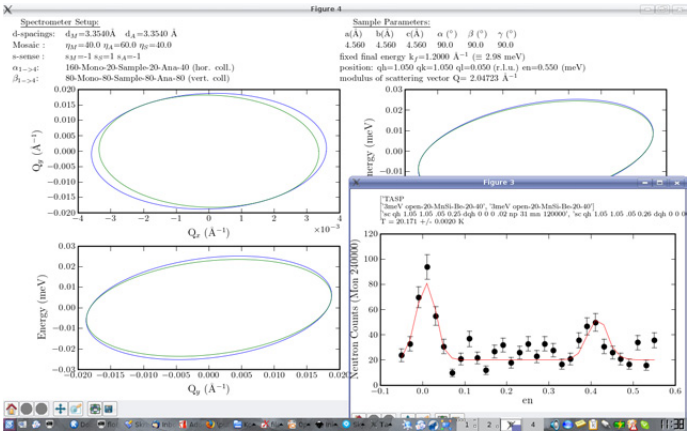

Figure 1: The figure shows a screenshot of a typical TASRESFIT session. The resolution ellipsoid was calculated and plotted for a special instrumental condition. In the bottom right window a fit of three axis data is shown.

References

[1] M. Popovici. *Acta Cryst.*, A31:507, 1975.
[2] G. van Rossum and F.L. Drake. `http://www.python.org`. *Python Reference Manual, PythonLabs, Virginia, USA*, 2001.

5.5 Multiple small angle neutron scattering: A new two-dimensional ultrasmall angle neutron scattering technique

Christian Grünzweig [1], **Murat Ay** [1], **Peter Böni** [2], **Roland Gähler** [3], **Robert Georgii** [2, 4], **Thomas Hils** [2], **Sebastian Mühlbauer** [2, 4]

[1] *Paul Scherrer Institut, CH-5232 Villigen, Switzerland*
[2] *Physik-Department E21, Technische Universität München, D-85748 Garching, Germany*
[3] *Institut Laue Langevin, -38042 Grenoble, France*
[4] *ZWE FRM-II, Technische Universität München, D-85748 Garching, Germany*

Small angle neutron scattering (SANS) is a powerful technique for studying the structure of materials with lateral correlation lengths in the range of about 0.6 nm up to about 600 nm. This corresponds to a q-range of 1 Å^{-1} to 10^{-3} Å^{-1}. Measuring correlation lengths in the micrometer range being of high interest for the research on biological samples, polymers, colloid systems, cements, micro-porous media leads to unacceptable losses in intensity by a factor 10^4 using the standard SANS technique. With the new MSANS technique we can overcome the intensity problem. The method is based on two 2D-multi-hole Cd-apertures one placed at the front end of the collimator of a common SANS instrument and the other close to the sample (Fig. 1).

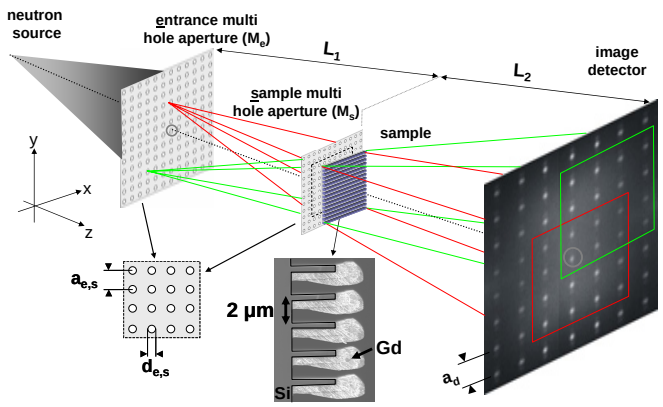

Figure 1: Schematic experimental setup of the MSANS option showing the 2D entrance multi hole aperture (M_e) with a lattice constant a_e and hole diameter d_e, and the 2D sample multi hole aperture (M_s) with lattice constant a_s and hole diameter d_s. Using appropriate values a_e= 5 mm, a_s= 2.5 mm and $L_1 = L_2$ = 2.6 m, the individual beams superimpose on the detector on a grid with the lattice constant a_d = 5.

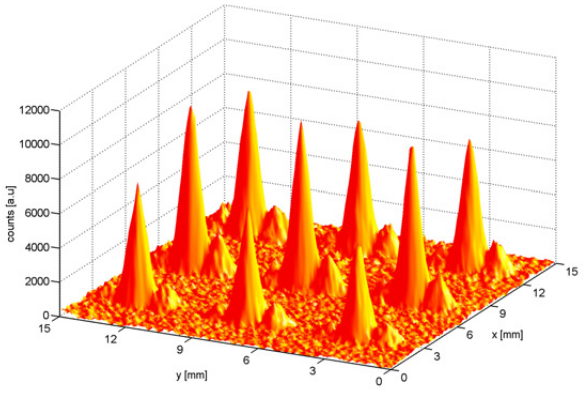

Figure 2: Section of an MSANS detector image of a 2 µm period Gd absorption grating.

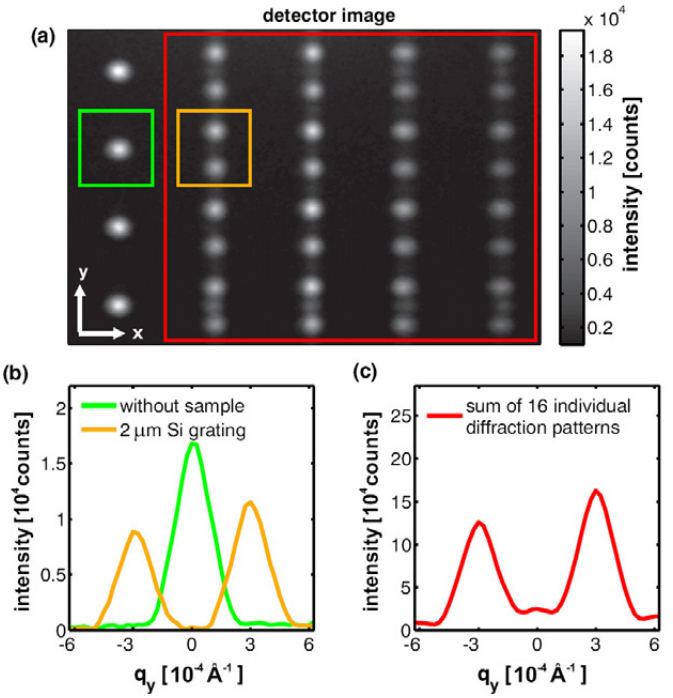

Figure 3: MSANS data of Si phase grating with a period of 2 μm. (a) Detector image. (b) Profiles along the y-axis through one hole pattern without sample in the beam (green box in (a)). The orange box in (a) showing the diffraction pattern of a 1D phase grating. (c) Section plot along the y-axis of 16 individual summed up diffraction patterns (red box in (a)).

By choosing the proper MSANS geometry, individual diffraction patterns are superimposed leading to a large gain in intensity. Using MSANS as an option for SANS beam lines, the q-resolution can be increased to 10^{-5} Å^{-1} without dramatically sacrificing intensity. The first demonstration experiment of the MSANS technique [1] was performed at the diffractometer beam line MIRA, where we already obtained a q-resolution of $3 \cdot 10^{-4}$ Å^{-1}. Fig. 2 shows a section of the detector image of a gadolinium (Gd) absorption grating with a period of 2 μm.

Fig. 3(a) shows the detector image from a silicon phase grating with a period of 2 μm. The large gain in intensity is clearly visible in Fig. 3(c).

Recently, a similar experiment has been performed using D11 at the Institute Laue-Langevin, where a grating with a pitch of 17 μm was resolved using the MSANS technique.

References

[1] C. Grünzweig and T. Hils and S. Mühlbauer and M. Ay and K. Lorenz and R. Georgii and R. Gähler and P. Böni, Appl. Phys. Lett., 91:203504, 2007.

5.6 Rotating Field Spin-Echo

Nikolas Arend [1], **Alexander Ioffe** [1], **Wicher Kraan** [2], **Robert Georgii** [3, 4]
[1] *Jülich Centre for Neutron Science - Outstation Garching, Forschungszentrum Jülich GmbH, 85747 Garching*
[2] *Interfacultair Reactor Instituut, Delft University of Technology , 2629 JB Delft, the Netherlands*
[3] *ZWE FRM-II, Technische Universität München, D-85748 Garching, Germany*
[4] *Physik-Department E21, Technische Universität München, D-85748 Garching, Germany*

Neutron Spin Echo (NSE) is a technique for quasi-elastic neutron scattering with very high energy resolution down to the sub-μeV range. The latter is achieved by comparing the Larmor precession angles of a polarized neutron beam in two well-known magnetic fields before and after scattering in a sample. This spin encoding or Larmor labeling can be accomplished by different technical methods, the most established variants being conventional NSE and Neutron Resonance Spin Echo (NRSE). During this beamtime at MIRA we investigated Rotating Field Spin Echo (RFSE) (see Figure 1 and 2), a technique targeting at measurements in the lower resolution domain.

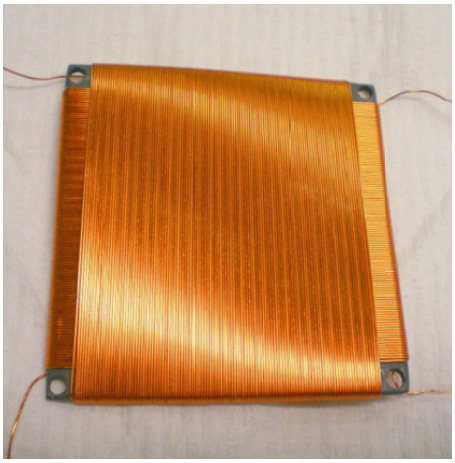

Figure 1: Rotating field coil

Figure 2: Spin echo setup

The experiments carried out had been divided in three parts: i) testing the bootstrap principle with rotating field coils for the first time, ii) installing a complete spin echo setup and recording the spin echo group (see Figure 3), and iii) performing first MIEZE measurements with this technique (see Figure 4). As opposed to Resonance Spin Echo, which uses coils that superpose a highly homogeneous static field and a superposed rotating (in practice: oscillating) field operated in resonance, Rotating Field Spin Echo implements rotating fields with the plane of rotation being perpendicular to the neutron beam path. Although no static fields are used in the latter technique, NRSE and RFSE are in principle equivalent and can be described similarly.

For the first time, a complete spin echo setup with rotating fields could be successfully operated and spin echo groups for two different frequencies were recorded. The same applies to proving the bootstrap principle to work with RFSE and the first rotating field MIEZE signal. A possible application of this new spin echo technique is to cover the frequency range from approx. 50 kHz and below. Here NRSE instruments usually cannot operate due to depolarization caused by the Bloch-Siegert shift which has its origin in the usage of oscillating instead of rotating fields in the resonance flipper coils.

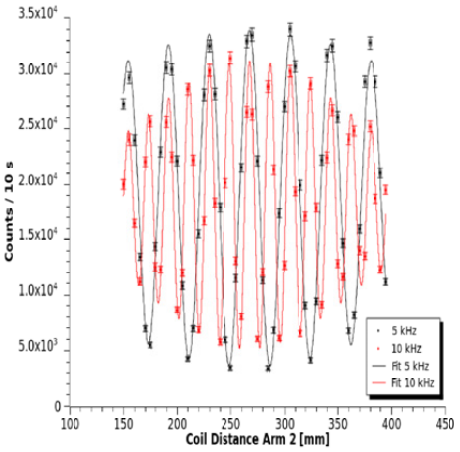

Figure 3: Spin echo groups for 5 and 10 kHz

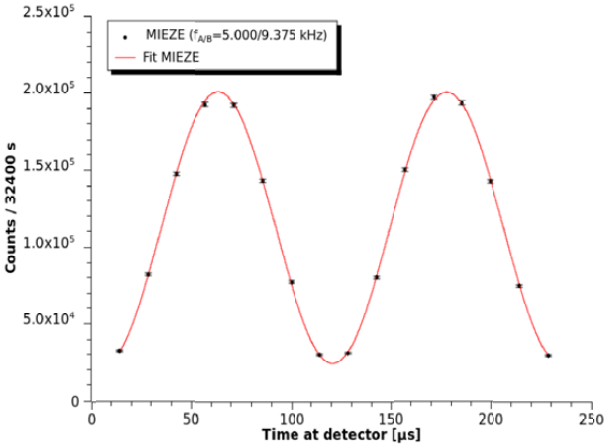

Figure 4: MIEZE signal for 5 / 9.375 kHz

5.7 MIRA – The beam line for very cold neutrons at the FRM-II

Robert Georgii [1, 2], **Peter Böni** [1], **Phillip Jüttner** [2], **Marc Janoschek** [3, 1], **Thomas Hils** [1], **Andreas Mantwill** [1, 2], **Sebastian Mühlbauer** [2, 1], **Christian Pfleiderer** [1], **Reinhard Schwikowski** [1]

[1] *Physik-Department E21, Technische Universität München, D-85748 Garching, Germany*
[2] *ZWE FRM-II, Technische Universität München, D-85748 Garching, Germany*
[3] *Laboratory for Neutron Scattering ETHZ & PSI, CH-5232 Villigen PSI*

MIRA is a versatile instrument for very cold neutrons (VCN) using neutrons with a wavelength $\lambda > 8$ Å (see Fig. **??**). The flux at the sample position is $5 \cdot 10^5$ neutrons/(cm^2 s) unpolarised. It is situated at the cold neutron guide NL6b in the neutron guide hall of the FRM-II. As the instrument set-up can be changed quickly, MIRA is ideally suited as a testing platform for realizing new instrumental set-ups and ideas. In particular, MIRA is unique in its possibilities of combining different neutron scattering methods as:

- Polarized or non-polarized reflectometry.
- Spherical Polarimetry.
- Polarized or non-polarized small angle scattering (SANS).
- Classical NRSE (Neutron Resonance Spin Echo) setup as well as using the MIEZE principle.

This year MIRA was again successfully operated for 5 reactor cycles. In total, 16 external and 18 internal proposals, several tests and service measurements were performed. A few selected of these experiments are shown in this annual report, see 2.2, 2.1, 4.2, 5.6 and 5.5. One Ph.D. thesis (Multi-Mieze measurements by Nikolas Arend (FRM II)) and several measurements for diploma thesis were finished using mainly data from MIRA. A total of 2 weeks was devoted to the Fortgeschrittenenpraktikum of the Physics Department for 35 students in total.

Currently the upgrade of MIRA to shorter wavelengths is in progress. The goal is to use neutons with wavelengths between 3 Å and 6 Å from the neutron guide NL 6a (beam area 120 x 60 mm^2) using a PG monochromator. Having neutrons with a wavelength closer to the maximum of the cold flux, having the PG mochromator a higher reflectivity as the current multilayer monochromator and using also a vertical focusing monochromator, MIRA will then show a significant increase in intensity. This year the new monochromator shielding has already been integrated in the guide NL 6a (see Figure 2) and all preparations for installing the new option in January 2008 have been taken.

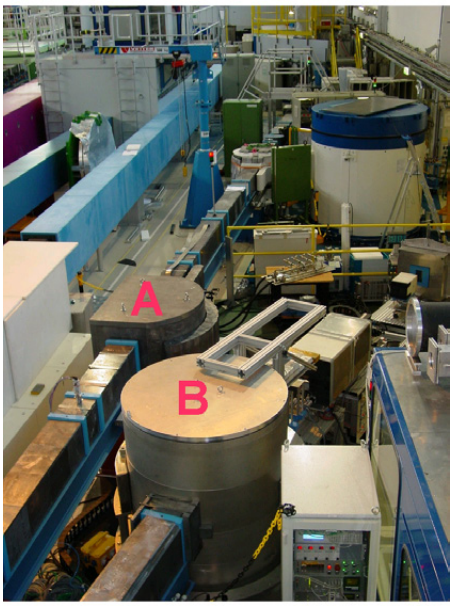

Figure 1: MIRA and the second monochromator shielding (A). The first monochromator is labeled (B).

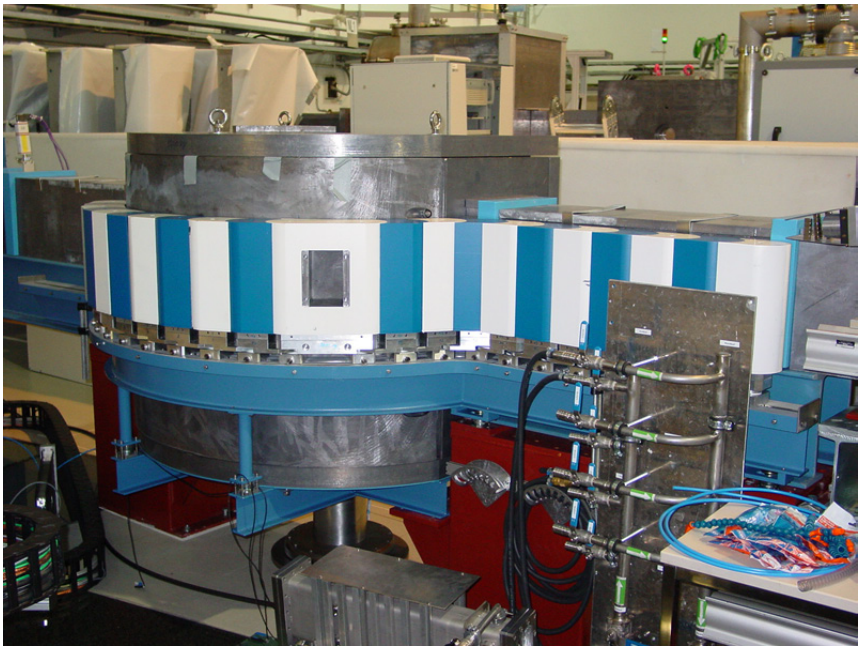

Figure 2: A close-up of the second monochromator shielding

5.8 Replacement of neutron guide and new polarizer at RESEDA

W. Häußler [1, 2], **M. Sandhofer** [1], **R. Schwikowski** [2], **A. Mantwill** [1], **P. Böni** [1]
[1] *Physik-Department E21, Technische Universität München, D-85748 Garching, Germany*
[2] *ZWE FRM-II, Technische Universität München, D-85748 Garching, Germany*

One major challenge in 2007 at the Resonance Spin Echo (NRSE) Spectrometer RESEDA has been the replacement of the neutron guide. The old, polarizing neutron guide NL5 had to be removed, due to non-tolerable activation of its magnetic supermirror layers. The new neutron guide NL5 consists of glass furnished with non-magnetic NiTi supermirrors. As a consequence, the neutron beam is no more depolarized. A supermirror cavity fixed at the very end of the guide is now used as a polarizer. Fig. 1 shows an image of the polarizing cavity, being 2 m long and optimized for neutron wavelengths $5 < \lambda < 8$ Å. A strong magnetic field produced by permanent magnets and iron plates around the polarizer provides sufficient polarizing field for the magnetic supermirrors. In order to maintain sufficiently strong magnetic field strength along the whole polarizer, several measures were taken. The beam shutter at the end of the neutron guide, having before partly covered the glass walls of the polarizer, had to be exchanged by a smaller, but nevertheless equally efficient shutter, because more space was needed for the iron plates of the guide field. The number of magnets was increased, in order to reach a field strength of about 400 G.

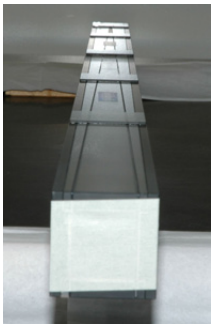

Figure 1: The new polarizing cavity, which is now mounted at the end of the neutron guide NL5, in front of RESEDA.

The instrument was moved on air pads about 80 cm aside the neutron guide, so that the polarization could be measured directly behind the polarizing cavity, i.e. before the neutrons traverse the instrument. After some improvements, the most significant one being a diaphragm, suppressing unpolarised neutrons at larger divergence angles and increased field strength at the end of the polarizer, the polarization reached a mean value over the whole beam cross section of 88% for $\lambda = 6$ Å. Fig. 2 shows a false color image of the polarization data acquired by means of a polarization measurement setup, consisting of two spin flippers, a He^3 cell (kindly provided by the FRM II - He^3 group, Dr. Masalovich and O. Lykhvar) used as analyzer and the detectors. For fast tuning of the spin flippers, we used a standard He^3 counter. For the final measurements providing spatially resolved polarization data, we used a CCD camera equipped with a neutron sensitive scintillator.

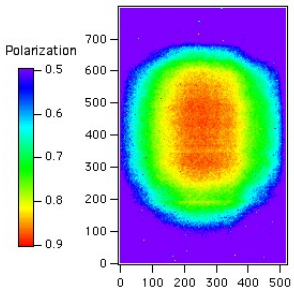

Figure 2: False color contour plot of the polarization measured directly behind the new polarizer at the end of NL5. The polarization reaches the maximum value 92%, the mean value is 88%.(200 pixels correspond to 25 mm)

In order to detect depolarization effects in the first spectrometer arm of RESEDA, it has been moved back to the neutron guide, and the polarization measurement setup described above was moved behind the first spectrometer arm. While moving RESEDA aside and back, it turned out that the air pads did not work properly. In order to avoid similar problems in future, construction of improved air pads has been started in mid 2007. Nevertheless, the instrument was positioned back and aligned according to the neutron beam. The very first polarization tests show, that the polarization is not equally distributed within the neutron beam behind the first arm of RESEDA. Fig. 3 shows a false color image of the polarization distribution. Improving the polarization will be continued during the first cycle in 2008.

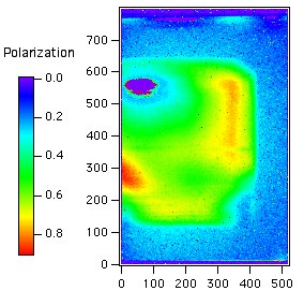

Figure 3: False color image of the result of the very first polarization test. The polarization measurement setup was placed behind the first spectrometer arm of RESEDA. The polarization shows some inhomogeneity of not yet known origin.(200 pixels correspond to 25 mm)

Last but not least, a significant effort in autumn 2007 was put into the relocation of the new RESEDA user cabin. Before having been able to install the user cabin, finishing work had to be done on it, including painting the inner walls and finishing installations. Subsequently, after having been put in place, the security installations of the cabin were installed, especially on the top of the cabin, where a most of the electrical installations and electronics is placed now. The NRSE coils, which have been supplied with motorized goniometers and rotation tables in early 2007, in order to provide fast and efficient positioning of the coils, will be put into operation again. Having finished the polarization measurements, we will start with spin echo test measurements, employing the NRSE coils together with new NSE coils that are used for measurements at small spin echo times.

5.9 Rod-casting-facility TGS and single crystal growth of MnSi and Mn_3Si

Andreas Neubauer [1], **Barbara Russ** [1], **Andrei Petrenko** [1, 2], **Christian Pfleiderer** [1]
[1] *Physics Department E21, Technical University Munich, 85748 Garching, Germany*
[2] *Columbia University, New York, New York, USA*

After successful implementation of the high purity (UHV) four mirror image furnace (OFZ) for floating zone crystal growth (see annual report 2006) first single crystals of intermetallic compounds were grown. Metallurgical, transport and thermodynamic properties of the crystals were investigated.

To prepare pure, homogeneous and geometrically well-shaped starting rods of the desired composition for use in the optical image furnace a rod-casting-facility (TGS) was constructed (Figure 1). Rods are cast in a Hukin-type cold crucible. The starting material is heated by a RF induction coil until the melt slightly levitates in the copper crucible. By pulling down a water-cooled copper rod at the bottom of the crucible the molten material flows into a water cooled copper mold (inset in Fig. 1) with a diameter of 6 mm and a length of 7 cm. The casting procedure takes place in high purity Ar atmosphere after UHV pumping the system.

Here we report on the growth of two systems; congruently melting MnSi and peritectic Mn_3Si. Below $T_c = 29$ K MnSi is a weak itinerant helimagnet with a spin spiral along the $\langle 110 \rangle$ - direction. Above a critical pressure $p_c = 14.6$ kbar MnSi shows a NFL-resistivity with a partially ordered magnetic phase [1]. MnSi is congruently melting with a melting temperature of $T_s = 1276°$C. Rods were cast with a stoichiometric composition of pure Mn (etched) and Si. Single crystals of MnSi were grown in the optical image furnace in a high purity Ar atmosphere. Optical investigation of metallurgical cuts, X-ray Laue diffraction and single crystal neutron diffractometry (RESI, FRM II) proved single crystallinity throughout the rod. Measurements of the specific heat confirm the magnetic transition at $T_c = 29$ K consistent with puplished data [2, 3].

Mn_3Si, an unusual itinerant antiferromagnet below $T_N = 23$ K [4], crystallizes in the cubic $L2_1$ Heusler structure. In contrast to congruently melting MnSi it solidifies in a peritectic formation. We therefore used self-flux-growth - the system drives itself into a molten zone of different composition. Two Mn_3Si crystals were grown (see e.g. Fig. 2 a). Fig. 2 b shows a longitudinal cut through the final zone of the crystal, nicely demonstrating the transition between the polycrystalline feed rod over off-stoichiometric flux to the single crystal (from left to right). Evidence of single cristallinity was obtained via X-ray Laue diffraction and neutron scattering. Specific heat and transport measurements are consistent with published data [4].

A.P. acknowledges financial support through the RISE program of the DAAD.

Figure 1: Rod-casting-facility (TGS) and copper mold with MnSi rod (bottom right corner).

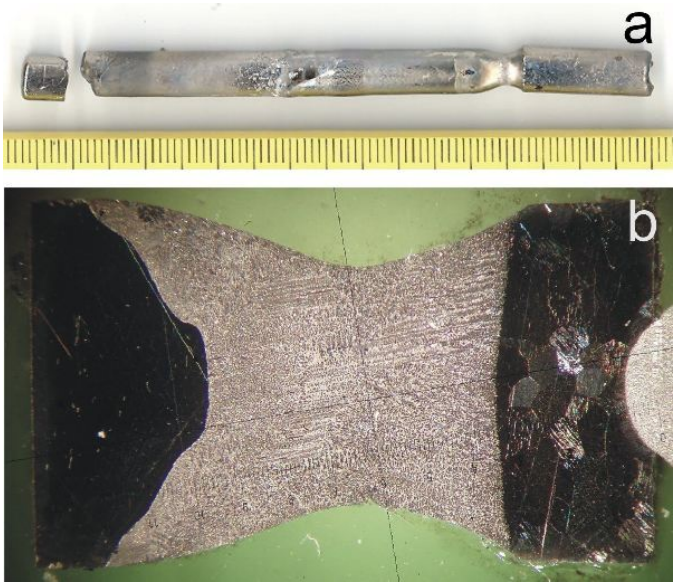

Figure 2: a) As grown Mn_3Si crystal. b) Longitudinal cut through final zone of the Mn_3Si crystal.

References

[1] C. Pfleiderer et al. Partial order in the non-Fermi-liquid phase of MnSi. *Nature*, 427:227–231, 2004.

[2] Daniel Lamago et al. Magnetic-field induced instability surrounding the A-phase of MnSi: Bulk and SANS measurements. *Physica B*, 385-386:385–387, 2006.

[3] C. Pfleiderer. Experimental studies of weakly magnetic transition metal compounds. *J. Magn. Magn. Mater.*, 226-230:23–29, 2001.

[4] C. Pfleiderer, J. Boeuf, and H. v. Löhneysen. Stability of antiferromagnetism at high magnetic fields in Mn_3Si. *Physical Review B*, 65:172404–1 – 172404–4, 2002.

5.10 Top-loading dilution refrigerator TL 400

S. Legl [1], **C. Pfleiderer** [1]
[1] *Physik-Department E21, Technische Universität München, D-85748 Garching, Germany*

Ultra-low temperatures are a key requirement in the search for novel ordering phenomena in intermetallic compounds. The most widely used technology for reaching mK temperatures are dilution refrigerators. However, an important technical constraint with conventional dilution refrigerators are the rather long turn-over times for sample changes. To reduce the turn-over time for sample changes, systems are now widely used where the dilution unit itself may be retracted from a bath cryostat by means of a sliding seal. Here cooling a sample from ambient temperature to base temperature typically takes 8 hours. Additional delays in are due to the time needed for changes of samples. An alternative dilution units, in which the sample is loaded directly into the mixing chamber, with a bespoke sample support. However, due to its design the base temperature of these systems is typically limited to about 20 to 30 mK, and the samples are immersed in the liquid.

We have inherited a dilution refrigerator from the experimental institute E12 (group of Prof. Krücken), that was previously used for particle physics experiments. The dilution fridge is based on an older design, which allows to load a sample into the inner vacuum can directly onto a tail attached to the mixing chamber. The loading mechanism is based on a load-lock feature along the central axis of the system. The sample is pre-cooled with a bespoke loading assembly, allowing extremely short turn over times.

To identify technical problems our dilution fridge, which had not been operated for nearly five years, was cooled-down twice to screen its technical status. Following this, the system was completely disassembled and all components leak tested and, where necessary, replaced. For our experiments state of the art electrical wiring was installed, along with low temperature signal transformers and RF filtering.

Following completion of these changes our top-loading dilution refrigerator immediately operated without any complications. Given some training we are now ambitious to come close to the old record for a sample turn-over of well below 3 hours between room temperature and the base temperature of the system of 5 mK.

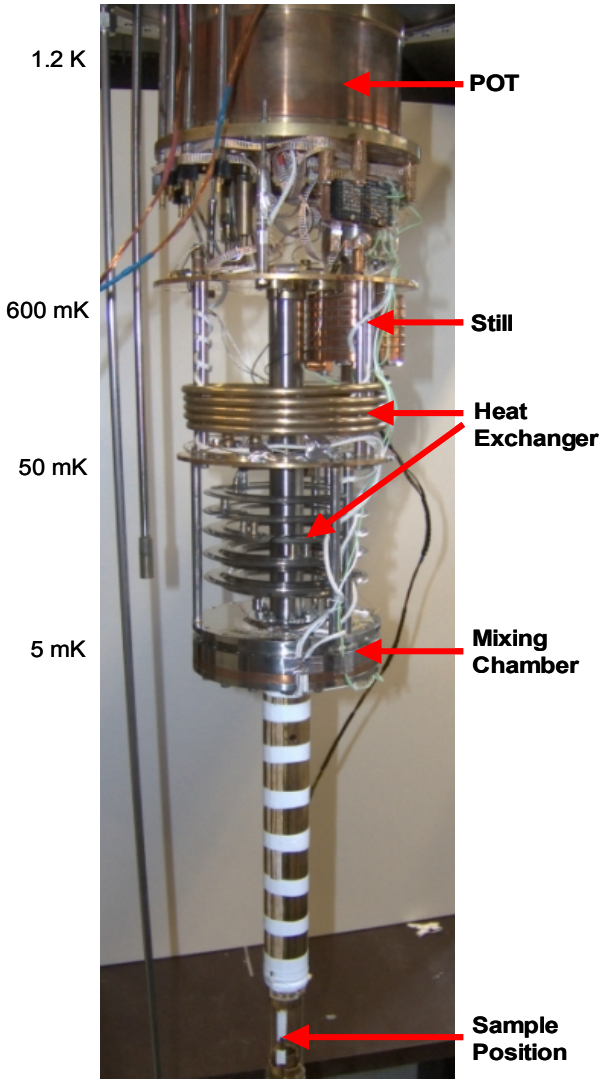

Figure 1: The dilution unit: The heart of the cryostat. The picture shows the He_4-POT, the Still, coiled tubular and sintered silver heat exchangers, the mixing chamber where the phase separation takes place and finally the sample position at the end of the tail.

6

Activities 2007

6.1 Lectures, Courses and Seminars

P. Böni	Lecture "Festkörperphysik I" (WS 06/07)
	Tutorials "Festkörperphysik I" (WS 06/07)
	Lecture "Festkörperphysik II" (SS 07)
	Tutorials "Festkörperphysik II" (SS 07)
	Lecture "Experimentalphysik I für Geodäsie und Geoinformation" (WS 07/08)
	Lecture "Polarized Neutrons", School on Pulsed Neutron Sources, Oct. 15-26 2007, The Abdus Salam International Centre for Theoretical Physics
	Seminar "Neutronen in Forschung und Industrie", together with W. Petry, K. Schreckenbach and W. Häußler
	Seminar "Experimentelle Methoden der Festkörperphysik", together with C. Pfleiderer and C. Hugenschmidt
R. Georgii	Lab course "Fortgeschrittenenpraktikum für Physiker" (at FRM-II)
W. Häußler	Seminar "Neutronen in Forschung und Industrie" together with P. Böni, W. Petry and K. Schreckenbach
C. Hugenschmidt	Seminar "Experimentelle Methoden der Festköperphysik", together with C. Pfleiderer and P. Böni
	Lab course "F-Praktikum Positronen-Annihilation"
M. Janoschek	Tutor "Festkörperphysik II" (SS 07)
	Tutor "Experimentalphyysik I für Geodäsie und Geoinformation" (WS 07/08)
T. Keller	Lab course "Elektronikpraktikum"
S. Legl	Tutor "Festkörperphysik I" (WS 06/07)
	Tutor "Festkörperphysik II" (SS 07)
	Tutor "Experimentalphysik I" (WS 07/08)
B. Löwe	Lab course "F-Praktikum Positronen-Annihilation"
K. Lorenz	Lab course "Elektronikpraktikum"
J. Mayer	Tutor "Experimentalphysik I" (WS 06/07)
	Tutor "Experimentalphysik II" (SS 07)
	Tutor "Experimentalphysik I" (WS 07/08)
C. Morkel	Lecture "Physics with Neutrons I" (SS 07)
	Lecture "Physics with Neutrons II" (WS 07/08)
M. Mühlbauer	Lab course "Elektronikpraktikum"
S. Mühlbauer	Tutor "Festkörperphysik I"(WS 06/07)
	Tutor "Festkörperphysik II"(SS 07)
	Tutor "Experimentalphysik I" (WS 07/08)
A. Neubauer	Tutor "Experimentalphysik I" (WS 06/07)
	Tutor "Experimentalphysik II" (SS 07)
	Tutor "Experimentalphysik I" (WS 07/08)

P. Niklowitz	Tutor "Festkörperphysik I" (WS 06/07)
	Tutor "Festkörperphysik II" (SS 07)
P. Pikart	Lab course "F-Praktikum Positronen-Annihilation"
C. Pfleiderer	Lecture "Experimentalphysik I" (WS 06/07)
	Tutorials "Experimentalphysik I"
	Lecture "Experimentalphysik II" (SS 07)
	Tutorials "Experimentalphysik II"
	Lecture "Experimentalphysik I" (WS 07/08)
	Tutorials "Experimentalphysik I"
	Seminar "Experimentelle Methoden der Festköperphysik", together with C. Pfleiderer, P. Böni and C. Hugenschmidt
	Seminar "Bose-Einstein-Kondensation und Supraleitung", together with W. Zwerger and R. Hackl (SS 07)
	"Münchner Physik Kolloquium", Coordinator (TUM)
	Lecture "Quantum order of chiral magnets", APCPT-MPI summer school on correlated electron systems, Aug 2007, Acian Pacific centre for theoretical physics, Pohang, Corea
C. Piochacz	Tutor "Festkörperphysik I" (WS 06/07)
	Tutor "Festkörperphysik II" (SS 07)
	Tutor "Experimentalphysik I" (WS 07/08)
	Lab course "F-Praktikum Positronen-Annihilation"
R. Ritz	Tutor "Experimentalphysik I" (WS 06/07)
M. Schulz	Lab course "Elektronikpraktikum"
B. Schillinger	Lab course "Elektronikpraktikum"
K. Schreckenbach	Lecture "Reaktorphysik und neue Methoden der Kerntechnik"
	Seminar "Neutronen in Forschung und Industrie", together with P. Böni, W. Petry and W. Häußler
	Lab course "Fortgeschrittenenpraktikum für Physiker" (at FRM-II)
M. Stadlbauer	Tutor "Festkörperphysik I" (WS 06/07)
	Tutor "Festkörperphysik II" (SS 07)
	Tutor "Experimentalphysik I" (WS 07/08)
	Lab course "F-Praktikum Positronen-Annihilation"

6.2 Seminar "Neutronen in Industrie und Forschung" 2007

Date	Speaker	Title
Jan 8	F. Tchirkova (TU München)	Neutronen-, Protonen- und Schwerionen-Bestrahlungstechniken
Jan 15	Dr. A. Gukasov (Laboratoire Leon Brillouin)	Single crystal neutron diffraction studies of composite chain-ladder compounds
Jan 22	T. Mayer (TU München)	Neutronen-Reflektometrie an weicher Materie
Jan 29	Prof. Dr. H.-J. Wester (Nuklearmedizinische Klinik und Poliklinik, TU München)	Zielgerichtete radioaktive Sonden in der Diagnostik und Therapie
Feb 5	N. Arend (TU München)	Intensitätsmodulation mit Resonanz-Spin-Echo
Feb 7	Dr. Amitesh Paul	Polarized Neutron Scattering of Exchange Coupled Multilayers
Feb 12	Dr. R. Schneider (HMI, Berlin)	Residual Stress Analysis From the Volume to the Surface
Feb 26	Martin Engelhardt (Siemens AG)	High-Resolution Differential Phase Contrast Imaging Using Microfocus X-ray Sources
March 5	Dr. F. Fleischer (MPI für Kernphysik, Heidelberg)	Das Positronium-Ion: eine Lebensdauer-Messung und Möglichkeiten für weitere Experimente am FRM II
April 2	Dr. J. Kohlbrecher (Laboratory for Neutron Scattering ETH Zurich and PSI)	The polarisation option on SANS-1 at SINQ-PSI
May 7	Dr. T. Unruh (FRM II)	Charakterisierung von kolloidalen Arzneistoffträgersystemen mittels Röntgen- und Neutronenstreuung
May 14	Dr. Marton Major (MPI f. Metallforschung, Stuttgart)	Domain transformations in antiferromagnetically coupled Fe/Cr multilayers
May 21	PD Dr. Walter Assmann (Department für Physik, LMU)	Entwicklung radioaktiver Implantate zur lokalen Strahlentherapie
June 4	Priv. Doz. Dr. F. Joachim Hartmann (TU München)	Ultracold neutrons
June 11	Prof. Dr. J.L. Urai (RWTH Aachen)	Microstructural investigations in Gamma-irradiated NaCl
June 18	Dr. W. Egger (Institut für Angewandte Physik und Messtechnik, UniBw München)	Das gepulste Positronenstrahlsystem PLEPS am FRM-II
July 2	Dr. R. May (Institute Laue Langevin, Grenoble)	Progress on D22: Technical developments and scientific achievements
July 9	F. Bernlochner (TU München)	3D-Polarisationsanalyse
July 16	Prof. Dr. R. v. Klitzing (Stranski-Laboratorium für Physikalische und Theoretische Chemie)	Correlation between interactions and structure formation in thin polymer films
July 30	Dr. A. Gaspar (FRM II)	The dynamical structure of disordered proteins as probed by time-of-flight neutron scattering

Date	Speaker	Title
Oct 1	Dr. K.-D. Liss (ANSTO)	The first diffraction instruments at OPAL reactor and upcoming studies
Nov 5	Dr. A. Schneidewind (TU Dresden)	Konkurrierende Supraleitung und Antiferromagnetismus in $CeCu_2Si_2$ untersucht mit Mu-SR und Neutronen
Nov 12	Dr. U. Rücker (Institut für Festkörperforschung - Streumethoden Forschungszentrum Jülich GmbH	Neutron Reflectometry in Nanomagnetism and Materials Science
Nov 19	Dr. R. Hackl (Walther-Meissner-Institut)	How can we find the generic properties of the cuprates?
Nov 26	Dr. S. R. Dunsiger (Physics Department E21)	Spin Liquid and Spin Ice : Tuning the Ground State
Dec 3	Dr. A. Pautz (Gesellschaft für Anlagen und Strahlensicherheit)	Überblick über moderne Rechenmethoden für die reaktorphysikalische Kernauslegung und Störfallanalytik am Beispiel des FRM-II
Dec 17	Prof. M. Sattler (Institute of Structural Biology)	Combining NMR and Small Angle Scattering for structural analysis of multi-domain proteins and complexes in solution

6.3 Invited Speakers at E21 in 2007

Date	Speaker	Title	Seminar
Aug 23	Prof. Dr. Jochen Mannhart (Center for Electronic Correlations and Magnetism, Universität Augsburg)	Interfaces between Complex Electronic Systems	Münchner Physik Kolloquium
May 10	Prof. Dr. Gertrud Zwicknagel (Institut für Mathematische Physik, TU Braunschweig)	Neue Komplexität bei elektronischen Korrelationen - 5f-Elektronen in Aktiniden	Colloquium on Solid-State Physics
June 11	Prof. Dr. Bernhard Keimer (Max-Planck-Institut für Festkörperforschung, Stuttgart)	Spectroscopy of correlated electrons	Münchner Physik Kolloquium
June 14	Prof. Dr. Ernst Bauer (Institut für Festkörperphysik, TU Wien)	Unconventional superconductivity in $CePt_3Si$ and materials without inversion symmetry	Kolloquium on Solid-State Physics
July 5	Priv.-Doz. Dr. Matthias Bode (Center for Nanoscale Materials, Argonne National Laboratory, USA)	Imaging magnetic nanostructures with atomic resolution	Colloquium on Solid-State Physics
Nov 19	Prof. Dr. Alois Loidl (Center for Electronic Correlations and Magnetism, Universität Augsburg)	Multiferroics	Münchner Physik Kolloquium
Nov 19	Dr. Rudi Hackl (Walther-Meissner-Institut)	How can we find the generic properties of the cuprates?	Neutrons in Science and Industry
Nov 22	Dr. Stephen Dugdale (H.H. Wills Physics Laboratory, University of Bristol, UK)	Probing electronic strucure with positrons and synchrotron light	Colloquium on Solid-State Physics
Nov 26	Dr. Sarah R. Dunsiger (Physics Department E21)	Spin Liquid and Spin Ice: Tuning the Ground State	Neutrons in Science and Industry
Dec 7	Dr. Ben Taylor (University of California, San Diego, USA)	The vortex solid to vortex liquid transition of type-II superconductors and the origin of universal scaling of the critical temperature	WMI Seminar on Current Topics in Low Temperature Solid-State Physics
Dec 17	Prof. Dr. Josef Zweck (Universität Regensburg)	Mikromagnetismus sichtbar gemacht - Nanostrukturen im Transmissionselektronenmikroskop	Münchner Physik Kolloquium

6.4 Workshops

Workshop on Neutron Scattering in Strongly Correlated Electron Systems
October 25-27, 2007
Organizers: C. Pfleiderer and W. Häußler

The workshop on Neutron Scattering in Strongly Correlated Electron Materials from October 25th to 27th, 2007 at the Technische Universität München had the aim to advertise the use of novel neutron scattering techniques for the study of selected problems in correlated electron systems. A total of 57 colleagues participated in the workshop with an additional 10 to 15 participants from TU München attending selected sessions. Participants came from all over Europe (France, United Kingdom, Switzerland, Greece, Bulgaria, Hungary,...), the USA and Russia. About 50% of the participants were students and young postdocs.
The workshop program consisted of 6 tutorial lectures and 18 contributed talks, plus an additional 9 poster contributions (some of which are not listed in the attached program). Thematically about 50% of the contributions addressed modern developments in neutron scattering techniques, while the other 50% concerned pressing issues and new results in strongly correlated electron systems. In addition we offered an extended guided tour of FRM II with special emphasis on new developments in instrumentation. The technical tutorials focussed on specific instrumentation for the study of strongly correlated electron systems at FRM II (Böni and Su), and neutron resonance spin-echo techniques of various kinds (Gähler). The scientific tutorials were dedicated to quantum phase transitions (von Löhneysen), frustrated magnets (Krimmel) and finally flux line lattices in superconductors (Forgan). The scientific program began in the afternoon of October 25th, 2007, followed by the poster session and a welcome reception with food and drinks. The program continued on the morning of Friday, October 26th 2007, followed by a scientific tour of FRM II in the afternoon. On Saturday, October 27th the official scientific program lasted until the early afternoon, interrupted by a brief lunch.

We gratefully acknowledge financial support through NMI3 and COST-P16 of the European Community, by the Technische Universität München and the team of FRM II.

Figure 1: Participants of the Workshop on Neutron Scattering in Strongly Correlated Electron Systems

European Workshop on Neutron Optics NOP'07
March 5-7, 2007
Organizers: J. Stahn (PSI) and P. Böni

The European Workshop on Neutron Optics NOP'07 was held at the Paul Scherrer Institute in Villigen, Switzerland from March 5 to 7, 2007. It was organized jointly by the Paul Scherrer Institute and the Physics Department E21 in order to present and discuss recent advances in the design of new neutron optical components being developed worldwide and in particular within the Joint Research Activity JRA3 that is supported by the European Union within the Sixth Framework Program. Part of the presented work was also supported by the Swiss National Science Foundation through the National Center of Competence in Research *Materials with Novel Electronic Properties - MaNEP*.
The recent years have witnessed significant progress in the development of improved focusing techniques using reflective and diffractive optics thanks to the progress made in the performance of supermirror coatings and of new concepts like non-linear tapering of guides, multiplexing of neutron beams, and focusing. These developments show already their impact at the FRM II as well as the new intense spallation sources SNS, J-PARC and TS-2 at ISIS. Therefore, the workshop was attended by a large number of experts (80) from almost all neutron scattering centers of the world.
Each of the four topics: Instrumentation, Guides, Focusing, and polarization were introduced by tutorial talks presented by well known experts in the respective fields, i.e. P. Böni (E21), R. Gähler (ILL), H. Shimizu (Riken), and K. Andersen (ILL) followed by oral presentations that were selected by an international program committee. In addition, two poster sessions were held giving the opportunity for lively discussions. Several companies, i.e. Umicore, SwissNeutronics, Mirrotron, and SDH displayed their newest products.
The refereed proceedings of the workshop were published in the scientific journal Nuclear Instruments and Methods A **586** (2008). The workshop was supported by the European Union within the sixth frame work program FP6 under contract n. 505925.

Figure 2: Participant of the European Workshop on Neutron Optics NOP'07

PLEPS Workshop and 2nd User Meeting at NEPOMUC

October 30, 2007

Organizers: C. Hugenschmidt (TUM) and W. Egger (UniBwM)

This second user meeting at NEPOMUC / FRM II has been dedicated to the pulsed low-energy positron system (PLEPS) which was transferred from the University of the Bundeswehr Munich (UniBwM) to FRM II. The one-day workshop at October 30th, 2007 at the Technische Universität München (TUM) was organized by our positron group at E21 and FRM II together with the research group of Prof. G. Dollinger at the institute for applied physics and measurement technology of the UniBwM.

The aim of the meeting was to advertise the feasibility of positron lifetime measurements for defect spectroscopy with variable depth using the PLEPS at the high intensity positron beam NEPOMUC. A total of 32 colleagues from all over Europe (France, Belgium, Finland, Hungary,...) attended the workshop. After welcome talks of Prof. W. Petry and Prof. G. Dollinger the positron beam facility (C. Hugenschmidt) and the PLEPS-apparatus (P. Sperr, W. Egger) were presented. The following sessions consisted of 18 short oral contributions concerning proposals for positron lifetime experiments. The attendees presented a large variety of experiments on defects in metals, irradiated samples, free volume of polymers and membranes. In addition we offered an extended guided tour of FRM II with special emphasis on the PLEPS apparatus and the other positron spectrometers located at NEPOMUC. In the evening the workshop was closed at the poster session, where all experiments of the FRM II were presented, and we had a Bavarian $Brotzeit$ together with the colleagues of the FRM II user meeting.

We gratefully acknowledge financial support through NMI3 of the European Community, by the Technische Universität München and the team of FRM II.

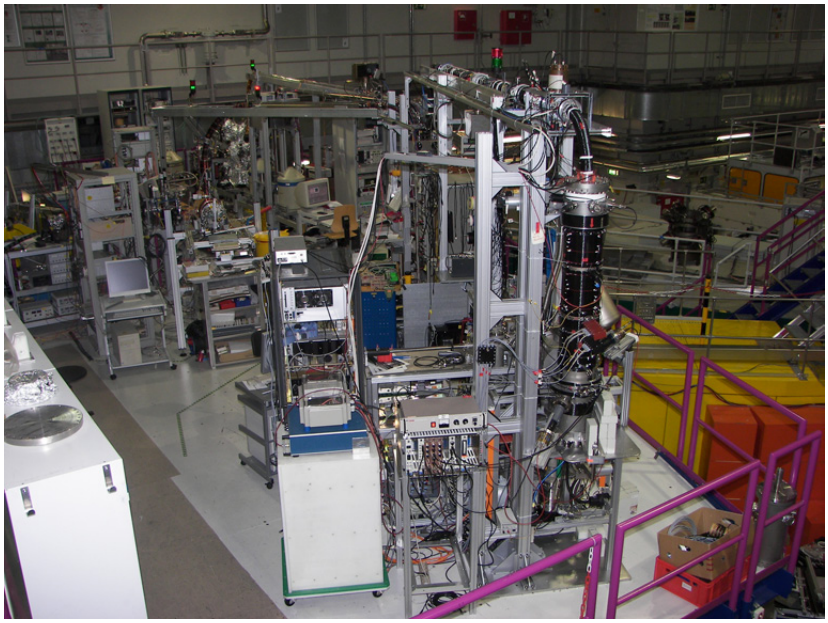

Figure 3: Experiments at the high intensity positron source NEPOMUC at FRM II

6.5 Publications 2007

[1] E. Babcock, A. Petoukhov, J. Chastagnier, D. Jullien, E. Lelièvre-Berna, K.H. Andersen, R. Georgii, S. Masalovich, S. Boag, C.D. Frost, and S.R. Parnell. Afp flipper devices: Polarized ^{3}He spin flipper and shorter wavelength neutron flipper. *Physica B*, 397:172–175, 2007.

[2] J. Baumann, Z. Kiss, S. Krimmel, A. Kuba, A. Nagy, L. Rodek, B. Schillinger, and J. Stephan. Discrete methods for nondestructive testing. *Advances in Discrete Tomography and its Applications*, pages 303–331, 2007.

[3] Y. Bodenthin, U. Staub, M. Garcia-Fernandez, M. Janoschek, J. Schlappa, E. I. Golovenchits, V. A. Sanina, and S. G. Lushnikov. Manipulating the magnetic structure by electric fields in multiferroic $ErMn_2O_5$. *Phys. Rev. Lett.*, 100:027201, 2007.

[4] P. Böni. Neutron optics and phase space transformers. *Notiziario Neutroni E Luce di Sincrotrone*, 12:26–27, 2007.

[5] H. B. Braun, J. Kulda, B. Roessli, D. Visser, K. Krämer, H. U. Güdel, and P. Böni. Chiral quantum excitations in the anisotropic antiferromagnet $CsCoBr_3$. *J. Magn. Magn. Mater.*, 310:1194–1196, 2007.

[6] T. Brunner and C. Hugenschmidt. Spectrometer for the investigation of temperature dependent Ps formation and material dependent moderation efficiency. *Phys. status solidi*, 4:3989–3992, 2007.

[7] A. Cervellino, M. Janoschek, L. Keller, V. Pomjakushin, B. Roessli, J. Schefer, G. Schuck, D. Sheptyakov, U. Stuhr, O. Zaharko, S. Klimko, and P. Böni. 10 years of neutron diffraction at the Swiss neutron spallation source SINQ. *SGK/SSCr Newsletter*, 73:6–12, 2007.

[8] F. Demmel, A. Diepold, H. Aschauer, and C. Morkel. The temperature dependent collective dynamics of liquid Rubidium. *J. of Non:Crystalline Solids*, 353:3164–3168, 2007.

[9] M. Engelhardt, J. Baumann, M. Schuster, C. Kottler, F. Pfeiffer, O. Bunk, and C. David. High-resolution differential phase contrast imaging using a magnifying projection geometry with a microfocus x-ray source. *Appl. Phys. Lett.*, 90(22):224101, 2007.

[10] M. Engelhardt, J. Baumann, M. Schuster, C. Kottler, F. Pfeiffer, O. Bunk, and C. David. Inspection of refractive x-ray lenses using high-resolution differential phase contrast imaging with a microfocus x-ray source. *Rev. Sci. Instrum.*, 78(9):093707, 2007.

[11] F. Fleischer, G. Gwinner, C. Hugenschmidt, K. Schreckenbach, P. Thirolf, A. Wolf, and D. Schwalm. The negative ion of positronium: measurement of the decay rate and prospects for further experiments. *Can. J. Phys.*, 85:487–495, 2007.

[12] R. Georgii, N. Arend, P. Böni, D. Lamago, S. Mühlbauer, and C. Pfleiderer. Scientific review: MIRA: Very cold neutrons for new methods. *Neutron News*, 18:25–28, 2007.

[13] R. Georgii, P. Böni, M. Janoschek, C. Schanzer, and S. Valloppilly. MIRA - a flexible instrument for VCN. *Physica B*, 397:150–152, 2007.

[14] R. Gilles, A. Ostermann, C. Schanzer, B. Krimmer, and W. Petry. The concept of the new small-angle scattering instrument SANS-1 at the FRM -II. *Physica B*, 385-386:1174–1176, 2006.

[15] S. V. Grigoriev, Maleyev, A. I. Okorokov, Y. O. Chetverikov, P. Böni, R. Georgii, D. Lamago, H. Eckerlebe, and K. Pranzas. Magnetic structure of MnSi under an applied field probed by polarized small-angle neutron scattering. *Phys. Rev. B*, 74:214414–(1–10), 2006.

[16] C. Grünzweig, T. Hils, S. Mühlbauer, M. Ay, K. Lorenz, R. Georgii, R. Gähler, and P. Böni. Multiple small angle neutron scattering (MSANS): A new two-dimensional ultra small angle neutron scattering technique. *Appl. Phys. Lett.*, 91:203504, 2007.

[17] J. Hagel, O. Ignatchik, J. Wosnitza, C. Pfleiderer, J. A. Schlueter, J. Mohtasham, and G. L. Gard. Pressure dependence of the electronic properties of the quasi-two-dimensional organic superconductor $(ET)_2SF_5CH_2CF_2SO_3$. *Physica C*, 460:639–640, 2007.

[18] W. Häussler, B. Gohla-Neudecker, R. Schwikowski, D. Streibl, and P. Böni. RESEDA - the new resonance spin echo spectrometer using cold neutrons at the FRM-II. *Physica B*, 397:112–114, 2007.

[19] W. Häussler, D. Streibl, and P. Böni. The resonance spin echo spectrometer RESEDA at the FRM II. *Neutron News*, 18:17–19, 2007.

[20] C. Hugenschmidt. NEPOMUC - the new positron beam facility at FRM-II. *Neutron News*, 18:29–32, 2007.

[21] C. Hugenschmidt, T. Brunner, S. Legl, J. Mayer, C. Piochacz, M. Stadlbauer, and K. Schreckenbach. Positron experiments at the new positron beam facility NEPOMUC at FRM-II. *Phys. status solidi*, 4:3947–3952, 2007.

[22] C. Hugenschmidt, J. Mayer, and K. Schreckenbach. Surface investigation of Si(1 0 0), Cu, Cu on Si(1 0 0), and Au on Cu with positron annihilation induced Auger-electron spectroscopy. *Surf. Sci.*, 601:2459–2466, 2007.

[23] C. Hugenschmidt, J. Mayer, and M. Stadlbauer. Investigation of the near surface region of chemically treated Al-coated PMMA by Doppler-broadening spectroscopy. *Radiat. Phys. Chem.*, 76:217–219, 2007.

[24] M. Janoschek, S. Klimko, B. Roessli, R. Gähler, and P. Böni. Spherical neutron polarimetry with MuPAD. *Physica B*, 397:125–130, 2007.

[25] R. Jungwirth, N. Wieschalla, W. Schmid, A. Röhrmoser, W. Petry, and C. Pfleiderer. Thermal conductivity of heavy-ion-bombarded U-Mo/Al dispersion fuel. *Proceedings of RRFM IGORR*, 2007.

[26] T. Lancaster, S. J. Blundell, D. Andreica, M. Janoschek, B. Roessli, S. N. Gvasaliya, K. Conder, E. Pomjakushina, M. L. Brooks, P. J. Baker, D. Prabhakaran, W. Hayes, and F. L. Pratt. Magnetism in geometrically frustrated $YMnO_3$ under hydrostatic pressure studied with muon spin relaxation. *Phys. Rev. Lett.*, 98:197203, 2007.

[27] S. Legl and C. Hugenschmidt. A novel time-of-flight spectrometer for PAES. *Phys. status solidi*, 4:3981–3984, 2007.

[28] J. Mayer, C. Hugenschmidt, and K. Schreckenbach. Positron annihilation induced Auger electron spectroscopy of Cu and Si. *Phys. status solidi*, 4:3928–3931, 2007.

[29] S. Mühlbauer, P.G. Niklowitz, M. Stadlbauer, R. Georgii, P. Link, J. Stahn, and P. Böni. Elliptic neutron guides - focusing on tiny samples. *Nuclear Instruments and Methods in Physics Research A*, 2007. doi:10.1016/j.nima.2007.11.047.

[30] H. Nozaki, M. Janoschek, B. Roessli, J. Sugiyama, L. Keller, J. H. Brewer, E. J. Ansaldo, G. D. Morris, T. Takami, and H. Ikuta. Neutron diffraction and muSR study on the antiferromagnet $BaCoO_3$. *Phys. Rev. B*, 76:014402, 2007.

[31] C. Pfleiderer. On the identification of Fermi-liquid behavior in simple transition metal compounds. *J. Low Temp. Phys.*, 147:231, 2007.

[32] C. Pfleiderer, P. Böni, T. Keller, U. K. Rössler, and A. Rosch. Non-Fermi liquid metal without quantum criticality. *Science*, 316:1871–1874, 2007.

[33] C. Pfleiderer and R. Hackl. High-temperature-superconductivity: Schizophrenic electrons (news and views). *Nature*, 450:492–493, 2007.

[34] C. Pfleiderer, D. Reznik, L. Pintschovius, and J. Haug. Magnetic field and pressure dependence of small angle neutron scattering in MnSi. *Phys. Rev. Lett*, 99:156406, 2007.

[35] C. Pfleiderer and U. K. Rössler. Condensed matter physics: Lets twist again (news and views). *Nature*, 447:154, 2007.

[36] C. Piochacz, W. Egger, C. Hugenschmidt, G. Kögel, K. Schreckenbach, P. Sperr, and G. Dollinger. Implementation of the Munich scanning positron microscope at the positron source NEPOMUC. *Phys. status solidi*, 4:4028–4031, 2007.

[37] C. Le Quellec, G. Dosseh, F. Audonnet, N. Brodie-Lindner, C. Alba-Simionesco, W. Häussler, and B. Frick. Influence of surface interactions on the dynamics of the glass former ortho-terphenyl confined in nanoporous silica. *Eur. Phys. J. Special Topics*, 141:11–18, 2007.

[38] A. Schmehl, V. Vaithyanathan, A. Herrnberger, S. Thiel, C. Richter, M. Liberati, T. Heeg, M. Röckerath, L. F. Kourkoutis, S. Mühlbauer, P. Böni, D. A. Muller, Y. Barash, J. Schubert, Y. Idzerda, J. Mannhart, and D. G. Schlom. Epitaxial integration of the highly spin-polarized ferromagnetic semiconductor EuO with silicon and GaN. *Nature Materials*, 6:882 – 887, 2007.

[39] M. Stadlbauer, C. Hugenschmidt, and K. Schreckenbach. Characterization of the chemical vicinity of open volume defects in magnesium and AZ31 with coincident Doppler broadening spectroscopy. *Phys. Stat. Sol.*, 4:3489, 2007.

[40] M. Stadlbauer, C. Hugenschmidt, K. Schreckenbach, and P. Böni. Investigation of the chemical vicinity of crystal defects in ion-irradiated Mg and a Mg-Al-Zn alloy with coincident Doppler broadening spectroscopy. *Phys. Rev. B*, 76:174104, 2007.

[41] Y. J. Uemura, T. Goko, I. M. Gat-Malureanu, J. P. Carlo, P. L. Russo, A. T. Savici, A. Aczel, G. J. MacDougall, J. A. Rodriguez, G. M. Luke, S. R. Dunsinger, A. McCollam, J. Arai, C. Pfleiderer, P. Böni, K. Yoshimura, E. Baggio-Saitovitch, M. B. Fontes, J. Larrea jr, Y. V. Sushko, and J. Sereni. Phase separation and suppression of critical dynamics at quantum phase transitions of MnSi and $(Sr_{1-x}Ca_x)RuO_3$. *Nature Physics*, 3:29–35, 2007.

[42] N. Volkov, G. Petrakovskii, P. Böni, E. Clementyev, K. Patrin, K. Sablina, D. Velikanov, and A. Vasiliev. Intrinsic magnetic inhomogeneity of Eu substituted $La_{0.7}Pb_{0.3}MnO_3$ single crystals. *J. Magn. Magn. Mater*, 309:1–6, 2007.

[43] N. Wieschalla, , A. Bergmaier, P. Böni, K. Böning, G. Dollinger, R. Großmann, W. Petry, A. Röhrmoser, and J. Schneider. Heavy ion irradiation of U-Mo/Al dispersion fuel. *Journal of Nuclear Materials*, 1-3:191–197, 2006.

6.6 Conference, Workshop and Seminar Contributions 2007

[1] P. Böni. Introduction to FRM II and strongly correlated electron systems. Talk. *Workshop on Neutron Scattering in Strongly Correlated Electron Systems, Oct 2007. Garching, Germany.*

[2] P. Böni. Materials science at FRM II. Talk. *DTU-TUM Meeting, June 2007. Garching, Germany.*

[3] P. Böni. Methods and techniques: Polarized neutrons. Talk. *Lectures on the occasion of the School on Pulsed Neutrons, International Centre for Theoretical Physics, Oct 2007. Trieste, Italy.*

[4] P. Böni. Neutronen in der Wissenschaft und Technik - Neue Quellen/moderne Optik. Talk. *Kolloquium der Physikalischen Gesellschaft Zürich, ETH, Oct 2007. Zürich, Switzerland.*

[5] P. Böni. New concepts in neutron instrumentation. Talk. *European Workshop on Neutron Optics NOP'07, March 2007. Villigen, Switzerland.*

[6] P. Böni, M. Janoschek, C. Pfleiderer, F. Bernlochner, B. Roessli, and A. Rosch. Spin waves in helical MnSi. Talk. *European Conference on Neutron Scattering ECNS 2007, 9^{th} SINQ Users Meeting, June 2007. Lund, Sweden.*

[7] M. Engelhardt, J. Baumann, O. Bunk, C. David, C. Kottler, F. Pfeiffer, C. Schroer, and M. Schuster. High-resolution differential phase contrast imaging using microfocus x-ray sources. Talk. *International Symposium on Digital Industrial Radiology and Computed Tomography (DIR 2007)*, 2007. Lyon, France.

[8] M. Engelhardt, J. Baumann, and K. Jefimovs. Investigation of size and intensity distribution of the focal spot of microfocus x-ray tubes. Poster. *International Symposium on Digital Industrial Radiology and Computed Tomography (DIR 2007)*, 2007. Lyon, France.

[9] M. Engelhardt, J. Baumann, M. Schuster, C. Kottler, F. Pfeiffer, O. Bunk, and C. David. Grating-based high-resolution differential phase contrast radiography and tomography using microfocus x-ray sources. Poster. *The 2007 Denver X-ray Conference (DXC 2007)*, 2007. Denver, USA.

[10] R. Georgii. MIRA – a flexible instrument for long wavelength neutrons at the Forschungsneutronenquelle Heinz Maier-Leibnitz (FRM II): recent results. Talk. *Frühjahrstagung der DPG, March 2007. Regensburg, Germany.*

[11] R. Georgii. MIRA - a versatile instrument for long wavelength at the FRM-II. Talk. *IFF-Seminar, Abteilung Th. Brückel, September 2007. Jülich, Germany.*

[12] C. Hugenschmidt. NEPOMUC - Neutron Induced Positron Source Munich and first positron experiments. Invited Talk. *The 11th International Workshop on Slow Positron Beam Techniques for Solids and Surfaces, July 2007. Orleans, France.*

[13] C. Hugenschmidt. NEPOMUC - Neutron Induced Positron Source Munich and first positron experiments. Invited Talk. *37th Polish Seminar on Positron Annihilation, September 2007. Ladek Zdroj, Poland.*

[14] C. Hugenschmidt, T. Brunner, J. Mayer, C. Piochacz, K. Schreckenbach, and M. Stadlbauer. Determination of positron beam parameters by various diagnostic techniques. Poster. *The 11th International Workshop on Slow Positron Beam Techniques for Solids and Surfaces, July 2007. Orleans, France.*

[15] M. Janoschek. Chiral magnetism investigated by neutron scattering. Talk. *Special seminar at Brian Maple's group at University of California, December 2007. San Diego, USA.*

[16] M. Janoschek. MuPAD: Neue Einsichten in magnetische Festkörper mit Neutronen. Talk. *Tag der Physik (day of physics) at the Physics Department of the Technische Universität München, July 2007. Garching, Germany.*

[17] M. Janoschek. Spherical Neutron Polarimetry with MuPAD. Talk. *Workshop on Neutron Scattering in SCES at the Physics Department E21 of the Technische Universität München, October 2007. Garching, Germany.*

[18] M. Janoschek. The magnetic structure of $NdFe_3(^{11}BO_3)_4$ investigated by spherical neutron polarimetry. Talk. *9th SINQ Users' Meeting which took place as a satellite conference to the 4th European Conference on Neutron Scattering (ECNS 2007), June 2007. Lund, Sweden.*

[19] M. Janoschek. Unique Determination of Complex Magnetic Structures by Spherical Neutron Polarimetry. Poster. *Korrelationstage 2007, Max Planck Institute for the Physics of Complex Systems, February 2007. Dresden, Germany.*

[20] W. Kaltner, K. Lorenz, A. Jentys, B. Schillinger, and J. A. Lercher. 3d neutron tomography: non-destructive testing of hollow sphere structures. Poster. *FRM-II User Meeting, Oktober 2007. Garching, Germany.*

[21] W. Häußler. Hydrodynamic functions measured by neutron spin echo spectrometry. Poster. *ESF-FWF Conference Water Interfaces in Physics, Chemistry and Biology, 2007. Obergurgl, Germany.*

[22] W. Häußler. Neutron (resonance) spin echo and diffusive dynamics. Invited Talk. *Seminar, 2007. Jülich, Germany.*

[23] W. Häußler. Neutron spin echo on ferritin. Talk. *Conference: Proteins at work, 2007. Perugia.*

[24] W. Häußler. Neutron spin echo studies on diffusion in protein solutions. Invited Talk. *Seminar, 2007. Tübingen, Germany.*

[25] W. Häußler. Polarized neutron technics, results of partner 4 (TUM). Talk. *NMI3 meeting, 2007. Vienna, Austria.*

[26] W. Häußler, B. Gohla-Neudecker, R. Schwikowski, D. Streibl, and P. Böni. RESEDA: Double and multi detector arms for neutron resonance spin echo spectrometers. Poster. *ECNS, 2007. Lund, Sweden.*

[27] W. Häußler, A. Ostermann, and P. Böni. Monte Carlo simulations and measurements of the neutron polarization at RESEDA. Poster. *ECNS, 2007. Lund, Sweden.*

[28] B. Löwe, K. Schreckenbach, and C. Hugenschmidt. Gas moderation of positrons. Talk. *The 11th International Workshop on Slow Positron Beam Techniques for Solids and Surfaces (SLOPOS-11), July 2007. Orleans, France.*

[29] B. Löwe, K. Schreckenbach, and C. Hugenschmidt. Gas moderation of positrons. Talk. *DPG Frühjahrstagung, March 2007. Regensburg, Germany.*

[30] J. Mayer, C. Hugenschmidt, P. Pikart, and K. Schreckenbach. Positron annihilation induced Auger electron spectroscopy (PAES) of thin metal layers on Cu and Si. Talk. *DPG-Frühjahrstagung, March 2007. Regensburg, Germany.*

[31] J. Mayer, K. Schreckenbach, and C. Hugenschmidt. Positron annihilation induced Auger electron spectroscopy of metal coated Si and Cu. Talk. *11th International Workshop on Slow Positron Beam Techniques for Solids and Surfaces, July 2007. Orleans, France.*

[32] J. Mayer, K. Schreckenbach, and C. Hugenschmidt. Positron annihilation induced Auger electron spectroscopy of thin metal layers on Cu and Si. Talk. *3rd FRM-II Workshop on Neutron Scattering, July 2007. Rothenfels, Germany.*

[33] C. Morkel. Neutron-based materials characterisation using the high flux neutron source FRM-II. Talk. *FEMAS start up meeting, 2 March 2007. Garching, Germany.*

[34] S. Mühlbauer. Poster. *Temperature and Field Dependence of the Magnetisation in Ferromagnetic Semiconductor EuO Thin Films. European conference on neutron scattering ECNS, June 2007. Lund, Sweden.*

[35] S. Mühlbauer. Poster. *Vortex lattice structures in Niobium, Vanadium and Tantalum. Summer school on strongly correlated electron systems, Paul Scherrer Institut, August 2007. Zuoz, Switzerland.*

[36] S. Mühlbauer. Talk. *Elliptic neutron guides - Focusing on tiny samples for high pressure experiments. Conference on Neutron Optics, March 2007. Paul Scherrer Institut, Switzerland.*

[37] S. Mühlbauer. Talk. *New methods in neutron scattering: Spin Echo, MIEZE and MuPAD. Condensed Matter Group Seminar, February 2007. University of Birmingham, UK.*

[38] S. Mühlbauer. Talk. *Vortex Structures in Niobium, Vanadium and Tantalum. DPG Frühjahrstagung, March 2007. Regensburg, Germany.*

[39] S. Mühlbauer, P. Böni, R. Georgii, A. Schmehl, D. G. Schlohm, and J. Mannhart. Temperature and field dependence of magnetisation in ferromagnetic semiconductor EuO thin films. Poster. *European Conference on Neutron Scattering*, June 2007. Lund, Sweden.

[40] A. Neubauer. Hall effect and magnetoresistance in weakly ferromagnetic $CeSi_x$ and heli-magnetic MnSi. Talk. *DPG Tagung, March 2007. Regensburg, Germany.*

[41] A. Neubauer. Optical heated floating zone crystal growth of intermetallic compounds. Poster. *PSI Summer School on Condensed Matter Research, August 2007. Zuoz, Switzerland.*

[42] A. Neubauer. Single crystal growth of intermetallic compounds at TUM: Vom Anfang bis zum Einkristall... Talk. *Arbeitskreistreffen der DGKK, September 2007. Dresden, Germany.*

[43] P. G. Niklowitz. Novel quantum states of magnetic metals. Colloquium Talk. *Condensed Matter Seminar, 29 March 2007. Royal Holloway College, Egham, UK.*

[44] P. G. Niklowitz, S. Mühlbauer, P. Link, Th. Keller, J. A. Mydosh, C. Pfleiderer, P. Böni, M. J. Steiner, G. G. Lonzarich, D. Braithwaite, G. Knebel, J. Wilson, and J. Flouquet. Advanced neutron-diffraction techniques for experiments at high pressure. Poster. *PORTFOLIO Workshop, 2 July 2007. St Andrews, UK.*

[45] C. Pfleiderer. Coupled order parameter phenomena in f-electron superconductors. Talk. *Workshop of the DFG Forschergruppe on High-Tc Superconductivity, Bayerische Akademie der Wissenschaften, Dec 18 2007.*

[46] C. Pfleiderer. Larmor diffraction of URu_2Si_2 under pressure. Talk. *Frühjahrstagung der Deutschen Physikalischen Gesellschaft, Universität Regensburg, March, 26 2007. Regensburg, Germany.*

[47] C. Pfleiderer. Let's twist again. Talk. *Physikalische Kolloquium Universität Regensburg, June 4 2007. Regensburg, Germany.*

[48] C. Pfleiderer. Let's twist again: Festkörperphysik mit magnetischer Chiralität. Talk. *Lange Nacht der Wissenschaft, Oct 13 2007. Garching, Germany.*

[49] C. Pfleiderer. MnSi at high pressure: Evidence for a novel metal? Talk. *Korrelationstage, Max-Planck-Institut für komplexe System, March, 1 2007. Dresden, Germany.*

[50] C. Pfleiderer. Non-Fermi liquid metal, partial order, blue phases and more: The strange world of MnSi. Talk. *Condensed Matter Physics Colloquium, University of Oxford, Nov 8 2007. Oxford, UK.*

[51] C. Pfleiderer. Non-Fermi liquid metal without quantum criticality. Talk. *User Meeting of FRM II, Oct 30 2007. Garching, Germany.*

[52] C. Pfleiderer. Quantenphasenübergänge: Nur Buzz-Word Bingo? Talk. *Geophysikalisches Kolloquium, Ludwig-Maximilians Universität, Jan, 26 2007. München, Germany.*

[53] C. Pfleiderer. Quantum order in chiral magnets: 3D non-Fermi liquid phase and blue quantum fog in MnSi. Talk. *Symposium on Quantum Order of Chiral Magnets March Meeting of the American Physical Society, March, 9 2007. Denver, USA.*

[54] C. Pfleiderer. Quantum order of chiral magnets. Talk. *Annual Meeting of the Dutch Condensed Matter Physics Community, University of Utrecht, Dec 7 2007. Utrecht, Holland.*

[55] C. Pfleiderer. Quantum order of chiral magnets. Talk. *Workshop, Universität zu Köln, Oct 10 2007. Köln, Germany.*

[56] C. Pfleiderer. Quantum order of chiral magnets. *Tutorial Lecture APCP T-MPI Summer School on Strongly Correlated Electron Systems, Acian Pacific Centre for Theoretical Physics, Aug 6 2007. Pohang, Corea.*

[57] C. Pfleiderer and P. Böni. Spin dynamics and spin freezing at ferromagnetic quantum phase transitions. Talk. *Begutachtung Forschergruppe, March 2007. Karlsruhe, Germany.*

[58] C. Piochacz. A positron remoderator for the high intensity positron source NEPOMUC. Talk. *The 11th International Workshop on Slow Positron Beam Techniques for Solids and Surfaces, July 2007. Orleans, France.*

[59] B. Schillinger. ANTARES. Poster. *Neutronenstrahlen für angewandte Forschung Materialentwicklung und Werkstofftechnik*, Oct 2007. Aachen, Germany.

[60] B. Schillinger. Concepts for a rebuilt ANTARES-II facility. Talk. *Meeting of the European Neutron Radiography Association*, March 2007. Berlin, Germany.

[61] B. Schillinger. Detection systems for static and for short-time stroboscopic and continuous neutron imaging. Talk. *9th International Workshop on Radiation Imaging Detectors*, July 2007. Erlangen, Germany.

[62] B. Schillinger. Detection systems for static and for short-time stroboscopic and continuous neutron imaging -and a little bit of everything: USANS at D11: The future of neutron tomography. Talk. *ILL seminar*, September 2007.

[63] B. Schillinger. Neutron computed tomography on rat lungs using a cooled CCD camera with a Zeiss planar high resolution lens. Talk. *3rd FRM-II Workshop on Neutron Scattering*, July 2007. Rothenfels, Germany.

[64] B. Schillinger. Neutronenradiographie und tomographie am instrument ANTARES. Talk. *Neutronenstrahlen für angewandte Forschung Materialentwicklung und Werkstofftechnik*, Oct 2007. Aachen, Germany.

[65] M. Schulz, E. Calzada, K. Lorenz, M. Mühlbauer, and B. Schillinger. Radiography with polarized and with monochromatic neutrons. Talk. *European Neutron Radiography Association workshop, March 2007. Berlin, Germany.*

[66] M. Stadlbauer, C. Hugenschmidt, and K. Schreckenbach. Element specific defect investigation on Mg-alloys by ion implantationwith coincident Doppler broadening spectroscopy. Talk. *Annual meeting of the german physical society, Session MM38.4, March 2007. Regensburg, Germany.*

[67] M. Stadlbauer, C. Hugenschmidt, and K. Schreckenbach. New design of the CDB-spectrometer at NEPOMUC for T-dependent defect spectroscopy in Mg by positron annihilation spectroscopy. Talk. *The 11th International Workshop on Slow Positron Beam Techniques for Solids and Surfaces, July 2007. Orleans, France.*

6.7 Services to the Community

P. Böni
- Reviewer of scientific proposals, GKSS, Geesthacht, Germany.
- TUM-Beirat für den FRM-II, Garching.
- Coordinator of Work Package on Neutron Optics, Joint Research Project JRA3: NMI3 FP6.
- Co-chairman of the European Workshop on Neutron Optics NOP'07, Villigen, Switzerland.
- Responsible professor for crystal laboratory at the Physik-Department.

C. Pfleiderer
- Reviewer of scientific proposals, Jülich Centre for Neutron Science, Jülich, Germany.
- Chair: Workshop on Neutron Scattering in Strongly Correlated Electron Systems, Technische Universität München, Garching, Germany.
- Coordinator of Münchner Physik Kolloquium (with D. Grundler, S. Kehrein, A. Burkert, J. Erdmenger).

K. Schreckenbach
- Chairman of the "Arbeitgemeinschaft Forschungsreaktoren" (German research reactor operation group).
- Chairman of the "Expert Advisory Comittee" at the Institut Laue Langevin, Grenoble.

B. Schillinger
- Board member of the International Society for Neutron Radiography.
- Vice President of the European Society for Neutron Radiology.
- Conference Board Member for the 8^{th} World Conference on Neutron Radiography, October 2006, NIST, Gaithersburg, USA.

W. Häußler
- Workshop secretary, Workshop on Neutron Scattering in Strongly Correlated Electron Systems, Technische Universität München, Garching, Germany.

6.8 PhD Theses

Nikolas Arend New Aspects of the MIEZE Technique and Verification of the Multi-level MIEZE Principle

6.9 Diploma Theses

Robert Ritz Phasenübergänge schwach magnetischer Metalle unter extremen Bedingungen

Philip Pikart Elementspezifische Analyse von Al-Sn-Al Schichtsystemen mit der Positronenannihilationsspektroskopie

Benjamin Löwe Entwicklung eines Gasmoderators für Positronen

6.10 E21 Members

Phone/Fax: +49-89-289- PH: Physics Department, RS: Reactor Station

Name	Phone	Fax	Room	email
Bernlochner Florian, diploma student	-12515	-14724	PH 1, 2373	Florian.Bernlochner@frm2.tum.de
Böni Peter, Prof. Dr.	-14711	-14713	PH 1, 2215	Peter.Boeni@frm2.tum.de
Böning Klaus, Prof. Dr.	-12150	-12191	UBA 0325	Klaus.Boening@frm2.tum.de
Bundschuh Ralph, Dipl. Phys.	+49-89-636-48015	+49-89-636-53810	Klinik für Nuklearmedizin	Ralph.Bundschuh@ph.tum.de
Dunsiger Sarah, Dr.	-14722	-14724	PH 1, 2207	Sarah.Dunsiger@frm2.tum.de
Engelhardt Martin, Dipl. Phys.	+49-89-636-45791	+49-89-636-53810	–	zfp.student@mchp.siemens.de
Franz Christian, diploma student	-14740	-14724	PH 1, 2207	Christian.Franz@frm2.tum.de
Gläser Wolfgang, Prof. emerit.	-12476	-12474	PH 1, 2279	wglaeser@ph.tum.de
Hils Thomas, Dr.	-14512	-14724	PH 1, 2367	Thomas.Hils@hils-consult.de
Janoschek Marc, Dipl. Phys.	-14725	-14724	PH 1, 2214	marc.janoschek@frm2.tum.de
Jones Sylvia, Secretary	-14712	-14713	PH 1, 2217	Sylvia.Jones@frm2.tum.de
Jonietz Florian, diploma student	-12512	-14724	PH 1, 2367	Florian.Jonietz@frm2.tum.de
Legl Stefan, Dipl. Phys.	-14740	-14724	PH 1, 2207	Stefan.Legl@frm2.tum.de
Loewe Benjamin, diploma student	-12129	-14620	Flachbau 10	Benjamin.Loewe@frm2.tum.de
Lorenz Klaus, Dipl. Phys.	-14741	-14997	RS, 146b	Klaus.Lorenz@frm2.tum.de
Mantwill Andreas, mechanician	-14887	–	–	FRM-II
Mayer Jakob, Dipl. Phys.	-12137	-14620	Flachbau 11	Jakob.Mayer@frm2.tum.de
Morkel Christoph, Dr. habil.	-14713	-14724	PH 1, 2214	Christoph.Morkel@frm2.tum.de
Mühlbauer Martin, Dipl. Phys.	-12106	-14997	RS, 125a	Martin.Muehlbauer@frm2.tum.de
Mühlbauer Sebastian, Dipl. Phys.	-12515	-14724	PH 1, 2373	Sebastian.Muehlbauer@frm2.tum.de
Münzer Wolfgang, diploma student	-12512	-14724	PH 1, 2367	Wolfgang.Münzer@frm2.tum.de
Neubauer Andreas, Dipl. Phys.	-12512	-14724	PH 1, 2367	Andreas.Neubauer@frm2.tum.de
Pikart Philip, diploma student	-12161	-14620	Flachbau 10	Philip.Pikart@frm2.tum.de
Pfleiderer Christian, Prof. Dr.	-14712	-14713	PH 1, 2205	Christian.Pfleiderer@frm2.tum.de
Piochacz Christian, Dipl. Phys.	-12179	-14620	Flachbau 10	Christian.Piochacz@frm2.tum.de
Reingen Gabriel, mechanician	-12656	–	PH 1, 1321	–
Ritz Robert, Dipl. Phys.	-12515	-14724	PH 1, 2373	Robert.Ritz@frm2.tum.de
Russ Barbara, Dipl. Ing.	-14717	-14713	PH 1, 2207	Barbara.Russ@frm2.tum.de
Sandhofer Mathias, diploma student	-12512	-14724	PH 1, 2373	Mathias.Sandofer@frm2.tum.de

Phone/Fax: +49-89-289- PH: Physics Department, RS: Reactor Station

Name	Phone	Fax	Room	email
Schreckenbach Klaus, Prof. Dr.	-12183	-14713	PH 1, 2201	Klaus.Schreckenbach@frm2.tum.de
Schulz Michael, Dipl. Phys.	-14718	-14997	RS, 125a	Michael.Schulz@frm2.tum.de
Stadlbauer Martin, Dipl. Phys.	-14631	-14620	Flachbau 12	Martin.Stadlbauer@frm2.tum.de

6.11 Associated Members at FRM-II

Phone/Fax: +49-89-289- PH: Physics Department, RS: Reactor Station

Name	Phone	Fax	Room	email
Calzada Elbio, Dipl. Ing.	-14611	-14997	RS, 126	Elbio.Calzada@frm2.tum.de
Georgii Robert, Dr.	-14986	-14989	NL-Halle, UYH 0336	Robert.Georgii@frm2.tum.de
Häußler Wolfgang, Dr.	-14921	-14989	NL-Halle, UYH 0334	Wolfgang.Haeussler@frm2.tum.de
Hugenschmidt Christoph, Dr.	-14609	-14620	Flachbau 9	Christoph.Hugenschmidt@frm2.tum.de
Röhrmoser Anton, Dr.	-14890	-14995	FRM-II, UYH 0328	Anton.Roehrmoser@frm2.tum.de
Schillinger Burkhard, Dr.	-12185	-14997	RS, 127	Burkhard.Schillinger@frm2.tum.de
Schwikowski Reinhard, technician	-14915	-14995	NL-Halle, UYH 0336	Reinhard.Schwikowski@frm2.tum.de

6.12 Longterm Guests

Phone/Fax: +49-89-289- PH: Physics Department, RS: Reactor Station

Name	Phone	Fax	Room	email
Gähler Roland, Dr. habil.	+33-4-7620-7189	+33-4-7648-3906	–	gahler@ill.fr
Keller Thomas, Dr.	-12164	-14997	RS, 106	Thomas.Keller@frm2.tum.de
Wieschalla, Nico, Dr.	+49-9131-1893018	+49-9131-1894705	Fuel Europe Engineering Materials	nico.wieschalla@areva.com
Niklowitz Philipp	+44-1784-44-3499	–	–	philipp.niklowitz@rhul.ac.uk

6.13 Short-term scientific Visitors

Name	Institute	Duration of stay
Syers Paul[1]	Emory University, USA	May 2007 - July 2007
Nampaisarn Thanasin[1]	MIT, USA	June 2007 - Aug 2007
Petrenko Andrej[1]	Columbia University, USA	June 2007 - Aug 2007
Duris Joseph[1]	University of California, USA	June 2007 - Sept 2007
Duncan Will[2]	Royal Holloway, UK	Sept 2007
Ivanenko Ludmilla, Dr.[3]	Balarussian State University, Minsk	June 2007 - Sept 2007

[1] DAAD-RISE: www.daad/rise.de

[2] European Community, COST P16

[3] DAAD

6.14 Guided Tours at FRM-II

The neutron source FRM-II is open for everybody to visit the scientific and experimental facilities (Experimental Hall, Neutron Guide Hall and Reactor Basin). Therefore, guided tours are organized by the „Besucherdienst“ and conducted by the scientists and the technical staff of FRM-II. In 2007 members of E21 guided approximately 140 officially registered tours at various occasions, thus contributing a significant amount of time and personal effort to help making the Neutron Source FRM-II a publically transparent and accepted research facility.

6.15 Third Party Funding

We gratefully acknowledge financial support from

- Deutsche Forschungsgemeinschaft (DFG)
- Bundesministerium für Bildung und Forschung (BMBF)
- European Community: COST-P16 Program
- European Community: NMI3 Program
- Bavaria California Technology Center (BaCaTeC)
- Deutscher Akademischer Austauschdienst (DAAD)
- Swiss National Science Foundation (SNF)

We also acknowledge beam time at:

- European Synchrotron Radiation Facility (ESRF)
- Hahn-Meitner-Institut (HMI)
- Institut Laue-Langevin (ILL)
- Paul-Scherrer-Institut (PSI)

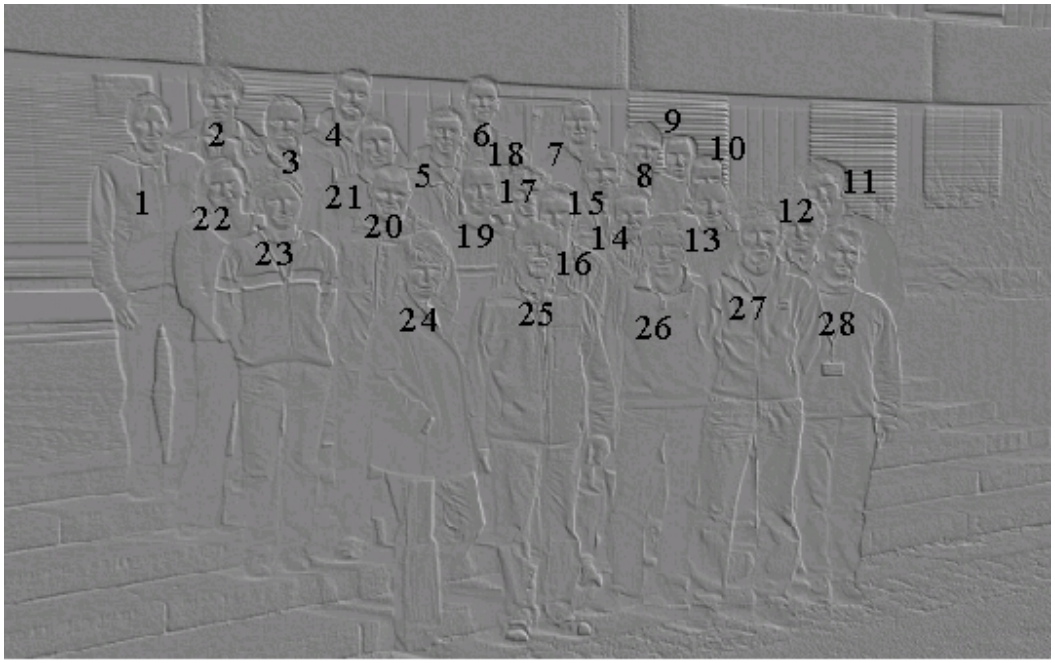

1	A. Neubauer	9	F. Jonietz	17	C. Weiß	25	R. Repper
2	K. Lorenz	10	M. Janoschek	18	M. Scheungraber	26	R. Schwikowski
3	K. Schreckenbach	11	H. Ceeh	19	B. Löwe	27	E. Calzada
4	B. Schillinger	12	C. Morkel	20	M. Stadlbauer	28	W. Häußler
5	R. Georgii	13	M. Sandhofer	21	M. Mühlbauer		
6	P. Pikart	14	C. Hugenschmidt	22	S. Jones		
7	W. Münzer	15	P. Böni	23	M. Schulz		
8	C. Pfleiderer	16	C. Franz	24	B. Russ		

Missing: F. Bernlochner, K. Böning, R. Bundschuh, S. Dunsiger, M. Engelhardt, W. Gläser, T. Hils, S. Legl, A. Mantwill, J. Mayer, S. Mühlbauer, C. Piochacz, G. Reingen, R. Ritz, A. Röhrmooser, T. Keller

E21 Gallery

Meanwhile bowling in January seems to be a tradition...

...like going to the Biergarten in summer.

This is what gloves are for

E21 group members searching for the Yeti

After a hard day at the DPG Frühjahrstagung

Closing the year with a christmas party

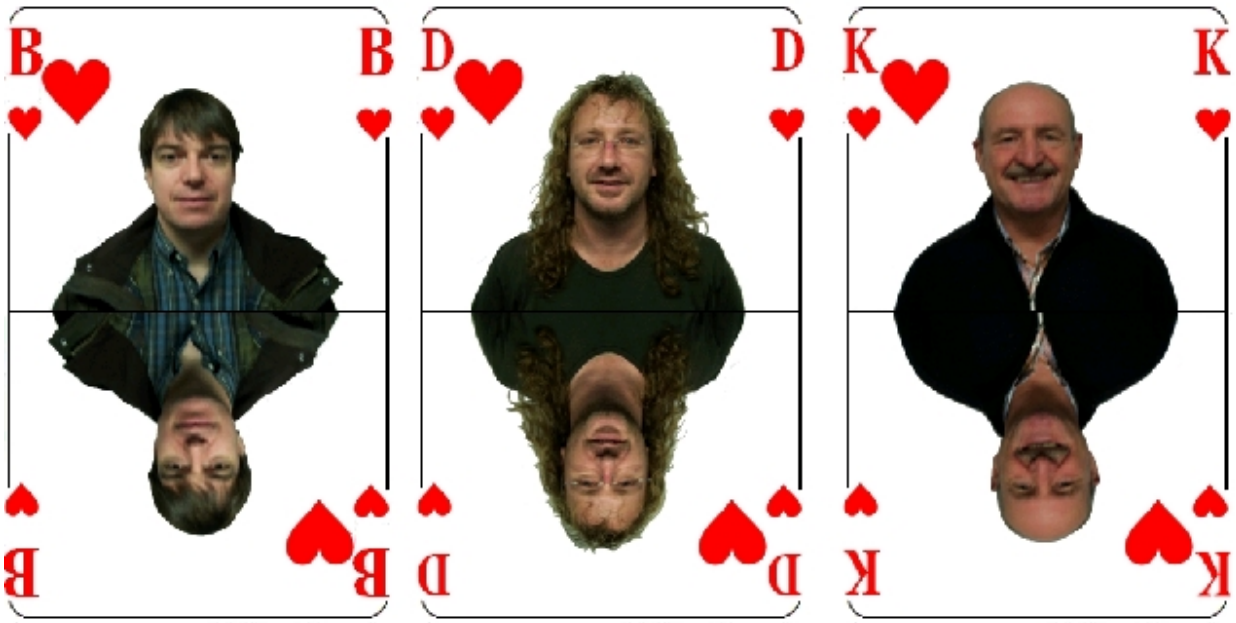

The team of *Experimentalphysik I*. Photos kindly provided by A. Weppner as prepared for the Christmas lecture 2007.